

*Research Report 44*

DECEMBER, 1960

# Composition of Sea Ice and its Tensile Strength



U. S. ARMY  
COLD REGIONS RESEARCH AND  
ENGINEERING LABORATORY

*Corps of Engineers*



# *Research Report 44*

DECEMBER, 1960

## **Composition of Sea Ice and its Tensile Strength**

by Andrew Assur

**U. S. ARMY SNOW ICE AND PERMAFROST  
RESEARCH ESTABLISHMENT**

**Corps of Engineers**

**Wilmette, Illinois**

16579



## PREFACE

This is a report of work performed on USA SIPRE\* Project 22.2-3 subtask a, Bearing capacity of floating ice sheets. The investigations were carried out by Dr. Andrew Assur, physicist, for the Applied Research Branch, Mr. W. K. Boyd, chief.

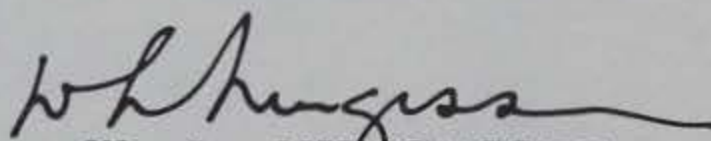
The following agencies and persons have provided help, support and assistance:

USAF Cambridge Research Center (Labrador and Greenland); Defence Research Board, Canada (Labrador); USA Engineer Arctic Task Force (Labrador and Greenland); USN Task Force 43 (Antarctica); US Committee for the International Geophysical Year (Antarctica).

Messrs. A. Landoldt, E. Remington, R. Benson, H. Hanson, and W. Johnson (IGY) assisted during this and many other test series at McMurdo Sound. Mr. T. Butkovich (SIPRE) kindly gave permission to use some of his unpublished test results in the analysis. Mr. D. Nevel (SIPRE) assisted in the preparation of some parts of the paper.

The author is especially indebted to Mr. D. Anderson and to Dr. W. Weeks who provided information about the dimensions and spacing of brine pockets used in this paper.

This report has been reviewed and approved for publication by the Office of the Chief of Engineers, U. S. Army.



W. L. NUNGESSER  
Colonel, Corps of Engineers  
Director

Manuscript received 24 January 1958

Department of the Army Project 8-66-02-400

\* Redesignated U. S. Army Cold Regions Research and Engineering Laboratory, 1 February 1961.



B2401  
6.44

4859490

## CONTENTS

	Page
Preface -----	ii
Summary -----	v
Introduction -----	1
List of symbols -----	3
Observed strength variations of sea ice -----	6
Observed phenomena -----	6
Testing procedures -----	8
Tensile strength tests -----	8
Salinity tests -----	10
Theoretical analysis -----	11
Some comments on stress concentration -----	11
Precipitation of salts -----	12
Effect of brine inclusions on the strength of sea ice -----	12
General theory -----	12
Specific models -----	18
Elliptical cylinders -----	18
Brine content -----	21
Chemical Analysis -----	22
Freezing point of brine -----	22
Some basic assumptions for "standard sea ice" -----	24
Methods for computing phase relations -----	25
Relative concentration of the main ions in brine as a function of temperature -----	25
Phase relations in "standard sea ice" -----	30
Relative volume of brine -----	32
Evaluation of ring tests results -----	33
Empirical analysis -----	37
Theoretical analysis of test results -----	37
Theory of reinforcement by salts -----	43
Conclusion -----	48
References -----	48
Appendix A: Relative volume of brine in standard sea ice -----	A1
Appendix B: Gravimetric constants for the main constituents in the brine-salt system of sea ice -----	B1

## ILLUSTRATIONS

Figure	Page
1. Observed vs computed strength of sea ice -----	7
2. Strength conditions of sea ice, depending on temperature and salinity -----	7
3. Relative tensile strength of sea ice as a function of temperature and salinity -----	13
4. Laminar structure of a sea-ice crystal -----	14
5. Cylindrical shape of brine inclusions -----	14
6. Freezing point of brine as a function of the ratio of dissolved salts to pure water -----	24
7. Relative loss of $\text{Ca}^{+}$ due to the precipitation of $\text{CaCO}_3 \cdot 6\text{H}_2\text{O}$ -----	26
8. Relative concentration of the principle ions in brine as a function of temprature -----	28
9. Relative amount of ions and salts in standard sea ice -----	30
10. Phase diagram for sea ice -----	32
11. Relative volume of brine in standard sea ice -----	33
12. Nomogram for relative brine volume in sea ice -----	33
13. Stresses at characteristic points in a "ring" under compression -----	35



## ILLUSTRATIONS (cont.)

Figure		Page
14.	Empirical relation of tensile strength of winter sea ice to relative brine volume -----	38
15.	Empirical relation of tensile strength of perennial ice to relative brine volume -----	39
16.	Measured tensile strength of sea ice versus relative volume of brine -----	40
17.	Two models for the transformation of brine pockets with changing temperatures -----	42
18.	Expected length of brine pockets as a function of the relative brine volume -----	44
19.	Reinforcement of brine pockets by salt-ice mixtures -----	44
20.	Increase of strength due to the precipitation of salts -----	46
21.	Hypothetical strength relations for perennial ice, compared with actual tests -----	47

## TABLES

Table		Page
I.	Dimensions of brine inclusions -----	6
II.	Absolute and relative concentration of the major ions in normal sea water -----	23
III.	Phase relations for standard sea ice (1957) -----	31
IV.	Condensed table of test results -----	36



## SUMMARY

Part of the salts contained in sea water are trapped in sea ice upon freezing. They form liquid and solid inclusions in a systematic pattern. The amount depends upon temperature and salinity. A detailed table of phase relations is given and a general theory is derived to show how the internal cavities may affect the strength of sea ice. The general theory leads to specific models. The principle of ring tensile strength tests is explained and a series for evaluation is given. Test data lead to a substantiation of theoretical principles and to an illustration of several hypotheses concerning the effect of solid salt inclusions upon strength. Observed sea ice phenomena are explained on the basis of internal structure.



# COMPOSITION OF SEA ICE AND ITS TENSILE STRENGTH

by  
A. Assur

## INTRODUCTION

In this paper the strength of sea ice is analyzed directly in terms of brine, rather than in terms of salinity and temperature, as has been done occasionally before.

The analysis was initially intended to be in the general form

$$\sigma' = c\sigma_f[1-f(v)] \quad (1)$$

where

$\sigma'$  — strength of sea ice

$c$  — coefficient

$\sigma_f$  — strength of fresh water ice, obtained by identical tests

$v$  — relative volume of brine, computed from temperature and salinity, considering the precipitated salts on the basis of phase relations.

The physical nature of  $f(v)$ , in the simplest case, is a relative reduction in area  $f(v) = \psi$  of the failure plane (the "plane porosity") due to brine inclusions, resulting in

$$\sigma' = c\sigma_f(1-\psi). \quad (1a)$$

In the more complicated case of precipitation of salts, the reinforcement by these salts must be considered. This reinforcement could explain the high strength of the sea ice at low temperatures.  $f(v)$  can be derived in empirical form from the data, but such an approach is not very satisfactory. On the other hand  $f(v) = \psi$  can be expressed by means of suitable models.

The laminar structure of sea-ice crystals (Fig. 4), with plates of fresh-water ice separated by layers with brine inclusions, has been known, in principle, since the turn of the century. This knowledge initially leads to an equation of the type (1a), but not much further.

The earliest attempt to study the relation of strength to internal cavities in sea ice was that of Tsurikov (1939). His equation 21\*

$$\sigma' = \sigma_0 \left( 1 - \sqrt{\frac{8}{\pi}} \sqrt{v} \right) \quad (2)$$

is based upon the assumption of circular uninterrupted cylindrical cavities.

$\sigma_0$  — strength of ice without pores

$v$  — porosity (internal voids)

It was obvious that further progress toward a rational approach to the properties of sea ice required a more detailed study of the geometry of the brine inclusions, leading to a formulation of  $\psi = f(v)$ . Dr. W. Weeks undertook the tedious task of preparing and analyzing numerous photomicrographs of the structure of sea-ice crystals with their brine inclusions and Anderson (1957) provided valuable information about the dimensions, spacing, and arrangement of brine inclusions.

They also proposed two models for  $f(v)$

$$\psi = \lambda = \sqrt{\frac{8v}{\pi}} \quad (3a)$$

$$\psi = \lambda = \frac{0.2116v + 0.0011}{0.0322} \quad (3b)$$

with

$2r_b$  — length of brine pockets,

$b_0$  — spacing of brine pockets, uninterrupted cylinders are assumed.

$\lambda$  — here defined as "line porosity" was substituted for the "plane porosity"  $\psi$ .

\*All cited equations are expressed in the symbols used in this report.



In the computation of  $\nu$ , Anderson (1957) follows the concept of Malmgren (1927) and Zubov (1945), neglecting the precipitated salts.

Eq 3a is based upon the assumption of circular cylinders and appears to be similar to Tsurikov's model (eq 2) in form, but is based upon a more advanced concept about the internal structure of sea ice. Model 3b, designated by Anderson as "elliptical", assumes changes of the brine pockets primarily within a plane. The constants are derived from measured dimensions.

The flexural strength of sea ice, measured in situ by cantilever tests, is far less than the tensile strength of fresh-water ice, as measured for example in laboratory tests by Butkovich (1954). Anderson (1957) attempted to explain this difference by

$$\sigma' = \frac{\sigma_b}{k} (1 - \lambda) \quad (4)$$

$\sigma_b$  - strength of fresh-water ice, using the bulk strength as measured by Butkovich (1954) in direct tension tests,

$k$  - stress concentration factor for brine inclusions in sea ice.

This equation offers a new concept in the treatment of sea-ice strength properties. It is identical to the approach used by engineers in computing the strength of perforated plates. For small circular isolated holes  $k \cong 3$ . This does not hold, however, for elliptical holes.

Eq 4 explains the difference in the strength of fresh- and salt-water ice primarily by stress concentrations. This key point is not necessarily supported by experimental evidence, as is shown below.

Eq 4 modified to

$$\sigma' = \frac{\sigma_s}{k} (1 - \psi) \quad (5)$$

where  $\sigma_s$  is the strength of small volumes of fresh-water ice, fits the experimental results better, but neither eq 3 alone or eq 4 with its concept of stress concentration is sufficient for a comprehensive approach to the problem.

In this report both eq 4 and 5 are discarded in favor of the concept

$$\sigma = \sigma_0 (1 - \psi) \quad (6)$$

where  $\sigma_0$ , the "basic strength" of sea ice, is the strength of an imaginary sample if all the brine pockets are filled with ice but stress concentrators remain (computed directly from sea-ice data by means of least squares),

$$\sigma = \sigma' \frac{\sigma_{10}}{\sigma_\theta} \quad (6a)$$

is the strength of sea ice, slightly modified by a factor reducing the strength of its fresh-water ice components to  $-10^\circ\text{C}$ . This is necessary so that the effect of temperature upon the strength of the fresh-water ice bridges in a sea-ice crystal need not be considered.

Eq 6 has the advantage that it does not rely upon stress concentration but can be used for any statistical combination of failure in tension with stress concentration or shear without stress concentration, which is actually the case at failure.

We will see that  $\sigma_0$  is not three times less than the corresponding value for fresh-water ice but comparable to it. Nevertheless some difference exists, which will be studied when all corresponding tests for  $\sigma_f$  are evaluated.

The physical meaning of  $c$  in eq 1 could be the ratio of stress concentration of fresh-water ice to the stress concentration in sea ice. (Recent information, March 1958, indicates that  $c < 1$ .)

In comparing the strength of sea ice and fresh-water ice, one must consider that ice in the presence of its liquid phase is weaker than ice tested in the air. The



interstitial liquid in sea ice weakens the minute ice bridges and  $c < 1$  can be explained by this phenomenon. It is not necessary to resort to the argument of a higher stress concentration in sea ice.

The next step is to present a general theory for  $\psi = f(v)$ , as a three-dimensional model, guided by some principles which can be used for a number of possible geometrical models, including eq 3a and 3b (two-dimensional concept), as well as for a more stochastic arrangement and shape of brine inclusions. In the latter case, actual statistical averages of certain dimensions must be compared with three "petrographic constants", arriving at three main groups of relations  $\psi = f(v)$ .

The third step is a new computation of the brine volume, considering the precipitation of salts and numerically deriving the phase relations in sea ice. This is a radical departure from the concept of Malmgren and Zubov, used by Anderson and Weeks (1958).

For the evaluation of strength data, a convenient series for the evaluation of the stress distribution in ring samples is given, and a condensed table of test results is presented (Table IV). An empirical derivation of  $f(v)$  is shown, illustrating the validity of the principal theoretical concepts and the necessity for a separate study of the effects of salts.

The possible effect of salts on strength is explained by models as the result of reinforcement of brine pockets by a salt-ice layer deposited on the walls.

(Note: The test results and their interpretation here are purely basic information for the properties of sea ice. They cannot be directly applied for trafficability purposes, by using the values for the required constants in plate equations.)

#### LIST OF SYMBOLS

- B-axis — Direction of brine pockets in the B-c plane (Fig. 5).
- Cl — Chlorinity, as measured by standard techniques. The actual concentration of chloride ions in normal sea water is  $Cl^- = 0.998942$  Cl.
- D — Diameter of sea-ice crystals, perpendicular to direction of growth G.
- $E_i$  — Young's modulus for ice.
- $E_s$  — Young's modulus for salt-ice mixture.
- F — Average area of brine pockets in the B-c plane, perpendicular to direction of growth G.
- $F_g$  — Average area of brine inclusions in the B-G plane, parallel to G.
- G-axis — Direction of growth of sea ice crystals (normally vertical) (Fig. 4).
- I — Ionic concentration in sea water (Table II).
- S — Salinity, weight of dissolved salts in sea water, brine or water, melted from sea ice, absolute or in ‰.
- $S_b$  — Salinity of brine.
- $S_s$  — Relative amount of solid salts in natural sea ice.
- V — Average volume of a brine inclusion.
- $Z = \frac{S}{1-S}$  — Salt content of brine: weight of dissolved salts divided by the weight of pure  $H_2O$ .
- $a_0$  — Spacing of parallel elementary ice plates or of layers with brine inclusions.
- b — Width of ice bridge along B-axis.
- $b_0$  — Spacing of brine pockets (center to center) in the B-direction, perpendicular to growth.



- br — Brine content by weight.
- c-axis — Principal crystallographic axis (Fig. 4).
- g — Length of brine cylinders in the G-direction.
- $g_0$  — Spacing of brine cylinders.
- k — Stress concentration factor (eq 4).
- $p_1, p_2, p_3$  — Petrographic constants (eq 23 a-c).
- r — Radius of brine pocket or of spherical brine inclusion.
- $2r_a$  — Width of brine pockets in the c-direction.
- $2r_b$  — Length of brine pockets in the B-direction.
- $r_1$  — Initial radius of brine pockets when a salt (NaCl) starts to precipitate.
- $\alpha_0 = \frac{a_0}{\sqrt{F}}$
- $\beta_0 = \frac{b_0}{a_0}$  — Relative spacing of brine pockets.
- $\gamma = \frac{F}{b_0 g_0} \cong 1 - \lambda_g = \frac{g}{g_0}$  — Relative length of brine cylinders in the G-direction.  
Also — actual density of sea ice.
- $\gamma_b$  — Density of brine.
- $\gamma_i$  — "Theoretical" density of sea ice, without air bubbles; can be computed from the composition of sea ice.
- $\epsilon = r_b/r_a$  — Elliptic ratio of brine pockets.
- $\theta$  — Ice temperature.  
Also — temperature of brine under phase equilibrium.
- $\lambda$  — "Line porosity" in the B-direction due to brine pockets.
- $\lambda_g$  — "Line porosity" in the G-direction due to brine pockets.
- $\nu = \nu(1) S$  — "Volume porosity". Relative volume of brine in sea ice, absolute or in  $\eta_0$ .
- $\nu_o = \frac{2d_o}{a_o}$  — "Anderson constant", for Condition  $A_0$  (Fig. 16).
- $\nu(1)$  — Relative volume of brine for  $S = 1\eta_0$ . For table see Appendix I.
- $\nu_s$  — Relative volume of brine when salts start to precipitate.
- $\sigma = \sigma' \frac{\sigma_{10}}{\sigma_\theta}$  (eq 6a).
- $\sigma'$  — Strength of sea ice.
- $\sigma_0$  — "Basic strength" of sea ice, computed by means of least squares on the basis of eq 6. Also a strength value in eq 2.
- $\sigma_1$  — "Basic strength" of sea ice, reinforced by  $\text{Na}_2\text{SO}_4$ .
- $\sigma_{10}$  — Strength of fresh-water ice, reduced to  $-10^\circ\text{C}$ . (eq 63).
- $\sigma_b$  — Bulk strength of fresh-water ice.
- $\sigma_f$  — Strength of fresh-water ice.



- $\sigma_s$  — Strength of small volumes of fresh-water ice (for example the bridges between the elementary plates within a sea ice crystal).
- $\sigma_t$  — Actual tensile stress (eq 66).
- $\sigma_\theta$  — Strength of fresh-water ice at the temperature  $\theta$ .
- $\psi$  — "Plane porosity"; relative reduction in area of the failure plane, due to brine inclusions.

Symbols used in computation of phase relations (eq 54-59):

- $a_1, a_2$  — Gravimetric "concentration" of the "first" ion in the salt.
- $x_1, x_2$  — Amount of salts to be computed.
- $\Delta I_0$  — Available amount of "reference ion".
- $\Delta I_1, \Delta I_2$  — Available amount of "first" ion.
- $\alpha_1, \alpha_2$  — Gravimetric "concentration" of the reference ion in the first or second salt.
- $\beta_1, \beta_2$  — Ratio of the concentration of the reference ion to the first or second ion in a given salt.
- $\beta_1 = \alpha_1/a_1.$
- $\beta_2 = \alpha_2/a_2.$
- $\rho_1, \rho_2$  — Observed ratio of the first or second ion to the reference ion.
- $\bar{\rho}_1 = \Delta I_1/\Delta I_0.$
- $\bar{\rho}_2 = \Delta I_2/\Delta I_0.$

Symbols used in evaluation of ring-test results:

- $A_n, D_n$   
 $P_n, S_n$  — Functions for evaluation of ring stresses (eq 62).
- $K$  — Concentration factor for evaluation of ring stresses (eq 61).
- $P$  — Load on ring (eq 61).
- $l$  — Length of cylinders in ring test (eq 61).
- $r$  — Distance from center in ring (eq 62).
- $r_0$  = Radius of ring.
- $r_i$  = Radius of hole in ring.
- $\rho = r_0/r.$
- $\bar{\rho} = r_0/r_i.$



Table I. Dimensions of brine inclusions adopted from Anderson and Weeks (1958).

$a_0 = 0.46$  mm, based upon 50 measurements. Weeks (1958) reports  $a_0 = 0.45$  mm with a variation between 0.2 and 0.8 mm. For Arctic pack ice, Assur recently found values more than twice as large.

$\beta_0 = \frac{1}{2}$ , varying over a large range. Anderson (1957) assumes values between  $\frac{1}{2}$  and 1. Weeks (personal communication, April 1958) measured most values below  $\frac{1}{2}$ .

$\beta_0 = 1$ , initial relative spacing in the second Anderson model.

$d_0 = 0.07$  mm, minimum width of parallel brine layer before splitting. Also width of brine pockets in second Anderson model.

$\nu_0 = \frac{d_0}{a_0} = 0.152$ , the "Anderson constant".

### OBSERVED STRENGTH VARIATIONS OF SEA ICE

"Sea ice is three times weaker than fresh water ice" is a statement repeated in many publications, although actual tests by SIPRE personnel and others do not agree with it. Sea ice can be weaker, much weaker, than fresh-water ice (tensile strength values below  $1 \text{ kg/cm}^2$  have been measured while the value for fresh-water ice is around  $20 \text{ kg/cm}^2$ ). But sea-ice strength can easily equal or even appreciably exceed the strength of fresh-water ice. It is this astonishing variation in the strength of sea ice which appeared worth study.

The source of the "one-third" rule of thumb was found to be a vague statement made by Moskatov (1938) 20 years ago without experimental evidence. It is rather amazing how this statement has dominated a certain line of our literature on the strength of ice, especially as other Russian test data do not support Moskatov's statement. The first serious arguments in favor of the "one-third" rule are given in a recent paper by Anderson (1957) who presents graphs relating strength to temperature down to  $-20^\circ\text{C}$ . This theory (eq 4) states in effect that the maximum possible strength of sea ice is one-third of the strength of fresh-water ice; the normal strength is always below. Data indicating that this might not hold were mentioned but not explained. Despite this deficiency, Anderson's paper should be considered as one of the best contributions to the mechanics of sea ice.

The actual tensile strength of sea ice, as measured by SIPRE (Fig. 1), ranges from practically zero in a state of deterioration to  $30 \text{ kg/cm}^2$ , as measured by ring tests. Assuming  $20 \text{ kg/cm}^2$  as the tensile strength of fresh-water ice would give about  $7 \text{ kg/cm}^2$  by the "one-third" rule. According to eq 4, it would never exceed this value, at least above  $-20^\circ\text{C}$ . This is not observed.

### OBSERVED PHENOMENA

The great increase in friction of sleds traveling over bare sea ice under cold weather conditions is well known to polar travelers. If the ice surface temperature drops below  $-23^\circ\text{C}$  (with an air temperature below some  $-30^\circ\text{C}$ ), travel by sleds becomes more difficult, a fact well known to Eskimos. At the same time the sea ice itself changes to a distinct whitish color. The explanation is the precipitation of NaCl, included in the brine pockets. If appearance and frictional characteristics change so suddenly, an effect on strength should also be suspected.

When drilling or chiseling a hole in such ice, even tools of the best high-strength steel become dull after a short time. In addition to becoming harder, the sea ice becomes appreciably more brittle.

Digging a pit under these conditions (below  $-30^\circ\text{C}$ ) will reveal a distinct top layer, grayish-white with a very definite texture and then a sudden transition to grayish-blue or greenish-gray ice underneath, depending upon illumination. A thermometer placed in the transition layer will show a temperature of about  $-23^\circ\text{C}$ .



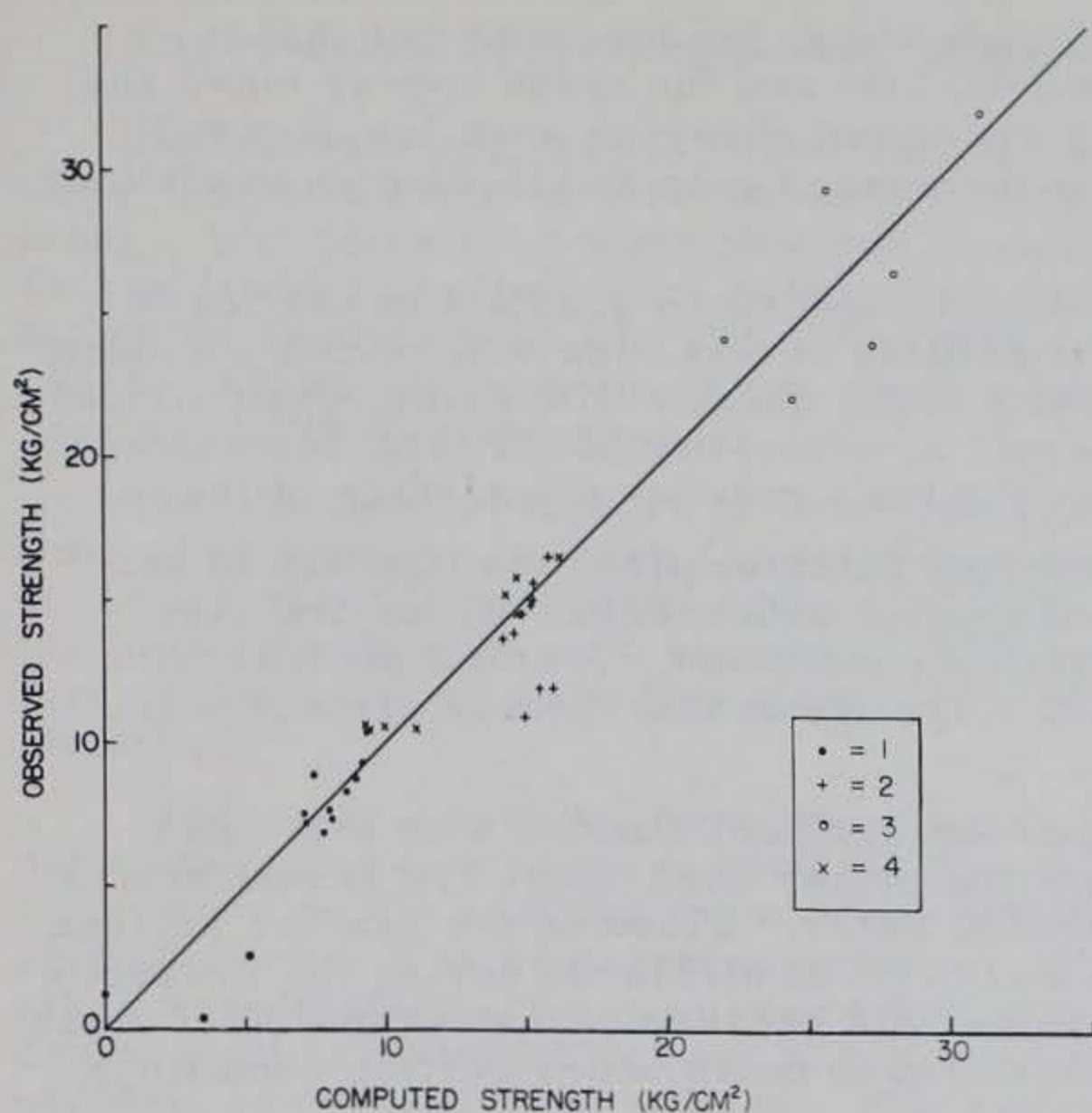


Figure 1. Observed vs computed strength of sea ice. 1. Winter ice, brine only, no precipitated salts.  $\theta \geq -8.2^\circ\text{C}$ . 2. Winter ice, precipitated  $\text{Na}_2\text{SO}_4 \cdot 10 \text{H}_2\text{O}$ .  $-8.2 > \theta \geq -22.9^\circ\text{C}$ . Three points failed to show the general relative strength increase of  $\frac{1}{3}$ . An increased ratio of  $\text{SO}_4^{--}/\text{Cl}^-$  is probably required for an increase in strength. 3. Winter ice, precipitated  $\text{NaCl} \cdot 2\text{H}_2\text{O}$ .  $\theta < -22.9^\circ\text{C}$ . 4. Perennial sea ice (Antarctica), probably with remaining solid  $\text{Na}_2\text{SO}_4 \cdot 10 \text{H}_2\text{O}$ .  $-1.3 \geq \theta > -9^\circ\text{C}$ . Points shown are averages of about 9 tests each. Observed values were obtained by ring tests (see "Testing procedures"). The computations were based on essentially three constants, determined from experiments with the help of suitable models, as explained later in this report.

With an ice surface temperature of about  $-15^\circ\text{C}$ , the top greenish-gray layer will show a fairly abrupt transition to a dark, almost black and wet layer underneath.\* The transition zone will have a temperature of  $-8$  to  $-10^\circ\text{C}$ . Samples from the different layers show a sharp distinction in strength. The lower layer is significantly weaker even if the samples are exposed to the same environmental temperature for some 12 hours or so.

All these very distinct layers of sea ice still have an appreciable strength. Figure 2 illustrates the temperature and salinity conditions under which sea ice has "normal strength" and the regions where its appearance changes so abruptly.

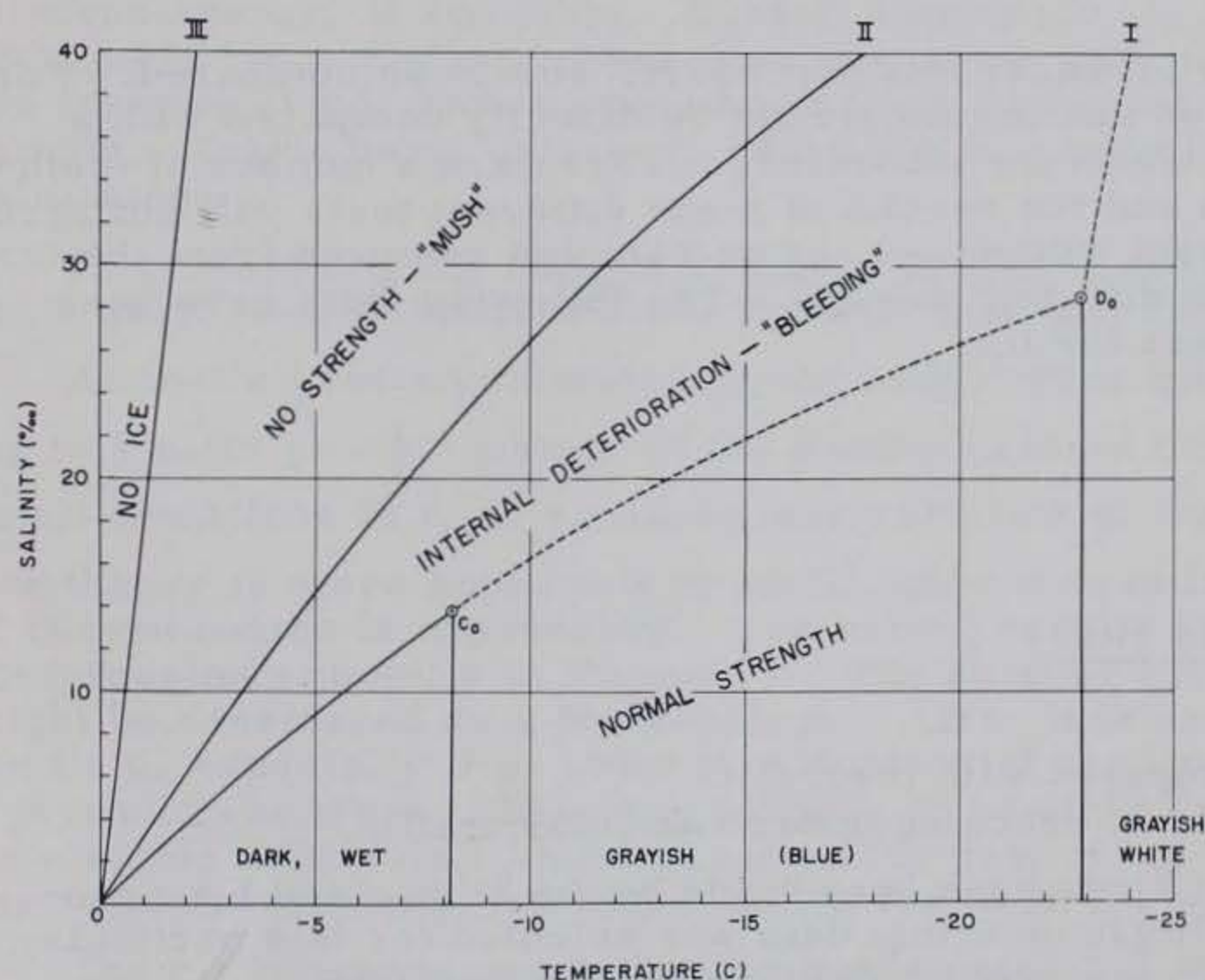


Figure 2. Strength conditions of sea ice, depending on temperature and salinity. Below I — "Normal strength", a wide range of strength conditions corresponding to values above line  $n$  in Fig. 3.  $C_0$  to  $D_0$  — precipitation of  $\text{Na}_2\text{SO}_4 \cdot 10 \text{H}_2\text{O}$ ; above  $D_0$  — precipitation of  $\text{NaCl} \cdot 2\text{H}_2\text{O}$ . I —  $\sqrt{v} = 0.3$ ;  $B_2$  on Fig. 14. I to II — Rapid deterioration and internal breakdown of sea ice, accompanied by distinct "bleeding" in pit or hole. II —  $\sqrt{v} = 0.3899$ ;  $A_0$  on Fig. 14. II to III — Ice "mush", usually consisting of incoherent plates without internal bridging. III — Freezing point  $\theta = -\frac{54.11S}{1-S}$ . Salinity scale is extended to  $40\text{‰}$ , far above the normal  $5\text{‰}$  salinity of sea ice, to show expected strength conditions for artificial salt-water ice produced by flooding.

\*The distinction by color holds for ice with even a low salt content, but not for fresh-water ice ( $S = 0\text{‰}$ ) (Fig. 2).



A deeper hole in sea ice will come to a layer where the ice is so wet that it "bleeds". Brine collects rapidly in a pit or drill hole and the chips appear more and more like slush. Although not evident to the untrained observer, such ice may still have an appreciable strength at that level but the phenomenon of bleeding is so distinct that it must be better defined.

With warmer weather in spring, the normal temperature gradient in sea ice is reduced and gradually reversed. Systematic drilling at this time will reveal a sudden transition to a condition where every hole and pit fills quickly with brine, even almost at the surface. This is the beginning of internal deterioration of the total ice sheet, characterized by the time when condition I in Figure 2 reaches the surface of the ice.

Possibly at a more advanced stage of internal deterioration, the cavities in sea ice are in actual hydraulic contact with the sea water underneath. Brine drainage holes as thick as a pencil or a finger support this conclusion. A small pit fills with high salinity water up to the hydrostatic level. The ice at that time is already weak although still intact.

Another well known phenomenon is that an ice surface, flooded with sea water, for example near the shore due to tides, remains mushy even under low temperatures. This is due to the high salinity of the overflowing water. Flooding the sea-ice surface in order to get rid of surface irregularities was tried at McMurdo during the Antarctic winter and was unsuccessful even under extreme cold because of the formation of mush. Even sea ice of low salinity can and does transform to mush under certain conditions (Fig. 2).

"Mush", which is also observed on top of young sea ice as "scum", still can be considered as a sort of ice, but finally there comes the condition when no ice is present and everything is transformed into brine (line III, Fig. 2).

It is also observed, and stressed, in the literature that perennial ice is stronger than one-season ice (winter ice).

A theory which explains not only some but all of these distinct phenomena, has not been available. This report attempts to present such a theory.

## TESTING PROCEDURES

### Tensile strength tests

Only strength data obtained by identical test procedures should be compared. For example, a cantilever test in situ on sea ice should not be directly compared with a direct tension test on fresh-water ice in the laboratory. There are a number of methods for measuring tensile strength and the results of these different tests will not agree. Tests can be made in situ, in contact with water, or on samples removed from the ice sheet and tested in the air, all with different results. The following tests have been used to obtain tensile strength values for ice:

- Direct tensile tests
- Flexural test on small beams
- Ring tensile tests
- Cylinder tensile tests
- Cantilever beam tests in situ
- Simply supported beam tests in situ
- Semi-infinite beam tests
- Tests on wedges
- Plate tests (first cracking compared with theory)
- Experiments with the frequency of cracking under vehicular traffic.

Thousands of tests of different kinds have been made by the author and his associates at SIPRE, but only one small group of test data was selected for this particular discussion, keeping in mind the requirement of identical test procedures.

The data used were obtained by ring tensile strength tests. This is a highly efficient test method, originally suggested for high-density snow by Mr. R. C. Philippe (OCE) and first applied for snow and ice by Butkovich (1956a, b).



The principle of the ring tensile strength test is shown in the inset of Figure 13.

The present analysis is based upon a total of 327 tests. Fifty-eight test results were computed from Mr. T. R. Butkovich's field data, obtained at Thule (NW Greenland). The remainder were obtained from field tests (145) performed by the author as a byproduct of other work at Hopedale (Labrador), Thule (Greenland), and McMurdo (Antarctica) or (124 tests) taken from SIPRE Research Report 20 (Butkovich, 1956). All samples, 3-in. diam, were taken from vertical cores obtained with the special SIPRE coring auger.

The standard procedure is to measure the ice surface temperature and note the time when the core is taken (to determine the duration of storage). The thickness of the ice sheet is measured and a sketch of the removed core pieces is made so that the initial position of each sample in the ice sheet can be identified later. The structure of the ice is noted at this time if necessary. In particular, snow-ice must be identified.

Frequently a parallel core was taken for salinity samples or parts of the core not suitable for testing were used for this purpose, but most of the salinity tests were made on the samples themselves after crushing, in particular all tests reported by Butkovich. It is preferable, however, to make some salinity tests on samples taken immediately after the core is removed from the ice sheet, because of the drainage of brine which occurs at higher temperature and creates an important problem in the testing of sea ice. The author tested the samples as soon as practical if the air temperature was above  $-10^{\circ}\text{C}$ . Below that temperature, the samples were allowed to adjust to the environmental temperature. The brine content is very high above  $-10^{\circ}\text{C}$ , but quite low at lower temperatures (see Curve M, Fig. 11).

Assur and Frankenstein found during recent tests on the Arctic pack ice (May 1958) that even at fairly low environmental temperatures the loss in brine is quite appreciable. For example ice of an initial salinity of 6‰ lost 24.4‰ of its salinity during a 24 hr storage at ambient temperatures of  $-9.5$  to  $-11.0^{\circ}\text{C}$ .

More emphasis should be placed in the future on obtaining a salinity profile immediately after removal of the core from the ice sheet.

The cores are cut in a miter box into short (3-in. long) cylinders. A bandsaw is advantageous, if available. Density determination is made by weighing the sample accurately (to 0.1 g) and measuring the length with calipers. Several measurements are taken to avoid random variations. It is important to check the diameter of the sample. Triple beam balances, which are normally used, should be checked and calibrated.

After weighing the sample a hole is drilled in the center of the cylinder, parallel to its axis. Any deviations from the true axis will cause systematic errors.

Almost all tests performed by the author were made with a  $\frac{1}{2}$ -in. hole, corresponding to a ratio  $\frac{r_i}{r_0} = \frac{1}{6}$ , instead of the  $\frac{1}{3}$  ratio used by Butkovich. With a smaller hole, small deviations in  $r_i$  or  $r_0$  cause less variation of the concentration factor  $K$  (eq 61).

The theory is more applicable to small holes than to larger holes, where the condition of curved beams is approached. The ratio  $\frac{1}{3}$  results in a small bending effect with compression at point 4 in Figure 13. The smaller critical volume with the ratio  $\frac{1}{6}$  might be considered as a disadvantage. Also, it is easier to prepare  $\frac{1}{2}$ -in. holes in the field, especially if an older type horizontal handcoring box must be used, as for a part of these tests. It is very difficult to use this arrangement at low temperatures. An electric drill with a stand was used for part of the tests and is recommended. (A very satisfactory hand-operated device for field use was also recently developed.)

The air temperature during testing is noted. It will not differ much from that of the ice sample at high temperatures. Large differences may exist if the sample is tested immediately after being brought from the ice sheet. Air temperature alone should never be used, as was done, for example, by Petrov (1955) for flexural tests on a Russian pack ice station, even when air temperatures were above freezing. Even



if the sample is well adjusted to the air temperature, sudden changes, caused, for instance, by opening the door of the shelter where tests are being made, will affect a thermometer placed in the air, but will not be reflected in the true temperature of the sample.

Therefore, the ice temperature of the sample was determined immediately after testing. In most cases, a Weston dial thermometer was used within the sample crushed to small pieces. This thermometer is sufficiently rugged for use in the field, but unfortunately is not very dependable. Repeated calibrations in an ice-water bath are necessary. At temperatures above about  $-5^{\circ}\text{C}$ , an accurate mercury-in-glass thermometer which can be read easily to  $1/10^{\circ}\text{C}$  is recommended.

The loading is accomplished by a press with a proving ring, with deformation measured with scale divisions of  $0.0001$  inch. The stem of the dial gage for measuring the deformation of the proving ring should have a brake for stopping at the maximum load. (This brake does not always work satisfactorily so that the dial must be watched.) Under cold conditions the gage sticks slightly, so that the stem of the gage must be carefully brought down in contact with the proving ring after each test.

#### Salinity tests

Samples taken for salinity tests either immediately after removal from the ice sheet or after testing are sealed in plastic containers ( $1\frac{1}{2}$ -pint square refrigerator containers are quite adequate) to minimize evaporation. The samples are later melted at room temperature. Melting can be accelerated by heating, being careful not to overheat the melt water; it is better to allow the last piece of ice to melt at room temperature. The melt-water temperature is kept close to  $15^{\circ}\text{C}$ , for which the hydrometer is calibrated. In practice temperatures from  $10$  to  $20^{\circ}\text{C}$  were allowed, applying proper corrections.

The hydrometer used (manufactured by the GM Company, New York) gives salinity in gradations of  $0.2\text{‰}$ ;  $0.1\text{‰}$  can be interpolated. The hydrometer should be read at the exact water level, looking slightly from below, not from above, because of the meniscus forming at the stem. The table supplied by the manufacturer for temperature correction of  $S$  was found to be very inconvenient due to the necessity of double interpolation. A special nomogram for easy interpolation was constructed for this purpose.

A hydrometer is not as accurate as titration for determining salinity, but it is much easier to use in the field than any other method. Titration is too complicated under the rough field conditions of polar regions. Also the  $S/\text{Cl}$  ratio in melt water from sea ice is not necessarily the same as in ocean water, for which Knudsen's formula applies.

The accuracy possible by titration ( $0.02\text{‰}$ ) is not needed. Natural variations in salt content cause a standard deviation of salinity of  $0.64\text{‰}$  for samples taken within 2 inches of each other.\* An accuracy of  $0.1\text{‰}$  is entirely adequate.

All salinity determinations made within a day or two, including those from other tests at the same location, were plotted in a profile, giving more weight to samples obtained immediately after removal from the ice sheet. This profile was used to define the salinity of each sample subjected to a mechanical test. This method, used on data obtained by the author, seems to be more adequate than the direct use of salinities obtained from individual samples with their appreciable scatter and systematic errors.

It is rather surprising to see that ice salinities in connection with determinations of sea-ice strength are extremely scarce in the Russian literature, despite the fact that Russian investigators have been studying sea ice for almost 60 years (Makarov, 1901). Petrov (1955) made more systematic determination of salinities, although not in adequate numbers. Since American investigations on the mechanics of sea ice began (unfortunately only since 1955), numerous salinity determinations have been a must during each field program. The testing procedure and technique are still being improved.

\*Analysis based upon field data furnished by Mr. O. Lee (then with USN Hydrographic Office).



## THEORETICAL ANALYSIS

Some comments on stress concentration

The main difference between fresh-water and salt-water ice is the presence of brine inclusions in the latter, forming systematically arranged holes. For mechanical properties, this system of holes can be analyzed as a perforated plate (eq 4) (Anderson, 1957). For such a plate under tension, the stresses could be computed on the basis of the reduced cross section. Theory and experiments have shown that these stresses are actually substantially exceeded in perforated plates. The so-called "stress concentration factor", which is the ratio between the actual maximum stresses produced and the stresses computed on the basis of the reduced cross section, depends on the ratio of diameter to spacing of the holes and on the shape of the holes. For small, circular, isolated holes, the stress concentration factor is 3.

If the phenomenon of stress concentration is considered the main difference between sea ice and fresh-water ice, as was proposed in connection with eq 4, it is reasonable to assume that the strength of sea ice can never exceed  $\frac{1}{3}$  of the strength of fresh-water ice. But this conclusion is erroneous because it assumes that fresh-water ice lacks this concentration of stresses.

Every sample of natural fresh-water ice is also subject to stress concentration due to the inclusion of minute cavities and air bubbles. SIPRE tests on the bulk strength of ice have shown that these stress concentrators are normally present in fresh-water ice.

Very small samples of fresh-water ice do have a considerably higher strength. The problem of small volumes does not arise in engineering computations of perforated plates, the concept on which eq 4 was based. To account for this effect, eq 4 can be modified to

$$\sigma' = \frac{\sigma_s}{k} (1 - \psi) \quad (5)$$

with  $\sigma_s$  - the strength of small volumes of fresh-water ice (bridges between the elementary plates), which is much higher than the bulk strength of fresh-water ice.

A further refinement can be introduced by keeping in mind that the actual shape of the brine pockets in the B-c plane (Fig. 5) is nearly elliptical with the long axis  $r_b$  in the B-direction. For an isolated elliptical hole, the stress concentration is (Timoshenko, 1941, p. 318)

$$k = 1 + 2 \frac{r_b}{r_a} = 1 + 2\epsilon \quad (5a)$$

$\epsilon$  - elliptic ratio. This leads to

$$\sigma' = \frac{\sigma_s}{1 + 2\epsilon} (1 - \psi). \quad (5b)$$

Assuming  $\epsilon = 1.5$ , for example, the stress concentration is 4, not 3.

The "basic strength" of sea ice is found to be  $14.2 \text{ kg/cm}^2$  (at  $-10^\circ\text{C}$ ). Assuming a stress concentration of about 4 (eq 5a), a strength of  $57 \text{ kg/cm}^2$  should be observed for fresh-water ice with no stress concentrators. Such ice can be produced under laboratory conditions if only small volumes are tested. Jellinek (1957) obtained tensile strength values from 15 up to  $70 \text{ kg/cm}^2$ , depending upon the dimensions of the specimen and particularly upon their volume. Considering the small volumes under critical stress between the brine inclusions in sea ice, the  $57 \text{ kg/cm}^2$  computed above as the actual strength of the pure ice without stress concentrators appears to be reasonable. Thus, modification (5) would make eq 4 correct, but the term  $\sigma_s/k$  does not explain the fundamental differences in the strength of fresh- and salt-water ice. In addition, not enough is known about  $\sigma_s$  and its dependence upon volume and dimensions of stressed small pieces of ice (bridges between elementary plates).



Figure 3 gives the strength of sea ice in terms of a computed "basic strength", equivalent to the tensile strength of an imaginary sample if all the brine pockets are filled with ice, but stress concentrators still remain. The reference value of 1.0 in Figure 3, on both left and right vertical scales, is roughly comparable to the strength of fresh-water ice as it occurs on rivers and lakes. (In glaciers the strength is much higher (Butkovich, 1958)). For the derivation of the relation in Figure 3 see corresponding sections below.

#### Precipitation of salts

The highest-strength sea ice of grayish-white color is characterized by rapidly increasing strength below  $-22.9^{\circ}\text{C}$  (Fig. 3), when large quantities of  $\text{NaCl} \cdot 2\text{H}_2\text{O}$  precipitate. Sea-ice strength can exceed the strength of fresh-water ice, especially at temperature below  $23^{\circ}\text{C}$ . The increase may be greater for young sea ice of high salinity than for perennial ice of low salinity. This is reasonable if the solid salt content determines the increase in strength. That portion of the graph, however, is primarily based upon a hypothetical model.

In the region from  $-8.2$  to  $-22.9^{\circ}\text{C}$  the presence of precipitated  $\text{Na}_2\text{SO}_4 \cdot 10\text{H}_2\text{O}$ , even in fairly small amounts, usually increases the strength by about one-third (Fig. 3, right scale) and there is very little change with temperature. In this region the strength of sea ice is quite comparable to the strength of fresh-water ice. Russian investigators (see Zubov, 1945) report flexural strength values in this region close to the strength of fresh-water ice. In addition, they report that they were unable to obtain a relationship with temperature, which is quite understandable from theoretical conclusions presented here.

Note the rapid decrease in strength of high salinity ice ( $S = 20\%$ ) if the temperature rises above  $-13^{\circ}\text{C}$ . It is often difficult to maintain a low temperature in flooded areas, especially if an ice crust is already formed and even a thin snow cover exists.

In perennial ice, we suspect, a great part of the enriched  $\text{Na}_2\text{SO}_4 \cdot 10\text{H}_2\text{O}$  does not return into solution above  $-8.2^{\circ}\text{C}$ . This explains the fact that the strength of perennial ice is about  $\frac{1}{3}$  greater than the strength of comparative one-season ice, even if the effect of lower salinity is considered. The short dashed line "m" indicates that perennial ice retains its strength even above  $-1.3^{\circ}\text{C}$  until all  $\text{Na}_2\text{SO}_4 \cdot 10\text{H}_2\text{O}$  goes into solution (hysteresis effect). Then the strength suddenly breaks down, an effect which was well demonstrated on an ice runway in the Antarctic summer of 1957.

Note that the breakdown of strength occurs more rapidly for low salinity perennial ice than for high salinity ice. In order to pick up strength variations along the breakdown line, temperature measurements have to be quite accurate, since fractions of a degree are important.

Normal one-season ice shows a strength which is characterized by the  $S = 5\%$  line at temperatures below  $-8.2^{\circ}\text{C}$ . Under moderate conditions, strength values in that range are to be expected.

### EFFECT OF BRINE INCLUSIONS ON THE STRENGTH OF SEA ICE

#### General theory

A normal sea-ice sheet consists of long vertical ice crystals, each usually several  $\text{cm}^2$  in cross section, but frequently much smaller. Numerous photographs taken under polarized light by Tabata and Ono (1957) illustrate this macrostructure very well; the microstructure was studied by Weeks (1958). The  $c$ -axis is perpendicular to the direction of growth, and the average cross-sectional "diameter"  $\underline{D}$  of the crystals increases linearly with depth  $\underline{h}$ , similar to fresh-water crystals with  $c$ -axis perpendicular to growth.

Dr. W. Weeks (personal communication) found on one sample of sea ice

$$\underline{h} = 29.16\underline{D} - 12.83 \text{ (cm).} \quad (7)$$



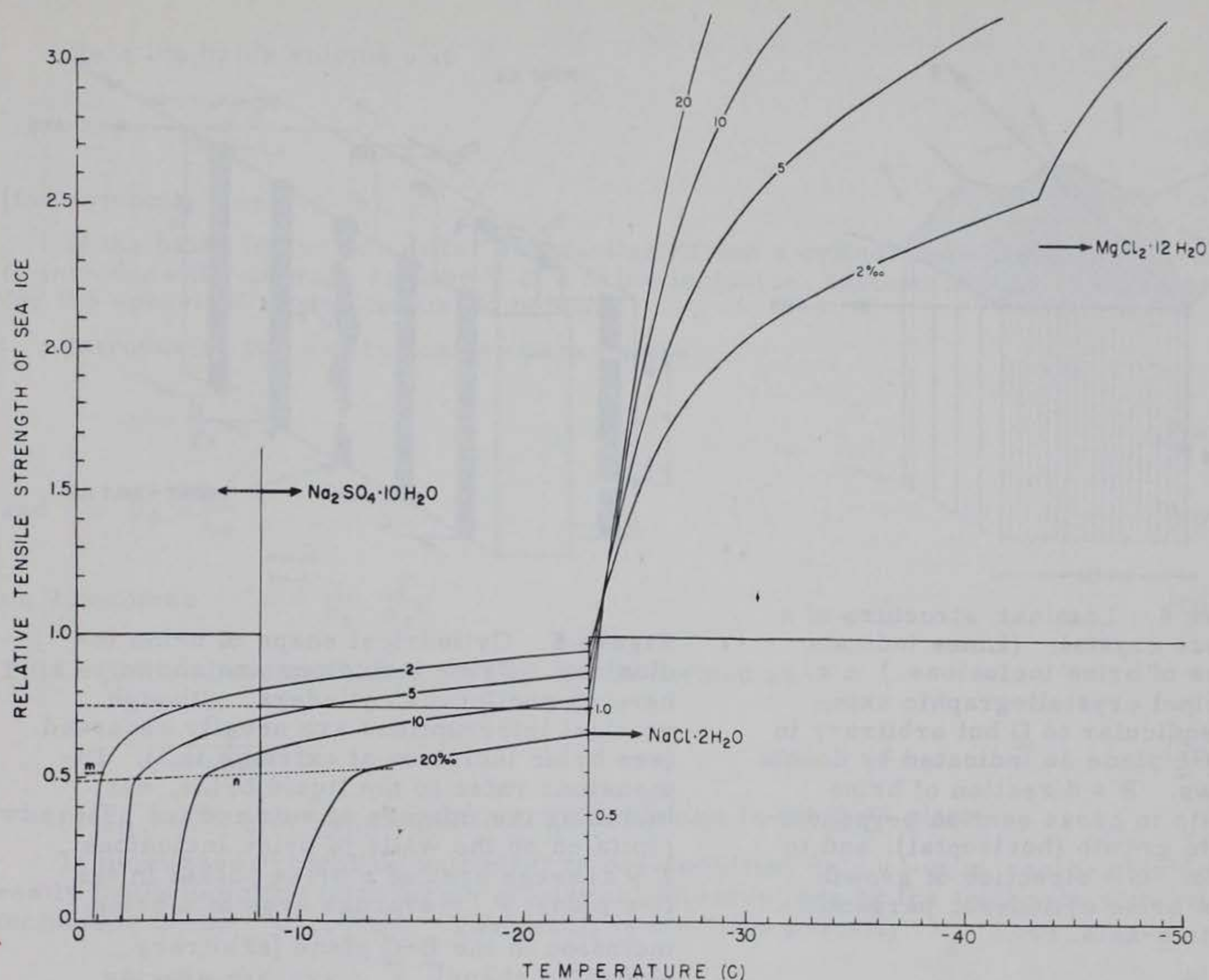


Figure 3. Relative tensile strength of sea ice as a function of temperature and salinity. The actual strength is divided by the "basic strength" of  $14.20 \text{ kg/cm}^2$ . For  $-8.2 < \theta \leq -22.9$  the presence of solid  $\text{Na}_2\text{SO}_4 \cdot 10\text{H}_2\text{O}$  increases the strength by  $\frac{1}{3}$ , as indicated by the right-hand scale. How rapid this transition is, is not known yet. The right-hand scale must be used also for perennial ice in the range  $-1.3 < \theta < -22.9^\circ\text{C}$ . The main salts responsible for variations in strength are indicated by arrows. The salinities correspond approximately to the following type of sea ice:  $S = 2\text{‰}$  — perennial sea ice;  $= 5\text{‰}$  — normal one-season sea ice in the middle of the winter;  $= 10\text{‰}$  — first formations of young sea ice;  $= 20\text{‰}$  — initial salinity to be expected in salt ice produced by flooding. n — line shows beginning of interior deterioration and bleeding. m = Value (right scale) to be expected for perennial ice shortly before transformation to slush.

This can be represented approximately by

$$D = \frac{h}{30} + 0.4 \text{ (cm)}. \quad (7a)$$

The diameter increased by 1 cm for every 30 cm in depth.

The sea-ice crystal consists of parallel plates in the direction of growth, with the brine inclusions located between these plates. The distance between brine inclusions is fairly constant. Brine volume depends strongly upon temperature and is proportional to the salinity at a given temperature.

We introduce two additional axes (Fig. 4): the  $\underline{G}$ -axis in the direction of growth (normally vertical) and the  $\underline{B}$ -axis in the direction of brine inclusions and perpendicular to  $\underline{c}$  and  $\underline{G}$ . It is quite obvious that the direction of weakest tensile strength is parallel to the  $\underline{c}$ -axis. Although the  $\underline{c}$ -axis is oriented randomly in the horizontal



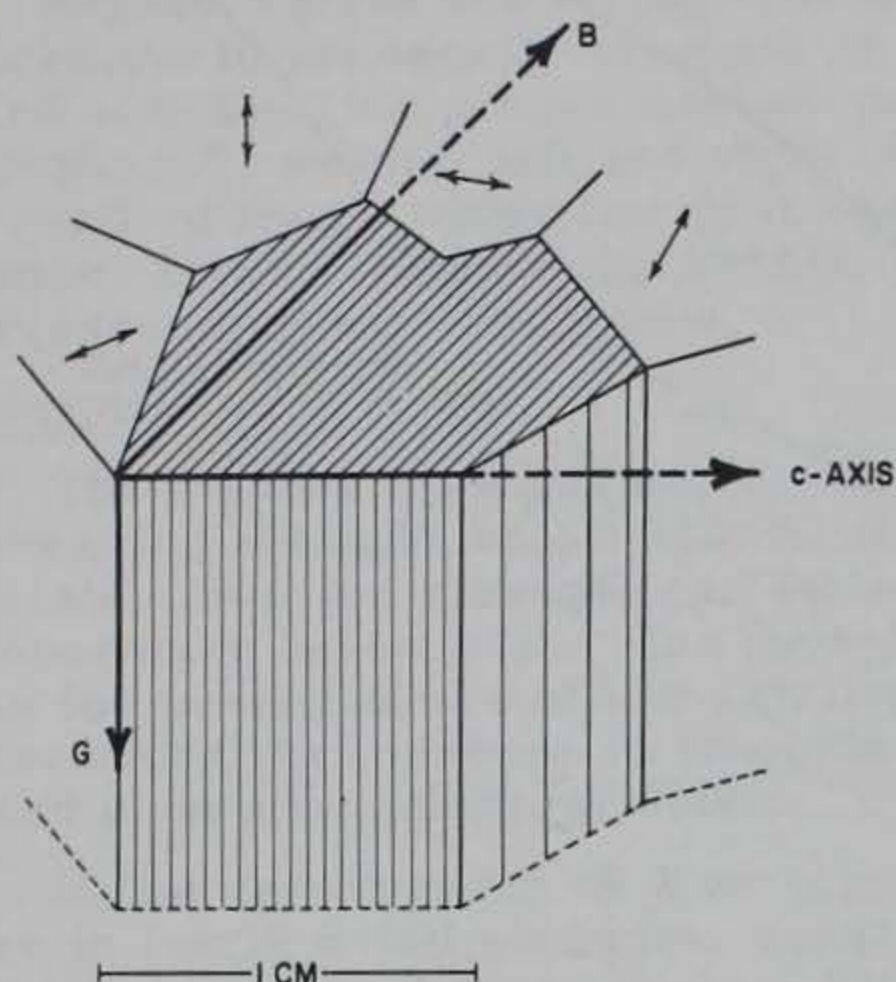


Figure 4. Laminar structure of a sea-ice crystal. (Lines indicate planes of brine inclusions.)  $c$  = principal crystallographic axis, perpendicular to  $G$  but arbitrary in the  $B$ - $c$  plane as indicated by double arrows.  $B$  = direction of brine pockets in cross section perpendicular to growth (horizontal), and to  $c$ -axis.  $G$  = direction of growth and of brine cylinders, perpendicular to  $c$ -axis.

(Tabata, 1957), there will always be a few crystals which have the critical  $c$ -orientation parallel to the tensile stresses. The critical shear stress is parallel to  $B$ . Failure of sea-ice samples is a statistical combination of tensile and shear failures on interlaminar planes. Rupture occurs in the  $B$ - $G$  plane due to geometrical reduction  $\psi$  of cross section  $1 - \psi$ .

Figure 5 shows the brine inclusions, drawn schematically as circular cylinders. In nature they do not necessarily have exactly this shape, but a general theory can be derived fairly simply even for arbitrary shapes. Photographs show the brine inclusions as elongated cylinders.

The elongated nature of brine inclusions was first shown by Wright and Priestley (1922), Tabata (1957, pl. LXV) shows it in a number of photographs and it appears most clearly in a photomicrograph by Weeks and Anderson (1958).

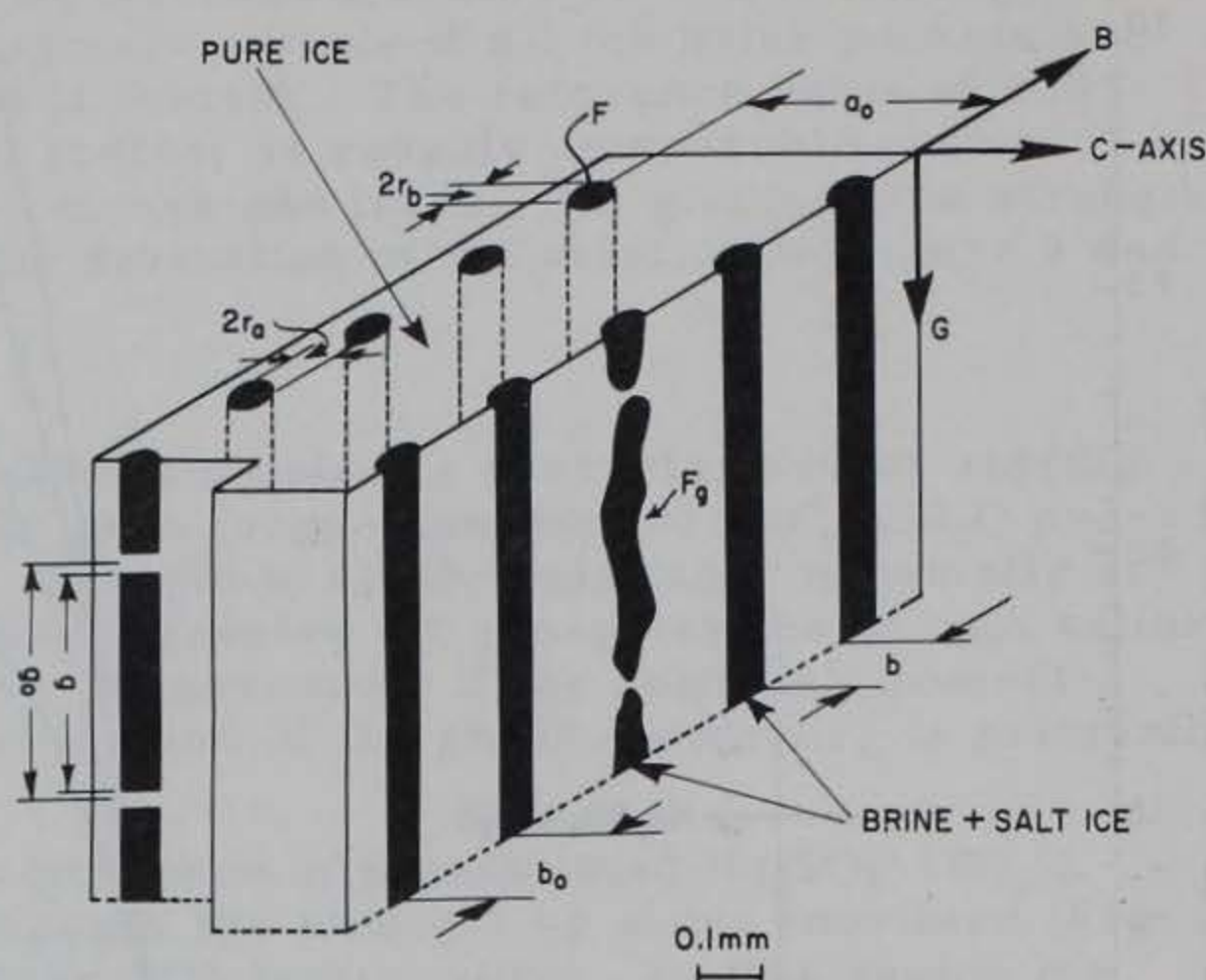


Figure 5. Cylindrical shape of brine inclusions. Brine inclusions are shown here as continuous cylinders, although vertical interruptions are usually observed (see brine inclusion at extreme left). Dimensions refer to the liquid brine, not including the mixture of salt and ice precipitated on the walls of brine inclusions.  $F$  = average area of a brine pocket in the  $B$ - $c$  plane;  $F_g$  = average area of a brine inclusion in the  $B$ - $G$  plane (arbitrary elongated shape);  $a_0$  = average spacing of parallel elementary ice plates or of layers with brine pockets (center to center) in the  $c$ -direction;  $b$  = width of plate along  $B$ -axis;  $b_0$  = average spacing (c-to-c) of brine pockets in the  $B$ -direction;  $g$  = length of brine cylinders in the  $G$ -direction;  $g_0$  = average spacing of brine cylinders in the  $G$ -direction;  $2r_b$ ,  $2r_a$  = maximum length and width of individual brine pocket in the  $B$ - $c$  plane.



Relative brine volume  $\nu$  is

$$\nu = \frac{Fg}{a_0 b_0 g_0} \quad (8)$$

(for symbols, see Fig. 5).

If the brine inclusions differ substantially from a cylindrical shape, it is better to introduce the average volume  $\bar{V}$  of a brine inclusion, instead of  $Fg$ . This is done for the spherical model discussed below.

Introducing two dimensionless parameters

$$\gamma = \frac{g}{g_0} \quad (9a)$$

$$\text{and } \beta_0 = \frac{b_0}{a_0} \quad (9b)$$

$$\text{eq 9 becomes } \nu = \frac{\gamma}{\beta_0} \frac{F}{a_0^2} \quad (10)$$

This equation becomes more general if  $\gamma$  is defined as

$$\gamma = \frac{Fg}{b_0 g_0} \quad (9c)$$

where  $F_g$  is the average area of a brine inclusion in the  $\underline{B}$ - $\underline{G}$  plane.

In most cases it will be sufficient to use definition 9a.  $\gamma = g/g_0$  can be obtained easily by dividing the total length of vertical interruptions by the total path with brine inclusions in the  $\underline{G}$  direction. The result is the "line porosity"  $\lambda_g$ . Then

$$\gamma = 1 - \lambda_g \quad (9d)$$

The most convenient way of measuring  $F$  is to find the maximum length  $2r_b$  and maximum width  $2r_a$  of individual brine pockets in the  $\underline{B}$ - $\underline{c}$  plane and averaging

$$F = \frac{\pi}{4} (2r_b \cdot 2r_a) \quad (11)$$

under the assumption of an elliptical shape, which is a good approximation.

It is also useful to find the average

$$\epsilon = \frac{2r_b}{2r_a} \quad (12)$$

as we shall see below (eq 27 ff).

A tensile stress applied in the direction of the  $\underline{c}$ -axis acts upon a reduced cross section, as does a shear stress. This reduction is

$$\psi = \frac{2r_b g}{b_0 g_0} \quad (13a)$$

with  $2r_b$  the average length of the brine pockets in the  $\underline{B}$ -direction.



The reduction can be expressed also as

$$\psi = \frac{\gamma}{\beta_0} \frac{2r_a}{a_0}. \quad (13b)$$

If the brine inclusions differ substantially from a cylinder, it is better to introduce the average area of the inclusions in the B-G plane instead of  $2r_b g$ . This was done for the spherical model, discussed below.

The effective strength due to the reduction in cross section becomes

$$\sigma = \sigma_0 \left( 1 - \frac{\gamma}{\beta_0} \frac{2r_b}{a_0} \right) \quad (14)$$

where  $\sigma_0$  is the basic strength of the ice (including the possible effect of stress concentration).

Now all depends on how  $2r_b$  and  $\gamma$  vary with the brine volume  $v$ . Different assumptions can be made.

If the brine inclusions are assumed to be geometrical bodies remaining similar during changes in the brine volume, all linear dimensions (including  $2r_b$  and  $g$ ) would change proportionally to the cube root of the brine volume. Since both  $\gamma$ , through  $g$ , and  $2r_b$  are involved, an equation of the following form results:

$$\sigma = \sigma_0 (1 - \text{const } \sqrt[3]{v^2}). \quad (15)$$

Another possible assumption is that the average length and spacing of the brine cylinders, and therefore  $\gamma$ , remain constant. Then the changes in brine volume are reflected only in the cross section B-c. Again we may assume that the cross-sectional shape of a brine pocket, whatever its form may be, stays geometrically similar. In that case all linear dimensions of the brine pockets in the cross section change proportional to the square root of the brine volume

$$\sigma = \sigma_0 (1 - \text{const } \sqrt{v}). \quad (16)$$

This assumption appears to be the most reasonable.

Finally it may be assumed that not only the relative length of the cylinders,  $\gamma$ , but also the width of the brine pockets stays constant. In that case  $2r_b$  must change proportional to the brine volume

$$\sigma = \sigma_0 (1 - \text{const } v). \quad (17)$$

The requirements of geometrical similarity in space, plane, or along a line (eq 15-17) are not the only conditions which might lead to equations of these three main types.

If we introduce another nondimensional parameter

$$\rho = \frac{2r_b}{\sqrt{F}} \quad (18)$$

then from eq 13b

$$\psi = \frac{\gamma \rho \sqrt{F}}{\beta_0 a_0}. \quad (19)$$

From eq 10



$$\sqrt{F} = \sqrt{\frac{\beta_0}{\gamma}} a_0 \sqrt{\nu} \quad (20)$$

so that

$$\sigma = \sigma_0 (1 - \rho \sqrt{\frac{\gamma}{\beta_0}} \sqrt{\nu}). \quad (21)$$

The nondimensional criterion

$$p_2 = \rho \sqrt{\frac{\gamma}{\beta_0}} \quad (22b)$$

must be constant if the strength reduces proportionally to  $\sqrt{\nu}$ .

By introducing the nondimensional ratio

$$a_0 = \frac{a_0}{\sqrt{F}} \quad (23)$$

and combining with eq 10 we have

$$\nu = \frac{\gamma}{\beta_0 a_0^2}. \quad (24)$$

Multiplying  $p_2$  by  $\nu^{-\frac{1}{2}}$  fulfills the condition of eq 17,

$$p_1 = p_2 \nu^{-\frac{1}{2}}$$

$$p_1 = \rho a_0. \quad (22a)$$

This nondimensional criterion has to be constant if a relation of the type of eq 17 holds. In that case

$$\sigma = \sigma_0 (1 - \rho a_0 \nu). \quad (25)$$

It is interesting to note that the spacings  $\beta_0$  and  $\gamma$  of the brine inclusions in the B-G plane do not enter into this relation.

To give eq 15,  $p_2$  has to be multiplied by  $\nu^{-\frac{1}{6}}$ :

$$p_3 = \frac{p_2}{\sqrt[6]{\nu}} = \sqrt[6]{\frac{\beta_0 a_0^2}{\gamma}} \rho \sqrt{\frac{\gamma}{\beta_0}}$$

$$p_3 = \rho \sqrt[3]{\frac{\gamma}{\beta_0}} a_0 \quad (22c)$$

and eq 15 now has the form

$$\sigma = \sigma_0 (1 - \rho \sqrt[3]{\frac{\gamma}{\beta_0}} a_0 \sqrt[3]{\nu^2}). \quad (26)$$

The three general groups of models can be represented by straight lines, in

$$\sigma, \nu \quad \sigma, \sqrt{\nu} \quad \sigma, \sqrt[3]{\nu^2} \quad (26a)$$



coordinates with the intercept  $\sigma_0$  on the  $\sigma$  axis for the maximum strength, the slope

$$\sigma_0 p_1 \quad \sigma_0 p_2 \quad \sigma_0 p_3 \quad (26b)$$

and the intercept

$$\nu_{\sigma=0} = \frac{1}{p_1} \quad \sqrt{\nu}_{\sigma=0} = \frac{1}{p_2} \quad \sqrt[3]{\nu}^2 = \frac{1}{p_3} \quad (26c)$$

for the condition of no strength, which leads to

$$\nu_{\sigma=0} = \frac{1}{\rho a_0} \quad \text{or} \quad \frac{\beta_0}{\rho^2 \gamma} \quad \text{or} \quad \sqrt{\frac{\beta_0}{\rho^3 \gamma a_0}}. \quad (26d)$$

To investigate the behavior of the three nondimensional criteria  $p_1$ ,  $p_2$ ,  $p_3$ , an album of photomicrographs should be assembled, each photo carefully identified as to original location of the specimen in the ice sheet, the salinity at that level, and the temperature at which each photo was taken. Available photomicrographs give valuable clues for some of the more important dimensions.

#### Specific models

Elliptical cylinders. Let  $\epsilon = r_b / r_a$  be the average ratio of the length of the elliptical brine pockets (in the B-direction) to the width of the pockets (in the C-direction). Then

$$F = \pi r_b r_a = \frac{\pi r_b^2}{\epsilon}. \quad (27)$$

Since  $\rho = 2r_b / \sqrt{F}$  we have

$$\rho = 2\sqrt{\frac{\epsilon}{\pi}}. \quad (28)$$

Considering eq 21 we obtain

$$\sigma = \sigma_0 \left( 1 - 2\sqrt{\frac{\gamma \epsilon}{\pi \beta_0}} \sqrt{\nu} \right). \quad (29)$$

The simplest possible case is the assumption of circular cylinders with  $\epsilon = 1$ . Neglecting the interruption of the vertical cylinders,  $\gamma = 1$ , we obtain

$$\sigma = \sigma_0 \left( 1 - \frac{2}{\sqrt{\pi \beta_0}} \sqrt{\nu} \right). \quad (30)$$

This equation for the "circular" model corresponds to the first Anderson model (1957), which was derived directly without establishing a general theory and without discussing a (true) elliptical model. His equation in our notations reads

$$\sigma = \frac{\sigma_b}{k} \left( 1 - \sqrt{\frac{4\nu}{\pi \beta_0}} \right) \quad (31)$$

with  $\sigma_b$  the (bulk) strength of fresh-water ice and  $k \cong 3$  the stress concentration factor at the brine pockets.

Detailed petrographic measurements are not absolutely necessary to check the validity of eq 29. Taking the strength  $\sigma$  as the ordinate and the square root of the relative brine volume  $\sqrt{\nu}$  as the abscissa gives a linear relation



$$\sigma = \sigma_0 - 2\sigma_0 \sqrt{\frac{\gamma\epsilon}{\pi\beta_0}} \sqrt{\nu} \quad (29a)$$

with the "basic strength"  $\sigma_0$  as intercept on the  $\sigma$  axis and  $2\sigma_0 \sqrt{\frac{\gamma\epsilon}{\pi\beta_0}}$  as the slope. The intercept on the  $\sqrt{\nu}$  axis with no strength is then given by the condition

$$\sqrt{\nu}_{\sigma=0} = \frac{1}{2} \sqrt{\frac{\pi\beta_0}{\gamma\epsilon}}. \quad (32)$$

Note:  $\gamma \leq 1$  by definition;  $\epsilon > 1$  from observation;  $\gamma\epsilon = 1$  transform the more general equation 29 into equation 30. It seems, however, that  $\gamma\epsilon > 1$ .

With sufficient strength data, this petrographic constant, in principle, could be determined accurately.

Now let us consider a constant width model corresponding to eq 17. Then

$$F = 4r_a r_b$$

$$\rho = \frac{2r_b}{\sqrt{F}} \quad a_0 = \frac{a_0}{\sqrt{F}}$$

and 
$$\rho a_0 = \frac{2r_b a_0}{4r_a r_b} = \frac{a_0}{2r_a}.$$

We introduce here the nondimensional ratio

$$\nu_0 = \frac{2r_a}{a_0} \quad (33)$$

which plays an important part in the understanding of sea ice. Eq 17 then becomes

$$\sigma = \sigma_0 \left( 1 - \frac{\nu}{\nu_0} \right). \quad (34)$$

Again, if this type of equation holds, the constants  $\sigma_0$  and  $1/\nu_0$  can be determined from the intercept of a straight line with the ordinate  $\sigma$  and the abscissa  $\nu$ . The no-strength condition is then

$$\nu_{\sigma=0} = \nu_0. \quad (35)$$

The assumption of rectangular brine pockets might appear unreasonable in this case. A refinement can be introduced, whereby the rectangular brine pockets have rounded ends. (Fig. 17, right side). Then

$$\begin{aligned} F &= 2r_a(2r_b - 2r_a) + \pi r_a^2 \\ &= 4r_a r_b - (2r_a)^2 \left( 1 - \frac{\pi}{4} \right). \end{aligned} \quad (36)$$

Combining with eq 10 and considering eq 33 we have

$$\nu = \gamma \nu_0 \frac{2r_b}{\beta_0 a_0} - \frac{\gamma}{\beta_0} \nu_0^2 \left( 1 - \frac{\pi}{4} \right)$$

and



$$\frac{2r_b}{a_0\beta_0} = \frac{\nu}{\gamma\nu_0} + \frac{\nu_0}{\beta_0} \left(1 - \frac{\pi}{4}\right). \quad (37)$$

Introducing this value into eq 14, we obtain

$$\sigma = \sigma_0 \left(1 - \frac{\nu}{\nu_0} - \frac{\left(1 - \frac{\pi}{4}\right) \gamma}{\beta_0} \nu_0\right). \quad (38)$$

This equation can be compared with Anderson's second model, which was derived in a different way and designated "elliptical" although it is really a constant width model. His equation in our notations is (see also eq 3b)

$$\sigma = \frac{\sigma_b}{k} \left(1 - \frac{\frac{b_0^2}{\beta_0} \nu - \pi r_a^2 + 4r_a^2}{2r_a b_0}\right). \quad (39)$$

The no-strength condition for our eq 38 is

$$\left(\frac{\nu}{\nu_0}\right)_{\sigma=0} = 1 - \left(1 - \frac{\pi}{4}\right) \frac{\gamma}{\beta_0} \nu_0. \quad (40)$$

This gives the intercept of a linear relation on the abscissa  $\nu$  if  $\sigma$  is the ordinate.

Interrupted cylinders are included in the derivation of eq 34 and 38, while eq 39 is derived on the assumption of uninterrupted cylinders.

As the simplest case of a model using eq 15, we select spherical brine inclusions, located between the plates in the B-G plane.

The volume of a brine inclusion of radius  $r$  is

$$V = \frac{4}{3} \pi r^3.$$

The relative volume of brine is then

$$\nu = \frac{(4/3) \pi r^3}{a_0 b_0 g_0}. \quad (41)$$

Using  $\beta_0 = b_0/a_0$  and  $\gamma_0 = g_0/a_0$  we have

$$\nu = \frac{4\pi/3}{\beta_0 \gamma_0} \left(\frac{r}{a_0}\right)^3 \quad (42)$$

and

$$\left(\frac{r}{a_0}\right)^2 = \left(\frac{\beta_0 \gamma_0}{4\pi/3}\right)^{\frac{2}{3}} \nu^{\frac{2}{3}}. \quad (43)$$

On the other hand, the reduction in cross section is

$$\frac{\pi r^2}{b_0 g_0} = \frac{\pi}{\beta_0 \gamma_0} \left(\frac{r}{a_0}\right)^2.$$

Considering (43) we obtain

$$\sigma = \sigma_0 \left(1 - \frac{1}{2} \sqrt[3]{\frac{9\pi}{2\beta_0 \gamma_0}} \nu^{\frac{2}{3}}\right). \quad (44)$$



Tsurikov (1939), apparently the first to propose a theory of sea-ice strength based upon the geometry of internal cavities, used a spherical model for cold sea ice (in the winter) and a circular (cylindrical) model for warm sea ice in the spring. However, his reasoning contains a number of discrepancies. He assumes a random distribution of spheres or cylinders, while the brine inclusions actually lie systematically in planes between the elementary plates. Tsurikov assumed that physically only gas inclusions are responsible for the reduction in strength. He does not give data on salinity or even temperature. The only variable he introduces is the air bubble content. We consider that the air bubble content has only a secondary importance compared with the brine content. Although density was measured, it is not considered in the report. The air content can be measured directly, but it can be also computed if density, salinity, and temperature are known. A study of the effect of density is still in progress. The air content could be added to the brine volume but careful further analysis is necessary to check such a concept.

It appears at present that neither the spherical, circular, or the constant width model will be entirely satisfactory, but our (true) elliptical model in eq 29 might emerge as the most adequate assumption. Final judgment must be reserved until the completion of further studies, but we will see later that it is not necessary to know the petrographic parameters accurately.

### BRINE CONTENT

All the models have one thing in common: The relative volume of brine must be known before an adequate theoretical explanation of the strength characteristics of sea ice can be attempted.

The only attempt to compute brine content was that reported by Malmgren (1933) and Zubov (1945). Anderson and Weeks (1958) follow the same concept, although they had the benefit of better original data, reported by Nelson and Thompson (1954). They present a graph of brine volume versus temperature and salinity, which does not allow sufficient accuracy in the determination of the brine volume.

All these attempts have one concept in common. The brine content  $br$  is computed as

$$br = S/S_b \quad (45)$$

where  $S$  = salinity of the ice

$S_b$  = salinity of the brine, determined from a relation of the freezing point versus salinity.

Eq 45 is equivalent to a statement that all the salts measured in  $S$  are completely dissolved in the brine inclusions, which is true only at higher temperatures. At lower temperatures, the assumption is completely inadequate, as shown by Figure 9. In addition, there is an enrichment in solid salts in natural sea ice beyond the amounts shown in Figure 9.

The correct equation is

$$br = \frac{S - S_s}{S_b} \quad (46)$$

with  $S_s$  = the relative amount of solid salts. The assumption that  $S_s = 0$  is not permissible.

The author's hypothesis that the measured high strength of sea ice at low temperatures is determined by the presence of precipitated salts also requires computing the amounts of solid salts.

The determination of the phase relations in sea ice proved to be a major and tedious job. The results should not be considered as final. The analysis is reported



in some detail in order to demonstrate some weak aspects. Further chemical studies should be made.

### Chemical Analysis

The data used are primarily those reported by Nelson and Thompson (1954). In addition, data obtained by Ringer (1906) were used, (but similar work by Gitterman (1937) was not available.)

Nelson presents a most valuable table for the concentration of the six major ions  $\text{Na}^+$ ,  $\text{Mg}^{++}$ ,  $\text{Ca}^+$ ,  $\text{K}^+$ ,  $\text{Cl}^-$ ,  $\text{SO}_4^-$  in brine, after the freezing of sea water. Values are given in ‰ with two decimals. Thirty-one tests are reported ranging in temperature from -2.2 to -43.15C. Ringer's data go down to -53C. Nelson (1953) gives brine densities, brought to 4C, which are used by us below. Nelson and Thompson report in some detail on their experimental procedure. Their primary purpose was to find whether and how palatable water could be obtained by freezing process. The "quantity of brine remaining after freezing of sea water", given by Nelson, has to be taken with reservations. He could collect only the brine which was left on the bottom of the container after the salt water ice itself was removed. He obviously, did not attempt to centrifuge the brine left within the ice. The actual amount of brine in phase equilibrium is substantially higher.

Nelson and Thompson (1954), plotted the grams of ions per 1000 g of brine. This ratio depends, of course, not only on the specific ion in question, but also upon the amount of brine, and upon any of the other ions in the brine. Changes in this ratio can be the result of formation of ice, precipitation of salts in which the given ion participates or of other salts in which it doesn't, as well as the result of the separation of crystalline water. All these factors were used by Nelson and Thompson to explain peculiarities in the graphical representation of this ratio.

We prefer to use only the relative concentration of two ions. In such a case it is easy to decide which of the two ions, or both, produce a change in the ratio.

### Freezing point of brine

Nelson and Thompson (1954) confirmed the qualitative conclusions of Ringer (1906) concerning the order and temperatures of precipitation of  $\text{Na}_2\text{SO}_4 \cdot 10 \text{H}_2\text{O}$ ,  $\text{NaCl} \cdot 2\text{H}_2\text{O}$ ,  $\text{KCl}$ , and  $\text{MgCl}_2 \cdot 12 \text{H}_2\text{O}$ . No further analysis or conclusions were reported except that Thompson's (1932) original equation for the freezing point of sea water

$$\theta = -0.0966 \text{ Cl} - 0.0000052 \text{ Cl}^3 \quad (47a)$$

was corrected to

$$\theta = -0.0966 \text{ Cl} - 0.0000035 \text{ Cl}^3 \quad (47b)$$

for brine with  $50 < \text{Cl} < 140\text{‰}$ . Below 50‰, eq 47a was found to be adequate. Cl is the chlorinity in its usual definition.

Our first task is to establish the relation of the freezing point of brine to the salt content. An attempt to express it in terms of Cl or the salinity  $\underline{S}$  in its usual definition would be too empirical. The proper parameter is  $\underline{Z}$  — the ratio of dissolved salts to pure water (the solvent), not to the brine (the solution). (See Fig. 6.)

It is known that a linear relation results for ideal solutions. This is the case for brine up to about 140‰ or -8C. There a break occurs because of the precipitation of  $\text{Na}_2\text{SO}_4 \cdot 10\text{H}_2\text{O}$ . Then the relation is linear again to about 300‰ or -23C, when  $\text{NaCl} \cdot 2\text{H}_2\text{O}$  begins to precipitate. More complicated relations appear below this temperature. Salinity was computed as the total of the 6 ions with a small correction, explained in Table II.



Table II. Absolute and relative concentration of the major ions in normal sea water.  $Cl = 19.00\text{‰}$ ,  $S = 34.325\text{‰}$ 

I	Absolute concentration	Relative concentration	
		$I/Cl^-$	$I/Cl$
$Cl^-$	18.9799	1	0.998942
$Na^+$	10.5561	0.556173	0.555584
$SO_4^{=}$	2.6486	0.139558	0.13940
$Mg^{++}$	1.2720	0.067018	0.066947
$Ca^{++}$	0.4001	0.02108	0.02106
$K^+$	0.3800	0.02002	0.02000
	34.2367		

Ratio  $SO_4^{=}/Na^+$  ---- 0.25091 $Mg^{++}/K^+$  ---- 3.3474

The data are computed from the table given by Sverdrup (1942, p. 173). The chlorinity  $Cl$  differs from the chloride concentration  $Cl^-$ , since other halides precipitate during titration. In addition, the international definition of chlorinity  $Cl$  introduces a small discrepancy. These differences are accounted for in the subsequent computation. The total of the 6 ions is  $34.2367\text{‰}$ . Adding the difference  $Cl - Cl^-$  we obtain  $34.2568\text{‰}$  which is still  $0.0682\text{‰}$  short of  $34.325\text{‰}$ , the salinity computed for  $Cl = 19.00\text{‰}$  according to the internationally adopted Knudsen's formula. All summations of the 6 ions have to be multiplied therefore by  $1 + \frac{0.0682}{34.2367} = 1.001992$ .

A least squares analysis was made for the first portion of the relation minimizing the absolute errors according to the expression

$a = [Z\theta]/[\theta\theta]$ . The result is

$$Z = -a\theta = -0.01848\theta_f. \quad (48)$$

If the salinity of the brine  $S_b$  is expressed as an absolute term (not in ‰) we have

$$\theta = -54.11 \frac{S_b}{1-S_b} \quad (49)$$

for the freezing point of the brine, or

$$\frac{1}{S_b} = 1 - \frac{54.11}{\theta} \quad (50)$$

for computing salinity of brine from the temperature. This relation is used below.

A relation of the type  $\theta = -\frac{1}{a} Z$  was once proposed by Lyman and Fleming (1940). They found  $1/a = 52.41$  for sea water as compared to our 54.11 for brine.

A least squares analysis of the second linear portion of the relation, minimizing the absolute errors of  $Z$  in relation to  $\theta$ , resulted in the equation

$$Z = -0.0103085\theta + 62.40 \quad (51)$$

measuring  $Z$  in absolute terms.



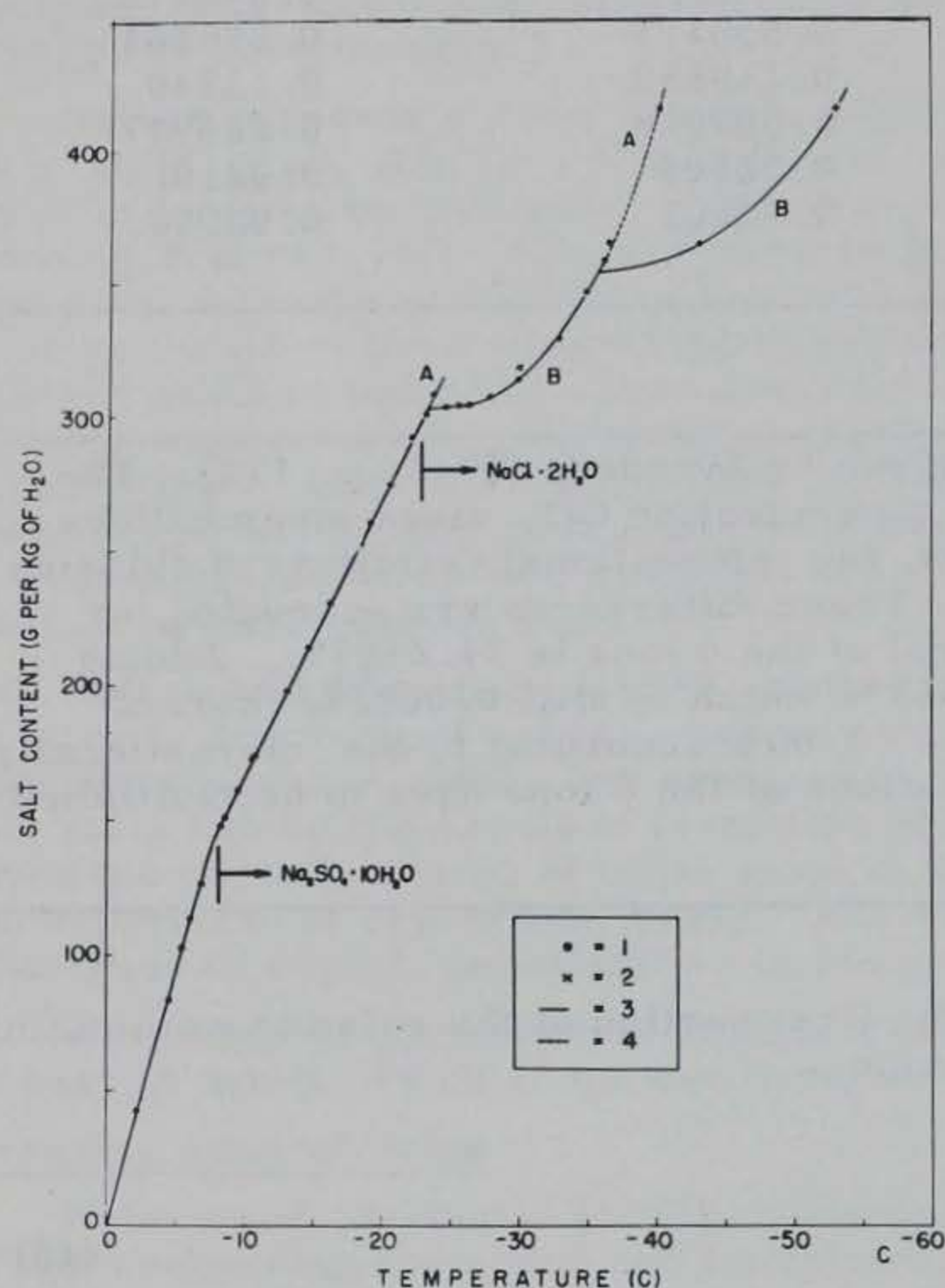


Figure 6. Freezing point of brine as a function of the ratio of dissolved salts to pure water (linear relations used to  $-24^{\circ}\text{C}$ ). 1 - Computed from data reported by Nelson (1954) for 6 major ions. 2 - Computed from Ringer (1906). 3 - Relation assumed for subsequent analysis (path B - B). 4 - Possible path (A - A), if salts precipitate in different order.

brine is assumed to be the same as for the liquid brine in the brine inclusions. There is no reason to suspect that this is not true. The change in freezing point for a curved surface is negligible because of the relatively large size of the brine inclusions. The capillary depression of the freezing point is of no consequence here, since the solid phase is always in contact with the brine, even when salts precipitate together with brine. The brine in the inclusions might not be under exactly the same pressure as the residual brine, but this effect certainly can be neglected.

It is also assumed that the concentration of the different ions is the same in relation to each other as in the residual brine left under the ice in the experiment. There is no reason to doubt this statement, and no process is known and investigated by which a different composition of the brine would be created. If there is a difference, there is no way of analyzing it at present.

The temperature coefficient with its standard error is  $0.010308$  ( $51 \pm 49$ ), which is a very high accuracy. The correlation coefficient is equally high,  $R = -0.9999(08 \pm 48)$ , with  $R = -1$  characterizing a perfect mathematical relation.

The two linear relations (48) and (51) cross at  $Z = 142.44\%$  and  $\theta = -7.71^{\circ}\text{C}$ , which is close to the temperature where  $\text{Na}_2\text{SO}_4 \cdot 10\text{H}_2\text{O}$  starts to precipitate.

Eq 51 can be expressed also in terms of an additional depression of the freezing point beyond that given by eq 48. We then have

$$\theta_1 = -54.11 Z \text{ for } Z < 0.142 \quad (52)$$

and

$$\theta = \theta_2 - \theta_1 = 42.8973 (Z - 0.14244) \quad (53)$$

for  $Z > 0.142$  up to about 0.300.

Below about  $-23^{\circ}\text{C}$  and  $-36^{\circ}\text{C}$  the freezing point relations show two possible paths (Fig. 6). Path A is barely indicated during the precipitation of NaCl, while path B is well covered by points.

During the precipitation of  $\text{MgCl}_2^*$ , two possible interpretations appear. Path B was selected due to its analogy with the NaCl path B, and because actually only one point supports the considerable deviation of path A below  $-36^{\circ}\text{C}$ . The points along path A are neglected in the subsequent analysis.

Some basic assumptions for "standard sea ice".

The freezing point of the residual

\* Precipitation of  $\text{MgCl}_2$  varies from sample to sample. Ringer (1928) did not obtain precipitation of  $\text{MgCl}_2$  even down to  $-80^{\circ}\text{C}$  in some cases.



It is known that the relative concentration of certain ions in melt-water samples from sea ice differs from the values observed in sea water. For example the  $\text{SO}_4^{2-}/\text{Cl}$  ratio is frequently higher in melt water from sea ice. This is readily explained.

A continuous drainage of brine occurs in sea ice. It is reasonable to assume that the solid salts, precipitated during cooling of sea ice, are not all suspended and then drained in the brine, but precipitate on the walls. In this way, ions which participate in the given salt are enriched in the melt water formed from sea ice. When sea ice goes through a warming cycle, only the amount of salt necessary to establish phase equilibrium in the brine will go into solution. The remainder will remain solid. This will certainly be the case below the temperature of precipitation of the given salt. Above this temperature the excess will stay solid until the eutectic point is reached, which is always higher than the temperature of the actual precipitation of the given salt, because of the presence of other ions. Even above the eutectic point the excess may stay solid, if the solution is saturated in relation to the ions participating in the given salts. The salt systems involved are not yet studied sufficiently to reach conclusions on the behavior above the eutectic point.

As a good approximation, the excess salts in sea ice may be assumed to be solid. The remaining brine within the ice should have the same relative concentration as the residual brine underneath. Once a substantial amount of chemical data for melt water from sea ice is available, the problem of excess salts can be attacked in principle. At present such data are meager.

Therefore, the concept of "standard sea ice" is introduced here. It is defined as sea ice of such a composition that its melt water would have the same relative concentration of ions (to each other) as normal sea water (Table II).

This concept will be very useful even when more is known about the chemical composition of normal sea ice. Our subsequent computations are based upon "standard sea ice" with the reservation that, eventually, adjustments will be made for normal sea ice.

#### Methods for computing phase relations

Relative concentration of the main ions in brine as a function of temperature. The relative concentration of individual ions in brine is shown in Figures 8a-f. Cl (chlorinity) rather than  $\text{Cl}^-$  (chlorine ion concentration) was used for the graphs. The small difference between these values (Table I) is accounted for in the final computations.

A number of different methods of computing the precipitated salts and brine content were tried.

Method I: The easiest method is to apply eq 45, not to the total salinity, but to individual ions which are known or expected to stay in solution without precipitating in a salt. This method proved to be highly inaccurate and unreliable, because the computed brine volumes differ greatly if different ions are used. In addition, some ions which were expected to stay in solution do precipitate in salts. It is not advisable to base the whole computation on just one unreliable ion, as this method would require at certain temperatures.

If the brine content  $\text{br}$  at different temperatures is known, the absolute amount of each ion in solution can be computed from the relative concentration. These absolute amounts then can be used to determine the absolute losses, from which the amount of precipitated salts can be computed. In practice, however, because of experimental errors or random variations of samples, the absolute amounts do not change as they should according to the gravimetric ratios in the salt.

Method II: A modification of method I. Instead of individual ions, all ions which are believed to stay in solution are combined. Greater accuracy results but the main deficiencies of method I remain, especially at low temperatures. This method is equivalent to taking weighted averages of brine amounts obtained by method I.

Method III: The first approximation for  $\text{br}$  is obtained by method II. The absolute amounts of ions are computed from this, and then the amounts of precipitated salts are computed from losses in the amounts of individual ions. Different values are obtained.



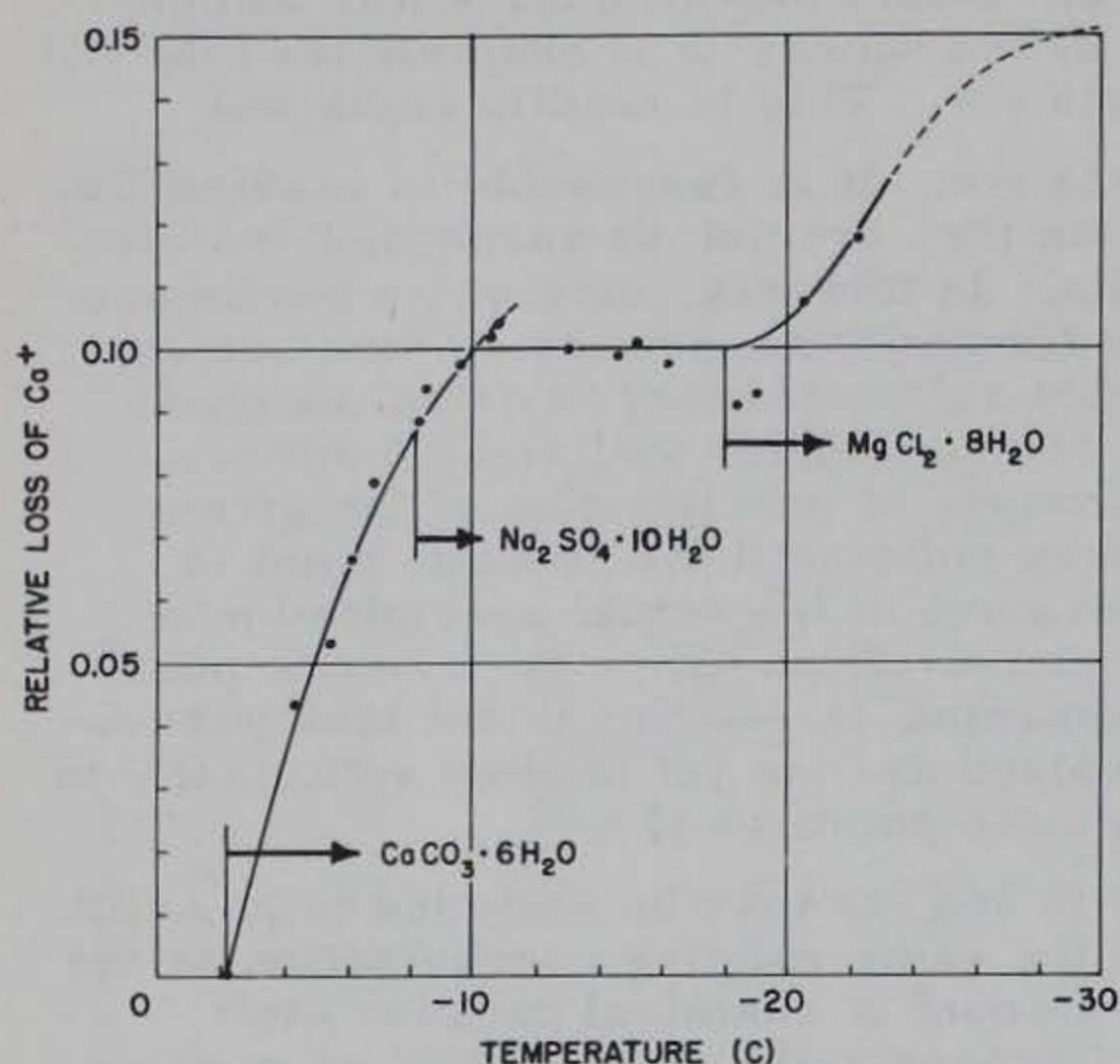


Figure 7. Relative loss of  $\text{Ca}^+$  due to the precipitation of  $\text{CaCO}_3 \cdot 6\text{H}_2\text{O}$ .  $\text{Ca}^+$  can be determined very accurately, accounting for the accurate values of precipitated  $\text{CaCO}_3 \cdot 6\text{H}_2\text{O}$ , which starts to precipitate at  $-2.2^\circ\text{C}$ . Precipitation ceases below  $-10^\circ\text{C}$  but seems to increase again after  $\text{MgCl}_2 \cdot 8\text{H}_2\text{O}$  starts to precipitate. A small correction was applied to the values due to the loss of Cl below  $-18^\circ\text{C}$ . Final value 0.151 is determined in such a way that the remaining  $\text{Ca}^+$  fully combines with Cl to  $\text{CaCl}_2$  below  $-54^\circ\text{C}$ . Note that the amount of  $\text{CaCO}_3 \cdot 6\text{H}_2\text{O}$  can be determined fairly accurately, although practically no effect is noticeable in the  $\text{Ca}^+/\text{Cl}$  ratio as plotted in Figure 8a.

$\Delta I_0$  — Available amount of "reference ion". (For example Cl in NaCl, Fig. 8d). Equal to amount in normal sea water minus the amount that might have already precipitated at a given temperature in other salts. This has to be determined by successive elimination. For example  $\text{Cl}^-$  has already precipitated in  $\text{MgCl}_2 \cdot 8\text{H}_2\text{O}$ , before NaCl starts to precipitate. This amount, however, was already determined with the help of method IV (Fig. 8c).

$\Delta I_1$  — Available amount of the "first" ion. Initial amount in normal sea water minus the amount already precipitated. A considerable amount of  $\text{Na}^+$ , for example, has precipitated in  $\text{Na}_2\text{SO}_4 \cdot 10\text{H}_2\text{O}$  (Fig. 8b) before  $\text{NaCl} \cdot 2\text{H}_2\text{O}$  begins to precipitate.

$\rho_1$  — Observed ratio of the absolute concentrations of the first ion to the reference ion (for example,  $\text{Na}^+/\text{Cl}$ , Fig. 8d).

$x_1$  — Amount of salt to be computed, for example  $\text{NaCl} \cdot 2\text{H}_2\text{O}$ .

$a_1$  — Gravimetric "concentration" of the "first" ion in the salt. For example

$$\frac{\text{Na}^+}{\text{NaCl} \cdot 2\text{H}_2\text{O}} = \frac{22.991}{94.480} = 0.24334$$

After computing weighted averages of the salts, new absolute amounts of ions in solution are determined. Eq 45 can be applied to the total of these, which gives a second approximation for  $\text{br}$ . With successive approximations higher accuracy can be achieved. Based upon the different amounts of computed salts, different brine volumes can be computed. The resulting error then can be minimized in the sense of least squares. This method proved to be very tedious and obvious experimental discrepancies could not be easily detected.

**Method IV:** If it is established beyond doubt that an ion does not precipitate at a given temperature range and its determination is sufficiently accurate, it can be used as a reference ion. The ratio of an ion precipitating in a salt to the reference ion is a reliable indicator of relative loss. From the initial absolute amount of the ion, absolute loss and amount of precipitated salt can be computed easily. This method was useful in determining  $\text{CaCO}_3 \cdot 6\text{H}_2\text{O}$  (Fig. 7) and  $\text{MgCl}_2 \cdot 8\text{H}_2\text{O}$  (Fig. 8c). Nelson does not mention the first salt, the second salt was not detected by Ringer or Nelson. Ringer mentions the precipitation of  $\text{CaCO}_3 \cdot 6\text{H}_2\text{O}$ , but did not determine the temperature of precipitation.

**Method V:** A very efficient method is to study the behavior of two ions precipitating in a given salt by plotting the ratio of their concentrations (Fig. 8b, d, f).

The amount of precipitated salts can be computed directly from this ratio.

The following designations are used:



The International Atomic Weights for 1956 were used throughout the analysis. For a convenient table of gravimetric constants see Appendix B.

$a_1$  — Gravimetric "concentration" of the reference ion in the salt. For example

$$\frac{\text{Cl}^-}{\text{NaCl} \cdot 2\text{H}_2\text{O}} = \frac{35.457}{94.480} = 0.37529.$$

The observed relative concentration of the two ions

$$\rho_1 = \frac{\Delta I_1 - a_1 x_1}{\Delta I_0 - a_1 x_1} \quad (54)$$

leads to

$$x_1(a_1 - a_1 \rho_1) = \Delta I_1 - \rho_1 \Delta I_0.$$

By introducing

$$\bar{\rho}_1 = \Delta I_1 / \Delta I_0 \quad (55)$$

which is known or computed beforehand, we obtain

$$\frac{a_1 x_1}{\Delta I_0} = \frac{\bar{\rho}_1 - \rho_1}{1 - \beta_1 \rho_1} \quad (56)$$

with

$$\beta_1 = a_1 / a_1 \quad (57)$$

the ratio of the concentration of the reference ion to the "first" ion. The molecular weight of the salt does not matter here;  $\beta_1$  can be directly obtained from the chemical formula of the given salt. It is  $\beta_1 = \text{Cl}/\text{Na} = 1.5422$  in the case of  $\text{NaCl} \cdot 2\text{H}_2\text{O}$  or  $\beta_1 = \text{Cl}_2/\text{Mg} = 2.9159$  in the case of both  $\text{MgCl}_2 \cdot 8\text{H}_2\text{O}$  and  $\text{MgCl}_2 \cdot 12\text{H}_2\text{O}$ .

Eq 56 can be conveniently evaluated since  $\rho_1$  is directly computed from the results of chemical analysis.  $\bar{\rho}_1$ ,  $\beta_1$ , and  $a_1$  can be computed from gravimetric constants.  $\Delta I_0$  is either the absolute amount of the reference ion in normal sea water or a reduced amount if the reference ion did or does participate in the precipitation of other salts.

Method V was used to determine  $\text{Na}_2\text{SO}_4 \cdot 10\text{H}_2\text{O}$  (Fig. 8b),  $\text{NaCl} \cdot 2\text{H}_2\text{O}$  (Fig. 8d),  $\text{KCl}$  (Fig. 8e), and  $\text{MgCl}_2 \cdot 12\text{H}_2\text{O}$  (Fig. 8f). The method is useful if two salts with a common ion do not precipitate simultaneously (for example,  $\text{NaCl} \cdot 2\text{H}_2\text{O}$ , while  $\text{Na}_2\text{SO}_4 \cdot 10\text{H}_2\text{O}$  is still precipitating). Fortunately, method V can be used in a region where most of the salt is precipitated anyhow.

The maximum available amount of a given salt which can precipitate can be computed from the amount of the most deficient ion. When the ratio of this maximum amount minus the salt already precipitated to the maximum possible amount is plotted on semilog paper, the small amount of the remaining precipitating salt can be easily extrapolated.

Method VI: Similar to method V. To be applied if two salts with a common ion precipitate at the same time. For this case we have two simultaneous equations:

$$\rho_1 = \frac{\Delta I_1 - a_1 x_1}{\Delta I_0 - a_1 x_1 - a_2 x_2} \quad (58a)$$

$$\rho_2 = \frac{\Delta I_2 - a_2 x_2}{\Delta I_0 - a_1 x_1 - a_2 x_2} \quad (58b)$$



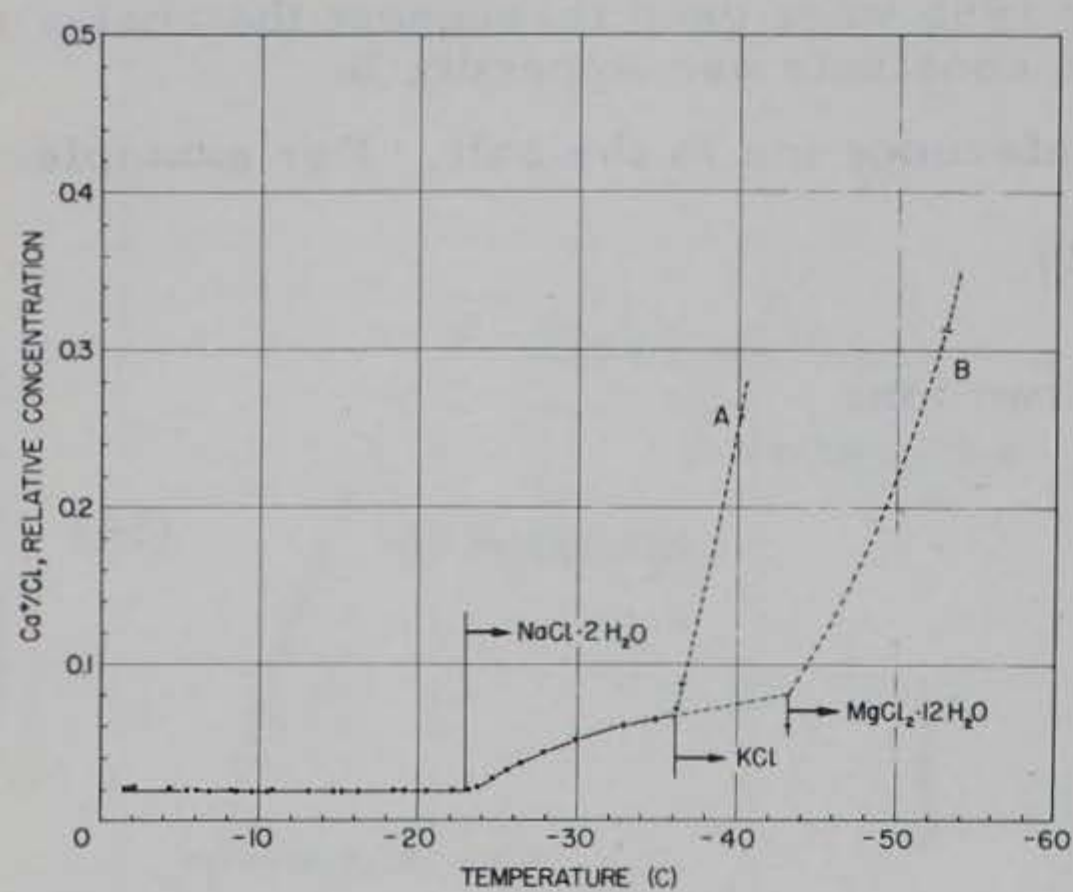


Figure 8a.

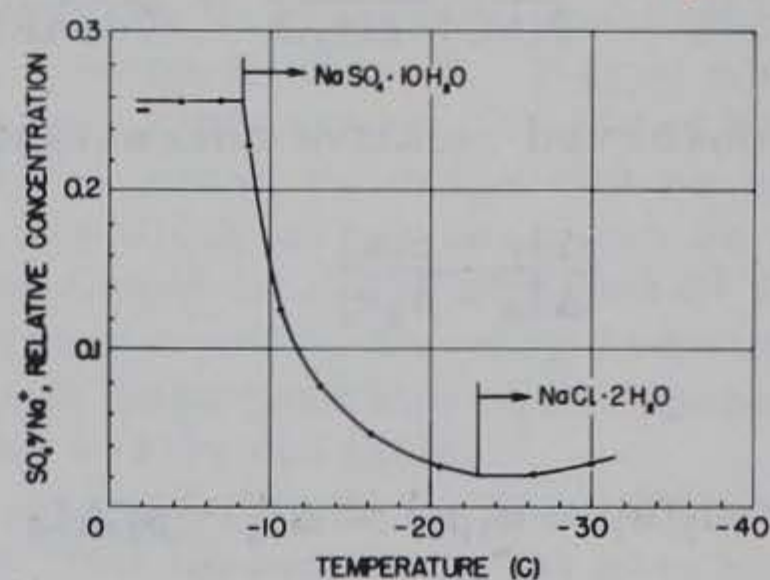


Figure 8b.

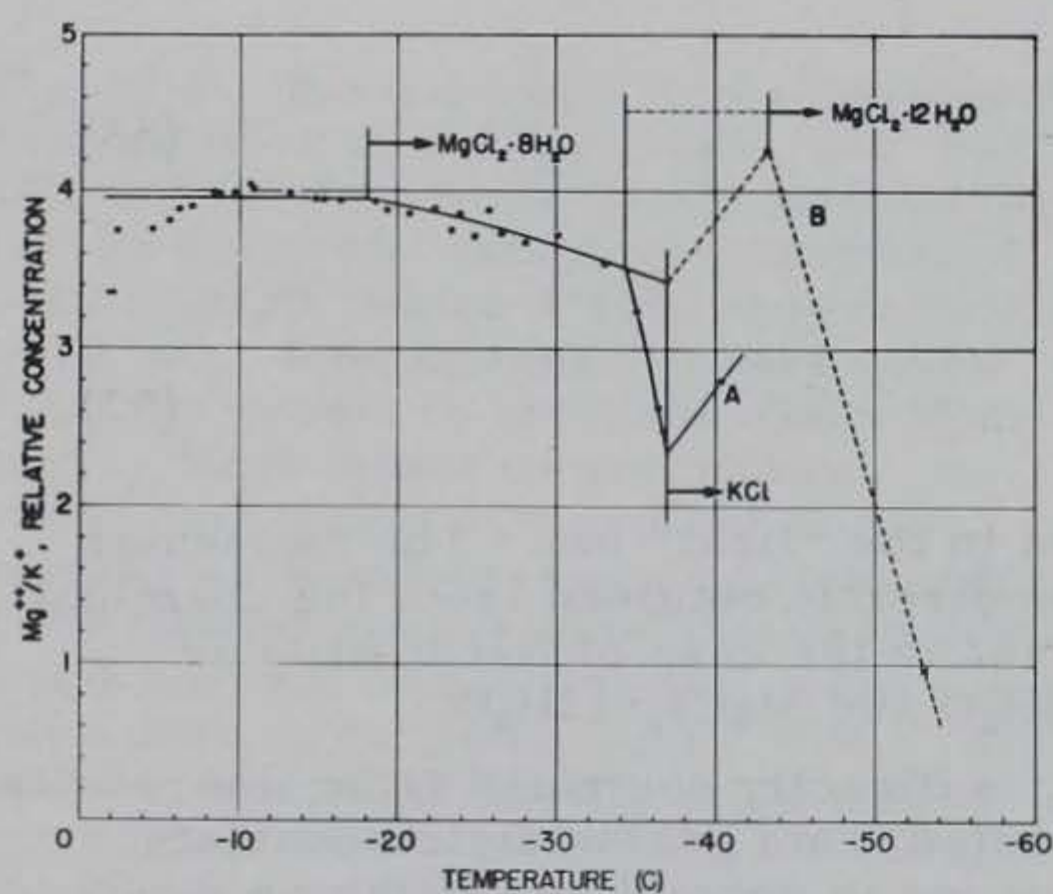


Figure 8c.

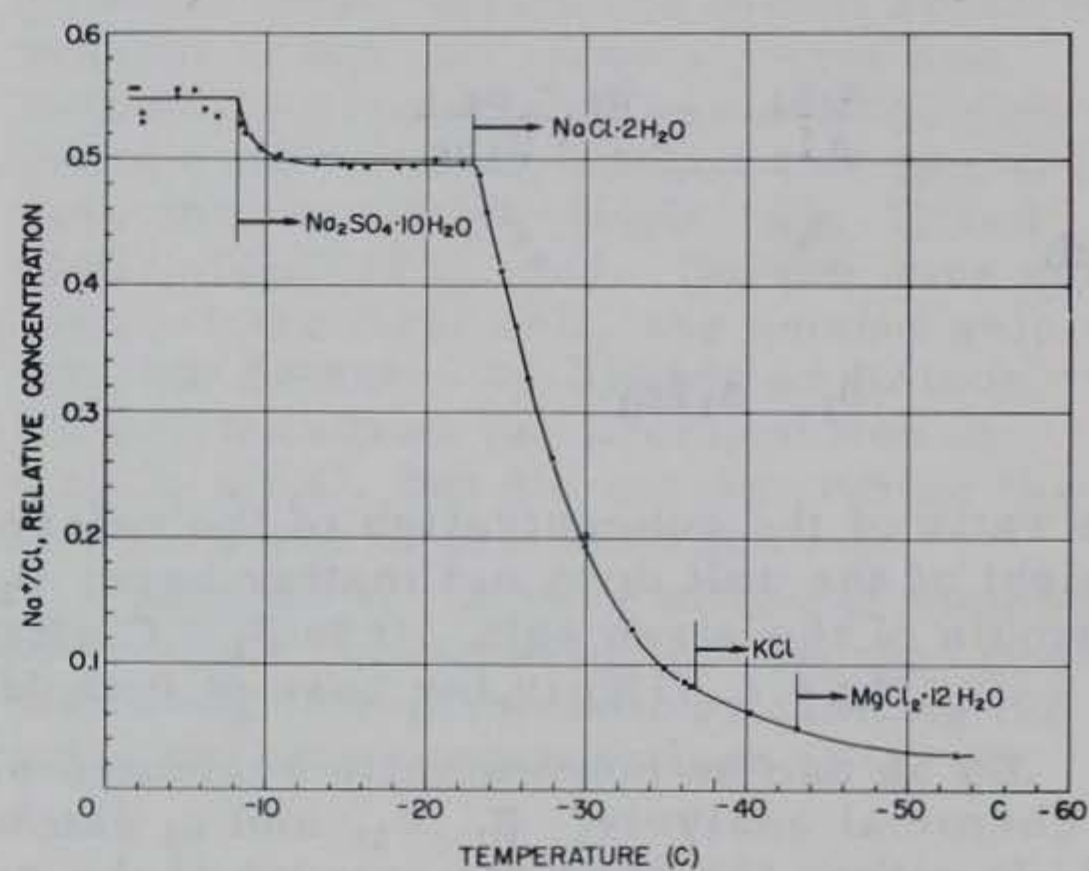


Figure 8d.

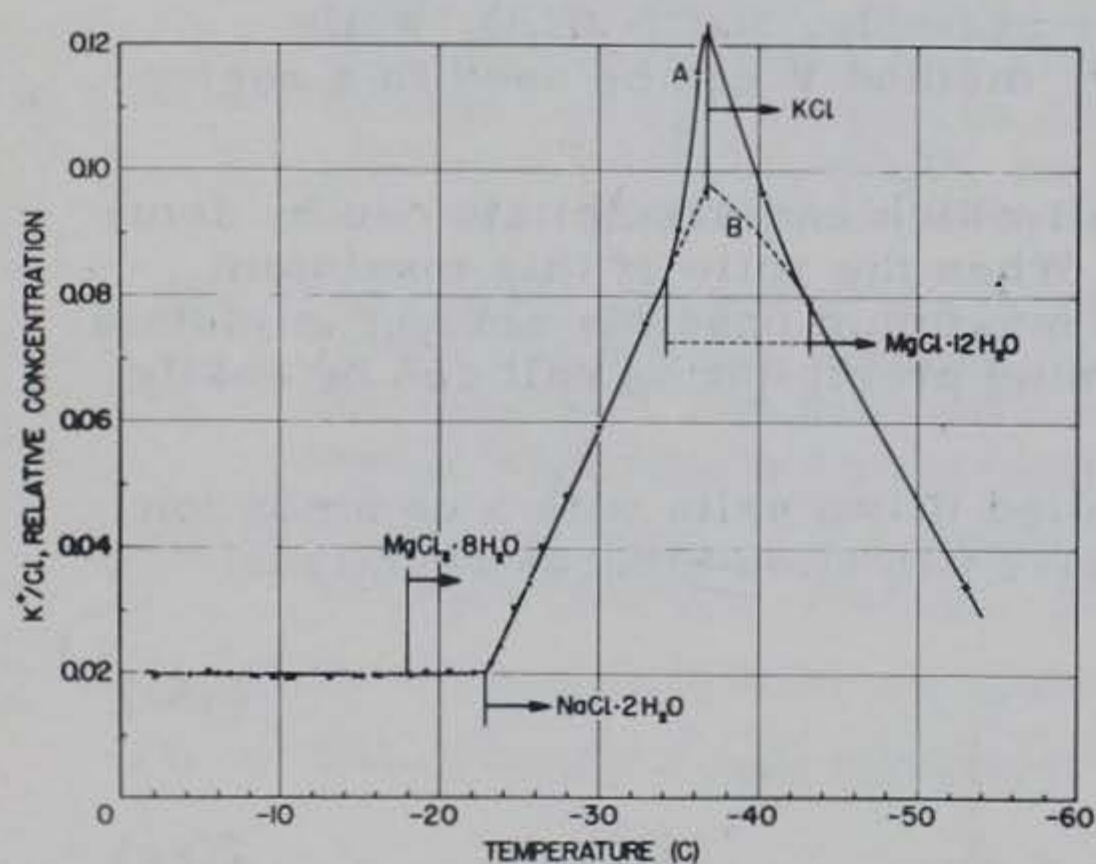


Figure 8e.

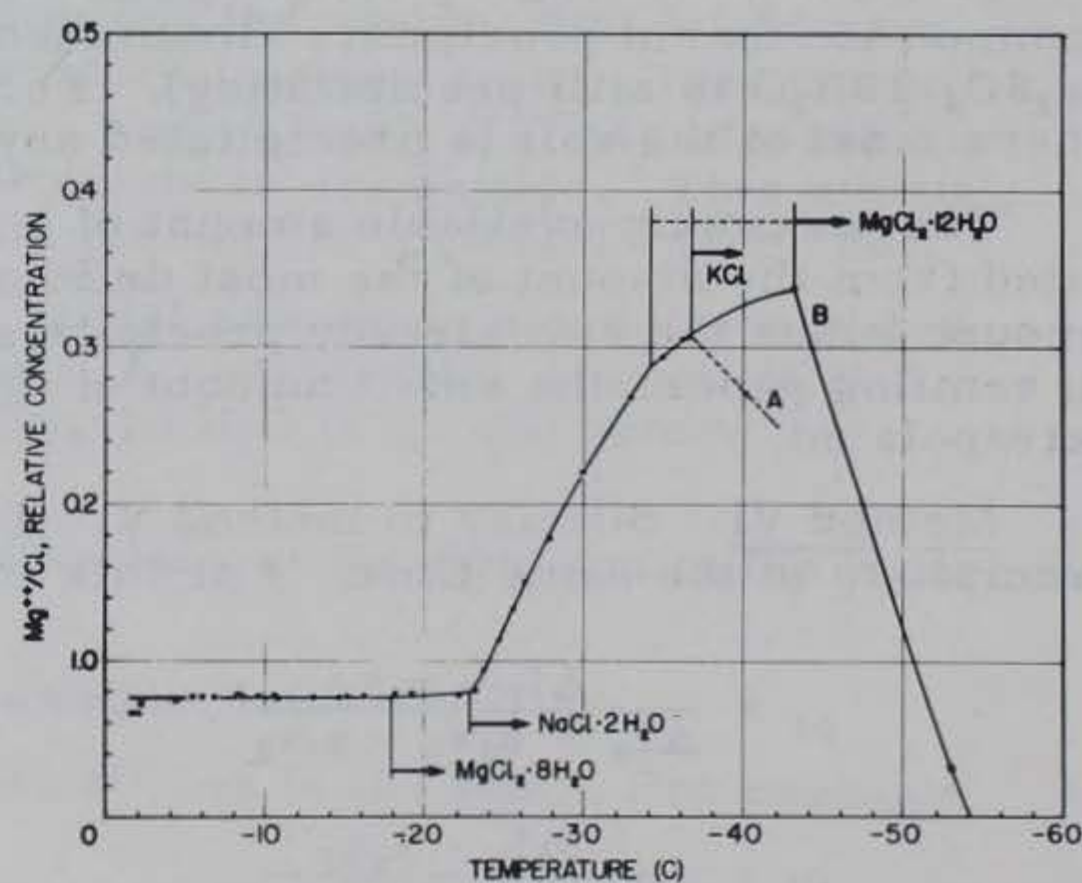


Figure 8f.

Figure 8. (see p. 29)



Figure 8. Relative concentration of the principle ions in brine as a function of temperature. Dots are computed from chemical test data reported by Thompson and Nelson (1954); "x's" are based on test data obtained by Ringer (1906). They are, generally, in good agreement with the rest of the points. Short heavy dash at the left side of each graph indicates relative concentration in normal sea water (Table II). Concentration of ions in the original sea water sample used is not given by Thompson and Nelson (1954) unless one uses their values for a brine at  $-2.2^{\circ}\text{C}$  for the relative concentration. It is difficult to decide whether and how much the samples differed systematically from normal sea water, or whether the discrepancies can be attributed to experimental errors. Arrows indicate where characteristic salts begin to precipitate. The most unreliable parts of the curves are indicated by dashed lines. Path B was selected for the further analysis (see Fig. 6).

- Relative concentration  $\text{Ca}^{+}/\text{Cl}$ . Not used in our analysis, since  $\text{CaCl}_2 \cdot 6\text{H}_2\text{O}$  precipitates only below  $-54^{\circ}\text{C}$ . The small amounts of  $\text{Ca}^{+}$  (not noticeable in this presentation) which precipitate at higher temperatures can be computed more efficiently by the method illustrated in Fig. 7.  $\text{Ca}^{+}$  should not be used as an indicator of the relative brine weight according to eq 45 (for individual ions) because (1) about 15% of  $\text{Ca}^{+}$  is already lost at higher temperatures, and (2) the  $\text{Ca}^{+}$  content below  $-36^{\circ}\text{C}$  is quite undetermined and unreliable.
- Relative concentration  $\text{SO}_4^{-}/\text{Na}^{+}$ . Used for computation of  $\text{Na}_2\text{SO}_4 \cdot 10\text{H}_2\text{O}$ , which begins to precipitate at  $-8.2^{\circ}\text{C}$ . Difficulty of Na determination might account for the small discrepancy with normal sea water (heavy dash).
- Relative concentration  $\text{Mg}^{++}/\text{K}^{+}$ .  $\text{K}^{+}$  was selected as reference ion, because of its systematic behavior (Fig. 8e), and to show that  $\text{MgCl}_2 \cdot 8\text{H}_2\text{O}$  starts to precipitate at  $-18^{\circ}\text{C}$ . The  $\text{Mg}^{++}/\text{Cl}$  graph (Fig. 8f) shows hardly any effect. Because of losses in  $\text{MgCl}_2 \cdot 8\text{H}_2\text{O}$ , Cl should not be used to compute brine content below  $-18^{\circ}\text{C}$  by eq 45. The considerable discrepancy with  $\text{Mg}^{++}/\text{K}^{+}$  in normal sea water may be due to experimental errors; chemical determination of  $\text{Mg}^{++}$  is traditionally difficult. Path B was selected for further analysis, although path A appears to be better covered with points. Final decision must be made on the basis of further chemical tests.
- Relative concentration  $\text{Na}^{+}/\text{Cl}$ . Used to compute  $\text{NaCl} \cdot 2\text{H}_2\text{O}$ , which begins to precipitate at  $-22.9^{\circ}\text{C}$ . The transition to  $\text{Na}_2\text{SO}_4 \cdot 10\text{H}_2\text{O}$  at  $-8.2^{\circ}\text{C}$  is rather vague on this graph. Note that chemical determination of  $\text{Na}^{+}$  is difficult.
- Relative concentration  $\text{K}^{+}/\text{Cl}$ . Used for computation of  $\text{KCl}$ , which seems to precipitate below  $-36.8^{\circ}\text{C}$  (see Fig. 8c, 8f). Dashed curve B is taken as a compromise, since 3 points along path A were deleted from the analysis after inspection of Fig. 6. A separate analysis could be based on path A.
- Relative concentration  $\text{Mg}^{++}/\text{Cl}$ . Used for computation of  $\text{MgCl}_2 \cdot 12\text{H}_2\text{O}$ . Precipitation assumed to begin at  $-43.2^{\circ}\text{C}$ . Path A was rejected after inspection of Fig. 6. Behavior of  $\text{MgCl}_2$  is erratic in general and not identical in all samples. Ringer (1906) cooled sea ice down to  $-80^{\circ}\text{C}$  without precipitation of  $\text{MgCl}_2$  in some cases.

The index  $_2$  refers here to the second salt, the index  $_0$  to the common ion.

The solution of this is

$$\frac{a_1 x_1}{\Delta I_0} = \frac{\beta_2(\rho_1 \bar{\rho}_2 - \bar{\rho}_1 \rho_2) + \bar{\rho}_1 - \rho_1}{1 - \beta_1 \rho_1 - \beta_2 \rho_2} \quad (59a)$$

$$\frac{a_2 x_2}{\Delta I_0} = \frac{\beta_1(\rho_1 \bar{\rho}_1 - \bar{\rho}_2 \rho_1) + \bar{\rho}_2 - \rho_2}{1 - \beta_2 \rho_2 - \beta_1 \rho_1} \quad (59b)$$

With  $\beta_2 = 0$ , eq 59a reduces to eq 56.



All the values leading to the determination of  $x_1$  and  $x_2$  are known or observed, but this set of equations should not be applied if one salt precipitates in only small quantities compared with the other. In addition, very accurate data are necessary in order to avoid discrepancies.

Method V was used primarily for the analysis of the phase relations. Method IV was used in some cases. The other methods were thoroughly studied, but the combination V - IV proved to be the most efficient. When more data are available, a more refined procedure can be used. A few corrections were applied to bring Nelson's data in agreement with data for normal sea water. The results were computed under the assumption that sea water of the composition given in Table II is frozen at a given temperature and brought to complete equilibrium.

#### Phase relations in "standard sea ice"

Table III is given as the most representative and important of the numerous tables computed in this connection. All the computations were carried out at 2°C intervals. The table is dated, since improved tables should be available in the future. Corrections can be expected, especially below -36°C.

The table shows the amount of different ions,  $H_2O$  in brine, different solid salts, and pure ice which are at equilibrium at the given temperature. All values are given assuming that 1 kg of normal sea water of the composition given in Table II ( $Cl - 19.00\%$ ) freezes at the temperature indicated. Phase relations for other salinities  $S$  (in ‰) can be obtained by multiplying all values except those for ice by  $\frac{S}{34.325}$ . The amount of ice is then 1000 minus the total amount of brine and salts.

After the salt-water sample freezes, the brine and salts are located either within the ice or underneath it. The relative distribution is not necessarily the same at these locations in the experiment, but it is assumed the same.

Most of the salts are given as hydrates. Vertical arrows indicate that the amounts do not change. The third decimal in the table is carried as a computational convenience, the experimental data have only two decimals.

Note that a considerable amount of  $H_2O$  is fixed within the salts as crystalline water. It is known that the strength of salts is higher when they are combined with crystalline water.

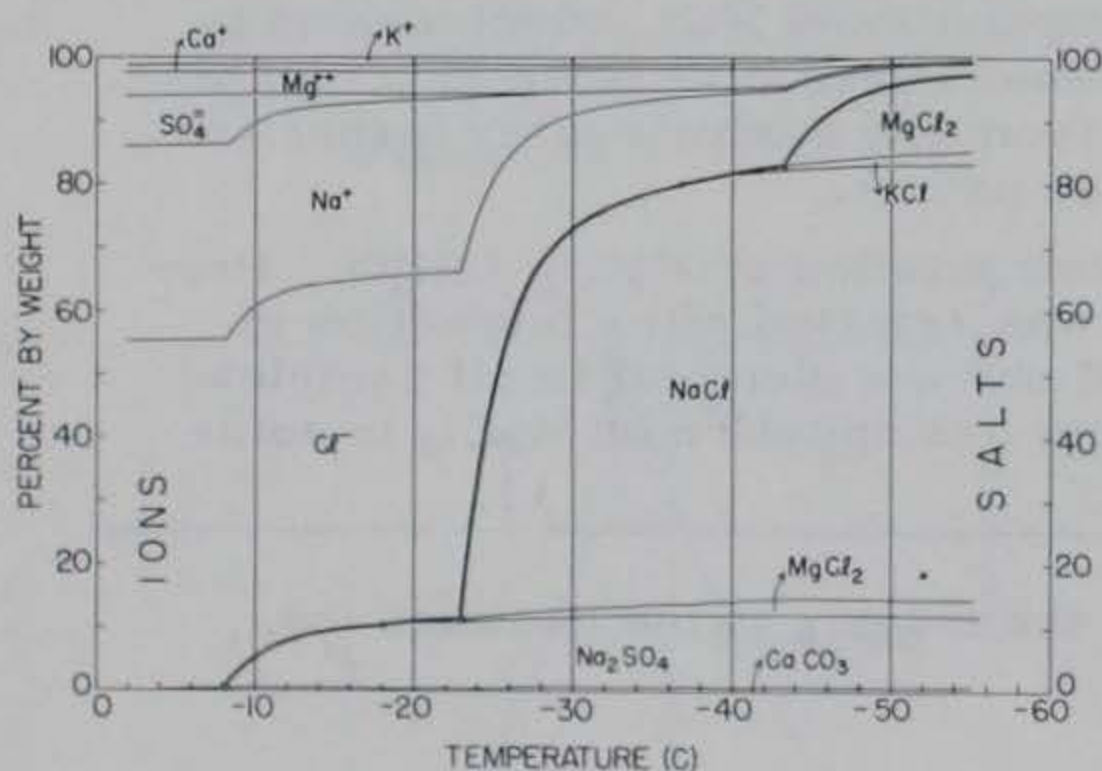


Figure 9. Relative amount of ions and salts in standard sea ice. Precipitation temperatures are shown by circles on the ion-salt line (heavy lines). Constructed from Table III by eliminating the amount of crystalline water in the salts and dividing the amounts of all ions and salts by 34.325.

Figure 9 shows the relative amount of the different ions and salts in sea ice. After the ice sample is melted all salts go into solution. At low ice temperatures most of the measured salinity refers not to the brine but to the solid salts. The percentage of solid salts is even greater if one considers that  $Na_2SO_4 \cdot 10H_2O$  is usually enriched several times, as proved by the observed increased ratio  $SO_4^{2-}/Cl$ . As a first approximation it can be assumed that the excess was precipitated in a solid salt ( $Na_2SO_4$  for example) in the original ice sample. The corresponding amount of the excess salt then has to be added to the values of the diagram, making the total more than 100%. The salts should play an important part in the strength characteristics of sea ice since they precipitate at the walls of brine inclusions, where the highest concentration of stresses occurs. We shall see that an increase in strength actually takes place.



Table III. Phase relations for standard sea ice (1957). Amount (g/kg) of ions, H<sub>2</sub>O in brine, salts, and ice under equilibrium at different temperatures. Salinity S = 34.325‰.

Temp (C)	Brine								Salts							Ice
	Uniden- tified ions	K <sup>+</sup>	Ca <sup>+</sup>	Mg <sup>++</sup>	SO <sub>4</sub> <sup>=</sup>	Na <sup>+</sup>	Cl <sup>-</sup>	H <sub>2</sub> O	MgCl <sub>2</sub> : 12H <sub>2</sub> O	KCl	NaCl· 2H <sub>2</sub> O	MgCl <sub>2</sub> · 8H <sub>2</sub> O	Na <sub>2</sub> SO <sub>4</sub> · 10H <sub>2</sub> O	CaCO <sub>3</sub> · 6H <sub>2</sub> O	Uniden- tified salts	
- 0	.088	.380	.400	1.272	2.649	10.556	18.980	965.675	0	0	0	0	0	0	0	0
- 2	.088	↓	↓	↓	↓	↓	↓	878.905	↓	↓	↓	↓	↓	↓	↓	86.770
- 4	.083	↓	.386	↓	↓	↓	↓	451.614	↓	↓	↓	↓	↓	.072	↓	515.008
- 6	.078	↓	.374	↓	↓	↓	↓	309.301	↓	↓	↓	↓	↓	.133	↓	656.227
- 8	.074	↓	.366	↓	↓	↓	↓	236.763	↓	↓	↓	↓	↓	.179	↓	728.781
-10	.072	↓	.360	↓	1.471	9.992	↓	195.293	↓	↓	↓	↓	3.951	.208	↓	768.021
-12	.072	↓	↓	↓	.885	9.712	↓	169.171	↓	↓	↓	↓	5.916	↓	↓	793.044
-14	.072	↓	↓	↓	.622	9.586	↓	151.078	↓	↓	↓	↓	6.798	↓	↓	810.644
-16	.072	↓	↓	↓	.456	9.506	↓	137.264	↓	↓	↓	↓	7.357	↓	↓	824.145
-18	.072	↓	↓	↓	.338	9.450	↓	125.778	↓	↓	↓	↓	7.750	↓	↓	835.412
-20	.071	↓	.358	1.261	.266	9.415	18.949	115.560	↓	↓	↓	.104	7.994	.217	↓	845.425
-22	.069	↓	.353	1.248	.213	9.390	18.910	106.717	↓	↓	↓	.235	8.171	.243	↓	854.071
-24	.058	↓	.347	1.232	.161	6.347	14.210	75.912	↓	↓	12.404	.389	8.346	.275	.009	879.930
-26	.038	↓	.343	1.216	.111	3.282	9.472	48.930	↓	↓	24.898	.553	8.513	.298	.028	901.938
-28	.029	↓	.341	1.198	.068	1.885	7.295	36.635	↓	↓	30.557	.733	8.656	.309	.035	911.879
-30	.024	↓	.340	1.178	.033	1.181	6.177	30.217	↓	↓	33.383	.927	8.775	.314	.040	917.031
-32	.021	↓	↓	1.158	.007	.803	5.557	26.537	↓	↓	34.883	1.122	8.862	↓	.043	919.973
-34	.019	↓	↓	1.134	0	.555	5.109	23.840	↓	↓	35.889	1.357	8.883	↓	.045	922.135
-36	.018	↓	↓	1.112	↓	.408	4.817	21.940	↓	↓	36.492	1.579	↓	↓	.046	923.671
-38	.017	.369	↓	1.080	↓	.304	4.577	20.386	↓	.021	36.921	1.811	↓	↓	.047	924.930
-40	.016	.332	↓	1.064	↓	.223	4.350	18.966	↓	.092	37.252	2.045	↓	↓	.048	926.075
-42	.016	.303	↓	1.040	↓	.166	4.165	17.797	↓	.147	37.486	2.284	↓	↓	.048	927.011
-44	.012	.260	↓	.747	↓	.123	3.206	13.385	3.747	.229	37.664	↓	↓	↓	.052	928.754
-46	.008	.200	↓	.369	↓	.092	2.000	8.124	8.593	.344	37.791	↓	↓	↓	.056	930.602
-48	.005	.119	↓	.188	↓	.069	1.363	5.384	10.914	.497	37.887	↓	↓	↓	.059	931.694
-50	.004	.050	↓	.096	↓	.052	1.007	3.896	12.086	.630	37.955	↓	↓	↓	.060	932.343
-52	.003	.019	↓	.037	↓	.041	.790	2.998	12.837	.689	38.002	↓	↓	↓	.061	932.702
-54	.003	0	↓	.003	↓	.033	.661	2.440	13.275	.725	38.034	↓	↓	↓	.061	932.944

COMPOSITION OF SEA ICE AND ITS TENSILE STRENGTH



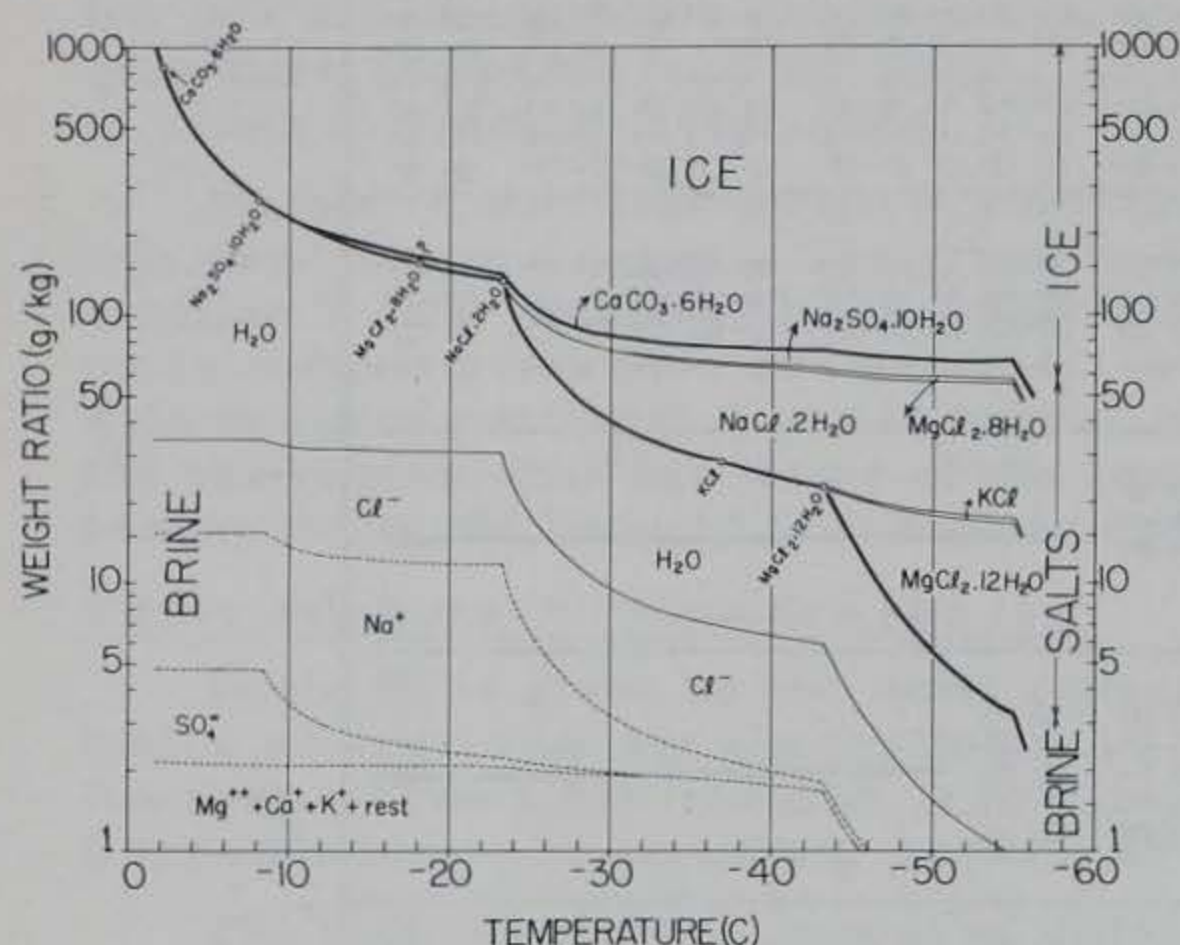


Figure 10. Phase diagram for sea ice. "Standard" sea ice is assumed. Salinity 34.325‰ is assumed corresponding to the salinity of normal sea water. For a given sea ice the values for salt and brine must be reduced in proportion to the salinities. Circles on the brine-salt line indicate temperatures at which the different salts precipitate. Path B-B (Fig. 6) was used for computing this phase diagram. A similar phase diagram can be constructed following path B-A (Fig. 6).

obtain the amount of brine. By subtracting the ions, the column  $H_2O$  in Table III was obtained. Dividing the amount of brine by 34.325 gave the amount of brine in standard sea ice of 1‰ salinity.

Nelson (1953) gives the density of the brine, obtained at different temperatures. All these densities of brines with different salinities were measured at (or reduced to?) 4°C. Nothing is known about the temperature dependence of these densities.

The amount of brine must be multiplied by the ratio  $\gamma_i/\gamma_b$ , with  $\gamma_i$  - the "theoretical" density of sea ice, and  $\gamma_b$  - the density of the brine. The actual density of sea ice depends upon salinity, temperature and air content. Here only the dependence upon salinity and temperature had to be considered, since the air content can be studied separately.

$\gamma_i$  can be computed from Table III, reduced to the given salinity, but this approach was considered impractical for routine use, since separate tables of the relative brine volume would have to be prepared for different salinities.

The theoretical densities of sea ice vary slightly, depending upon temperature and salinity (Zubov, 1945). An average value  $\gamma = 0.926$ , corresponding to  $\theta = -10^\circ C$  and  $S = 6\text{‰}$ , was assumed. The relative brine volume  $v$  then can be computed as strictly proportional to the salinity. This greatly simplifies the application of this concept. The  $v$  values for  $S = 1\text{‰}$  are tabulated in Appendix A.

Figure 11 shows the relative volume of brine in relation to temperature. The very rapid increase of the brine volume at high temperatures (line M) readily explains the well-known rapid weakening of sea ice in the spring.

A simple, although rough approximation for observed relations (dashed line, Fig. 11) gives the relation (in decimal logarithms)

By adding the values of Table III consecutively, a phase diagram for standard sea ice is obtained (Fig. 10). The changing amounts of different ions,  $H_2O$  in brine, different salts as hydrates, and the ice itself are caused by transitions (water to ice, ions to salts) as the result of changing temperatures. The phase diagram is plotted on a semi-log scale to show small amounts.

The objection has been made that the relatively small amount of solid salts cannot possibly have an effect on strength. One must consider, however, to what degree the mechanical properties of steel are affected by small changes in the enclosed carbon.

Mr. Anderson (personal communication) has recently succeeded in determining the phase relations in sea ice. As a first approximation his determination was made primarily on the basis of method I, whereas our computations were made on the basis of methods IV - V.

#### Relative volume of brine

When the amounts of precipitated salts were computed, the amount of ions in solution were easily determined by subtraction from the initial amounts in Table II. Once the absolute amount of ions was known, their total was obtained, and eq 45 could be directly applied to



$$\lg v = \lg 65 - \frac{\theta}{23}, \quad v \text{ in } \text{‰} \quad (60)$$

indicating that the brine volume drops to one-tenth of its value if the temperature decreases by 23C. A sudden transition to  $v = 1000\text{‰}$  must be assumed at the melting point.

Figure 12 is a nomogram for the determination of the relative volume of brine.

Note: There is a method available for determining the content of liquid brine directly (Savel'ev 1954, 1957), but experimental results are not available as yet. Savel'ev's method does not yet have corrections for the presence of solid salts.

### EVALUATION OF RING TESTS RESULTS

The tensile strength is equal to

$$\sigma' = K \frac{P}{l \pi r_0} \quad (61)$$

$l$  = length of cylinder

$P$  = failure load (half the weight of the ring cylinder is added to the load, but the correction is very small)

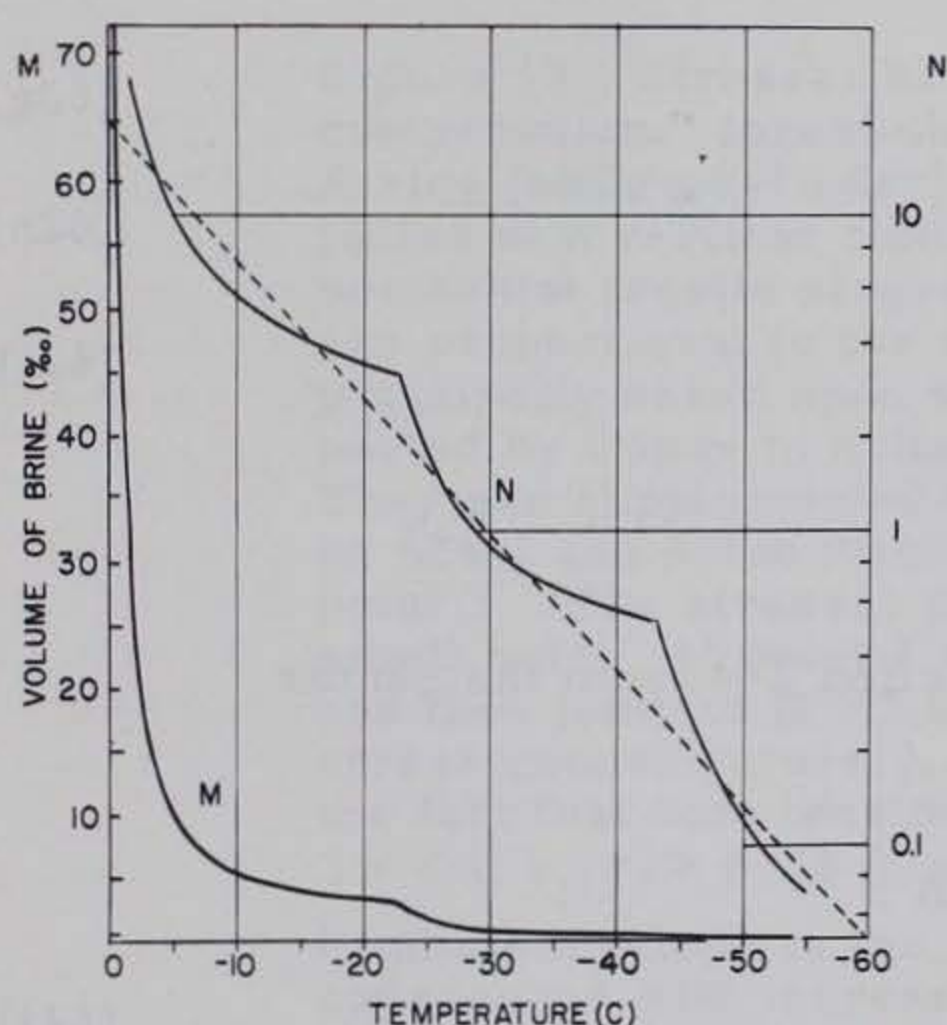


Figure 11. Relative volume of brine in standard sea ice of  $S = 1\text{‰}$ . Brine volume for any salinity  $S$  can be obtained by multiplying the values by  $S$ . Temperature measurements above  $-5\text{C}$  must be very accurate to evaluate brine volume. Arithmetic presentation (line M, left scale) shows rapid increase of brine volume with rising temperature. Semilog presentation (line N, right scale) shows sharp breaks due to precipitation of  $\text{NaCl}$  and  $\text{MgCl}_2$ . A linear relation (dashed line; right scale) gives a rough approximation (a sudden transition to  $v = 1000\text{‰}$  must be assumed).

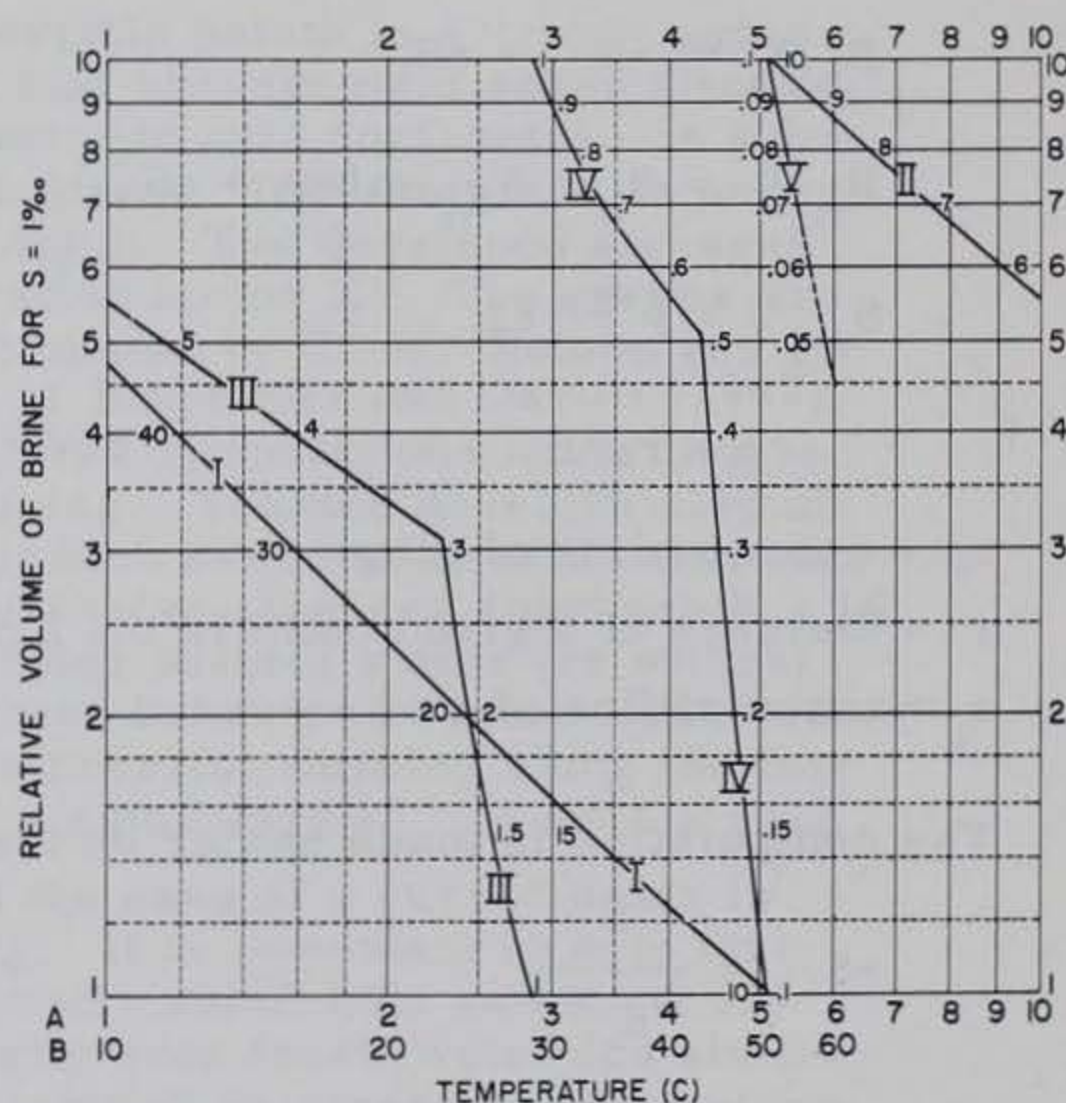


Figure 12. Nomogram for the determination of the relative brine volume in sea ice for  $S = 1\text{‰}$ . Left, right and upper scales are given for orientation purposes. Use curves I and II with temperature scale A and curves III, IV and V with temperature scale B. For other salinities  $v = Sv(1)$ . The curves in this nomogram can be expressed with good approximation as power functions  $v = \text{const} (-\theta)^{-n}$ , valid in specific ranges.



$r_0$  = outer radius of ring.

The concentration factor  $\underline{K}$  is a complicated function of the ratio  $r_i/r_0$ , which has to be evaluated in series. An expression given by Ripperger and Davids (1947) was found to be inconvenient and impractical for computations.

A new set of equations, numerically identical but more convenient, was derived for the change of  $\underline{K}$  along the line 2-4 (Fig. 13). It reads:

$$K = 1 + \frac{\rho^2+1}{\bar{\rho}} - 2B_2 + \sum_n^{\infty} [P_n \rho^{-n} - Q_n \rho^{n+2}] \quad (62a)$$

with  $\underline{n} = 2, 4, 6 \dots$

$$P_n = (n+2)(A_n - B_{n+2}) \quad (62b)$$

$$Q_n = n(C_n - D_{n+2}) \quad (62c)$$

$$R_n A_n = S_n + nS_1 \quad (62d)$$

$$R_n B_n = S_n + nS_{-1} \quad (62e)$$

$$R_n C_n = -S_{-n} - nS_{-1} \quad (62f)$$

$$R_n D_n = -S_{-n} + nS_1 \quad (62g)$$

$$R_n = S_n + S_{-n} - n(nS_1 + nS_{-1}) \quad (62h)$$

$$S_n = \bar{\rho}^{-2n-1} \quad (62i)$$

$$\rho = r_0/r \quad \bar{\rho} = r_0/r_i$$

$r_0$  = outer radius of ring

$r$  = distance of a given point in the critical section 2-4 from the center

$r_i$  = inner radius of ring.

The computation is made easier by the relation

$$-S_{-n} = \frac{S_n}{S_n + 1} \quad (62j)$$

Note that the coefficients have different meanings than in Ripperger and Davids (1947).

The stress distribution in a ring sample was evaluated in considerable detail by eq 62a-j, but space does not permit more attention to it here.

The critical concentration factor at point 2 can be computed by substituting  $\bar{\rho}$  for  $\rho$  in the set of equations. We obtain  $K = -10.9171$  for  $\bar{\rho} = 3$  and  $K = -7.09257$  for  $\bar{\rho} = 6$ .

The theory predicts  $K = 1$  for a solid cylinder without a hole. But even an infinitesimally small hole would create a concentration factor of  $K = 6$  (see curve 2, Fig. 13). Butkovich (SIPRE) recently performed parallel tests on solid cylinders and rings prepared from glacier ice. The author initiated a similar study on snow-ice and clear fresh-water ice, performed by L. Hansen (SIPRE). The results essentially confirm our theoretical prediction of  $K = 6$ , which is direct experimental evidence of the presence



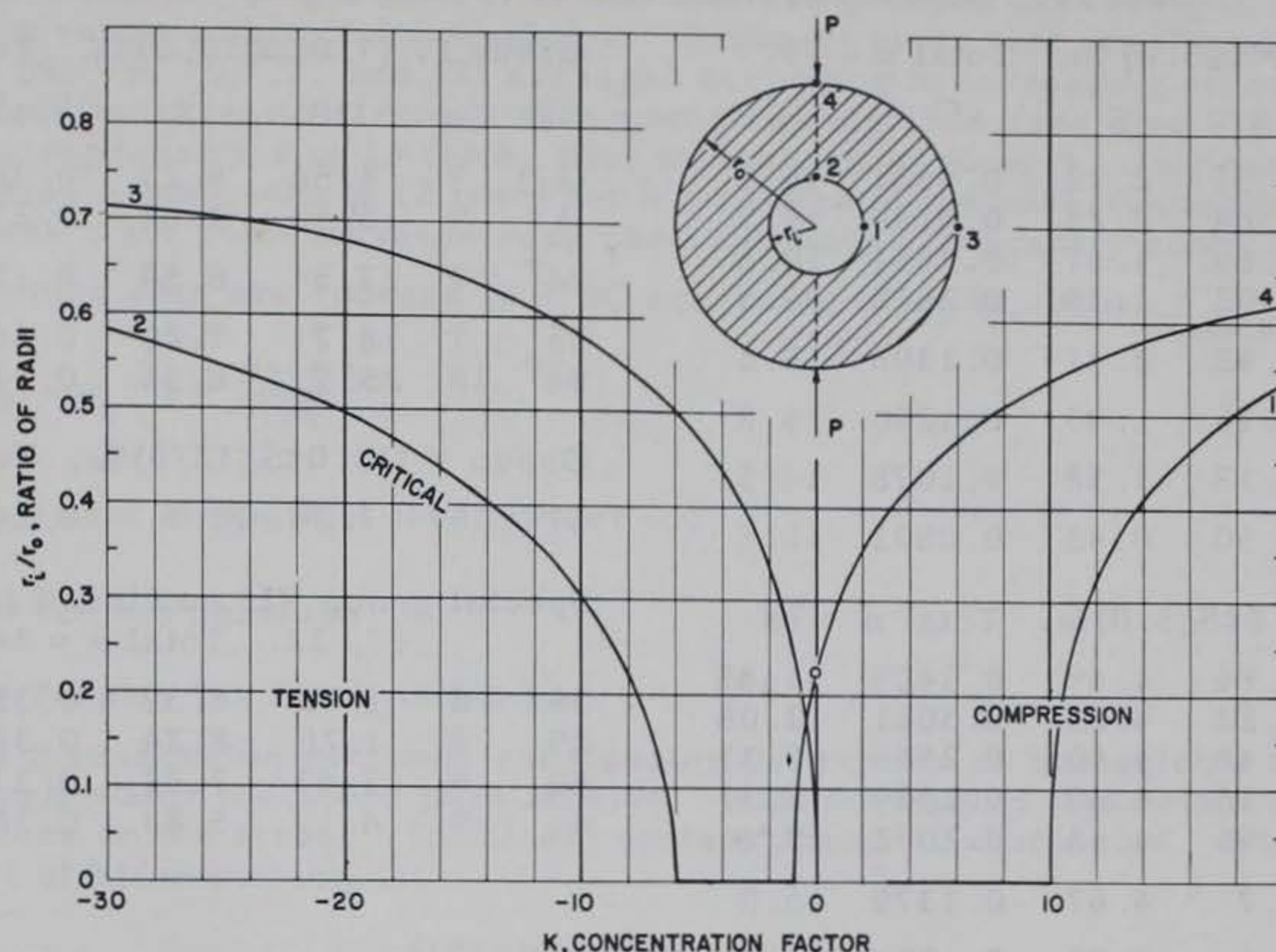


Figure 13. Stresses at characteristic points in a "ring" under compression. Insert shows the test arrangement schematically. A ring (hollow cylinder), lying with its axis horizontal is subjected to a vertical compressive force. The sample fails under horizontal tensile stresses at point 2. The developed stresses are proportional to the concentration factor  $K$ . The curves are principally based upon values computed by C. W. Nelson and reported by Popov in a discussion of Ripperger and Davids (1947). They are supplemented by additional computations according to eq 62a-j and some further reasoning. Tension develops also at point 3. The stresses there approach zero for an infinitesimally small hole. At point 1 the compressive stresses approach  $K = 10$  and then jump to  $K = 3$  for a cylinder without a hole (or without stress concentrators!). The stress behavior at point 4 illustrates the fact that both tension and compression develop along the line 2 - 4 if  $r_i/r_o > 0.22$  (marked by a small circle). In such a case bending develops in the ring and the case of a curved beam is approached with increasing  $r_i/r_o$ . It is important to note that  $K = 6$  at point 2 for an infinitesimally small hole and  $K = 1$  for a cylinder without a hole. Actually even fresh-water ice always has very small holes and irregularities as stress concentrators so that similar tests performed on solid cylinders should and do show a stress concentration factor of about  $K = 6$ . Stresses are horizontal at 2 and 4, vertical at 1 and 3. This explains why the stresses at 2 and 1 are not equal for  $r_i/r_o = 0$ .

of stress concentrators in fresh-water ice. These test series are the strongest argument against the assumption that stress concentration in the brine pockets causes the strength differences between fresh-water and sea ice.

Even when conditions which effect the strength of sea ice are kept constant, the results of strength tests will vary considerably, because of random structural defects in the samples. This is a common phenomenon for ice and especially for sea ice. The effect of this natural variation in strength under identical conditions has to be reduced by using group averages. Table IV gives the data used for the analysis, condensed



Table IV. Condensed table of test results (April 1958)\*

Group I ( $0.0 < S \leq 3.0$ ) ‰. Total n = 75.

#	n	$\theta$	S	$\sqrt{v}$	$\sigma$
1	9	0.51	2.13	0.4631	10.5
2	10	0.64	2.23	0.4149	10.7
3	10	0.69	1.87	0.3651	10.6
4	10	1.02	1.38	0.2612	10.5
5 <sup>x</sup>	12	6.43	2.41	0.1396	15.2
6 <sup>x</sup>	8	6.16	1.95	0.1290	15.8
7 <sup>x</sup>	8	6.19	1.58	0.1078	14.5
8 <sup>x</sup>	8	7.50	0.92	0.0803	16.5

Group II ( $3.0 < S \leq 5.0$ ) ‰. Total n = 68.

(9)	8	1.84	4.49	0.3425	1.45
(10)	8	2.22	4.25	0.3061	2.08
11	8	3.46	4.60	0.2546	7.31
12	8	4.16	4.30	0.2309	8.31
13	11	5.91	4.53	0.2002	10.4
14 <sup>+</sup>	6	15.7	4.67	0.1379	15.0
15 <sup>+</sup>	10	17.1	3.98	0.1221	11.9
16 <sup>o</sup>	9	27.1	4.42	0.0828	29.3

Group III ( $5.0 < S \leq 7.0$ ) ‰. Total n = 134.

(17)	9	1.87	5.71	0.3912	2.09
18	9	3.58	6.39	0.2960	7.17
19	9	4.03	5.82	0.2685	6.87
20	9	5.33	6.02	0.2411	8.73
21	10	6.67	5.77	0.2125	9.26
22 <sup>+</sup>	8	15.1	6.55	0.1605	13.8
23 <sup>+</sup>	9	16.7	6.04	0.1522	10.9
24 <sup>+</sup>	9	17.9	5.96	0.1476	14.8
25 <sup>+</sup>	9	17.3	5.57	0.1444	15.6
26 <sup>+</sup>	9	18.1	5.47	0.1406	11.9
27 <sup>+</sup>	9	20.1	5.58	0.1370	16.5
28 <sup>o</sup>	8	24.4	6.08	0.1089	24.1
29 <sup>o</sup>	8	24.9	6.11	0.1030	22.0
30 <sup>o</sup>	9	26.1	6.02	0.0935	26.4
31 <sup>o</sup>	10	27.1	5.65	0.0828	32.0

Group IV ( $7.0 < S \leq 10.0$ ) ‰. Total n = 42.

#	n	$\theta$	S	$\sqrt{v}$	$\sigma$
(32)	9	4.56	8.23	0.3036	6.86
33	9	5.33	7.62	0.2716	7.62
34 <sup>+</sup>	7	17.5	8.54	0.1780	13.6
35 <sup>+</sup>	7	18.7	7.29	0.1606	14.5
36 <sup>o</sup>	10	25.7	8.36	0.1163	23.9

Group V ( $10.0 < S \leq 12.0$ ) ‰. Total n = 8.

37	8	7.24	11.6	0.2909	8.86
----	---	------	------	--------	------

Special group VI, combined from # 9, 10, 17, 32. Total n = 34.

38	8	1.61	8.39	0.3270	0.336
39	8	1.76	8.24	0.3601	1.14
40	9	2.63	7.37	0.3191	2.43
41	9	4.17	5.83	0.3014	7.24

## Symbols

- n - Number of tests.  
 $\theta$  - Average temperature of ice samples (-C).  
S - Average salinity ‰ (g of salts per kg of ice).  
 $v$  - Ratio of the volume of brine contained in sea ice to the volume of the ice.  $\sqrt{v}$  is computed as an average from individual tests. It does not necessarily correspond exactly to the average  $\theta$  and  $S$  of the group.  
 $\sigma$  - Ring tensile strength (kg/cm<sup>2</sup>), multiplied by  $(1 - \frac{\theta - 10}{150})$ . (See eq 63 and eq 6a).  
o - Tests with precipitated NaCl.  
+ - Tests with precipitated Na<sub>2</sub>SO<sub>4</sub>.  
x - Perennial sea ice with suspected precipitated Na<sub>2</sub>SO<sub>4</sub>.

\* Revision of the analysis will be necessary, primarily on account of newly available test data which could not be utilized yet. About 300 additional tests on sea ice are now available; many more are expected after the summer of 1958 in connection with participation in an IGY project. Dr. E. R. Pounder (McGill University, Canada) has similar data available for young and warm sea ice (personal communication). In addition, several hundred similar tests on fresh water ice were performed at SIPRE.

A preliminary examination of newly available information reveals that the strength interpretation for temperatures between -25 and -30C has to be reduced, probably some 15%, unless new test data become available. More supporting material is now available for the increase in strength due to Na<sub>2</sub>SO<sub>4</sub>, and also for the effect of hysteresis during cooling and warming cycles. New evidence explains why precipitation of Na<sub>2</sub>SO<sub>4</sub> is not always associated with an increase in strength. This preliminary condensed table will be replaced by a more substantial and comprehensive table of test data, when it becomes practical to publish.



from all test results. In groups I - V, the data are grouped according to salinity and the results given in order of decreasing  $\nu$ . Group VI gives test results with an average  $\sqrt{\nu} > 0.300$  (No. 9, 10, 17, and 32) arranged according to increasing strength, to show the rapid increase in strength with a small change in  $\nu$  (see also Fig. 17). Each test number represents 6 to 13 tests, with an average of about 9. Jellinek (1957a) had to combine a minimum of 12 tests for his studies of the adhesive strength of ice, although these tests could be made very carefully under laboratory conditions.

All strength data are reduced to  $-10^\circ\text{C}$  according to eq 6a, with

$$\sigma_{10} = \sigma_b \left( 1 - \frac{\theta - 10}{150} \right) \quad (63)$$

$\sigma_b$  = bulk strength of fresh-water ice

$\theta$  = ice temperature

which holds roughly for fresh-water ice.

This is a reasonable relation, considering the results of Butkovich's tests (1954) made on fresh-water ice under pure tension. With the help of this relation, the effect of temperature on the strength of the elementary plates is eliminated. What remains is the effect of brine inclusions.

#### EMPIRICAL ANALYSIS

As the first step, group averages of strength values (not corrected to  $-10^\circ\text{C}$ ) for different narrow ranges of salinities were plotted versus temperature, giving a family of curves with constant salinities. One empirical result was that, at a given temperature, the reduction in strength is proportional to  $\sqrt{S}$ .

As brine volume is also proportional to salinity at a given temperature, we can assume that reduction in strength is proportional to  $\sqrt{\nu}$  at constant temperature. The relation for different temperatures is not known as yet, but a reduction proportional to  $\sqrt{\nu}$  (eq 16) is the most reasonable assumption.

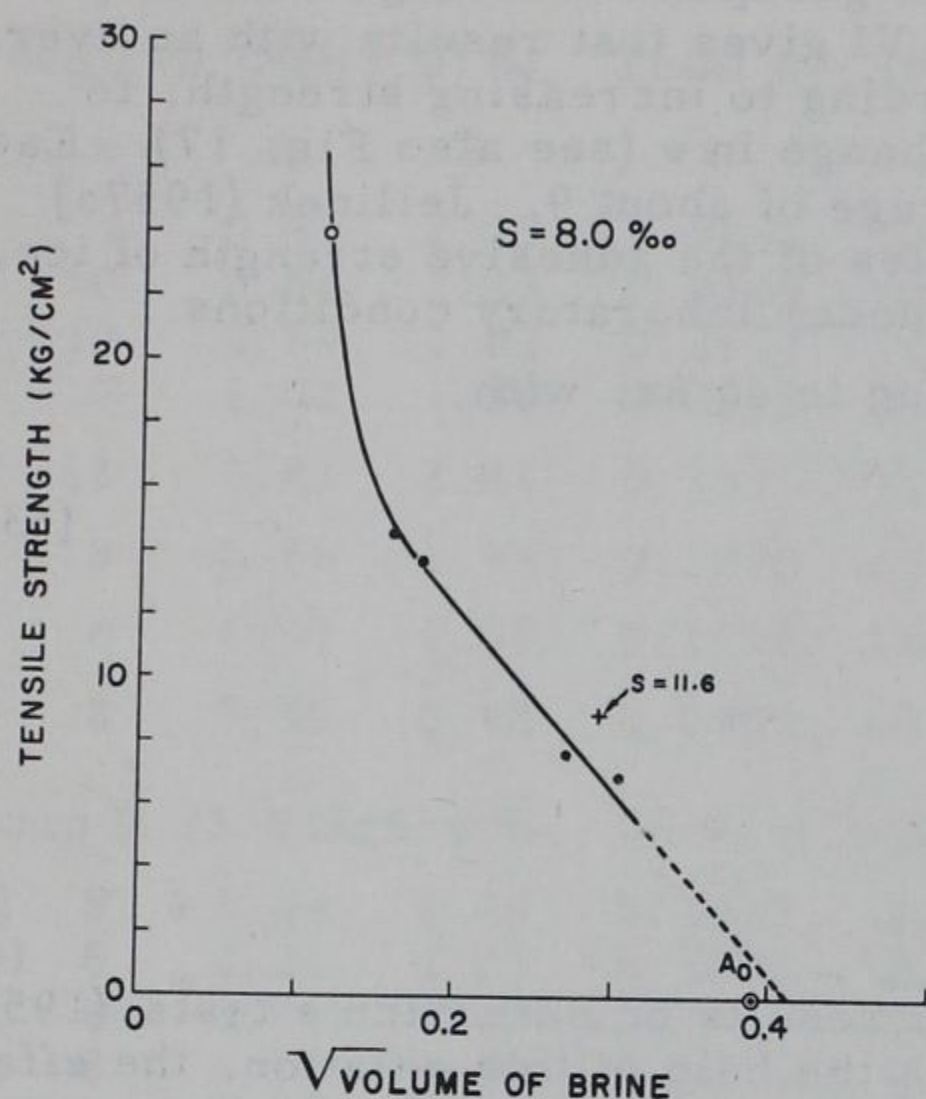
The empirical strength results (without any adjustment) plotted against  $\sqrt{\nu}$  for selected salinities (Fig. 14a-c) give a relation which is practically identical for any salinity except perennial ice (Fig. 15). The curves demonstrate a systematic and rapid increase of strength when NaCl precipitates. For high  $\sqrt{\nu}$  a linear relation results, leading to an intercept of zero strength somewhere near  $A_0$  with  $\sqrt{\nu} = 0.390$ . In all cases, however, a rapid increase in strength is observed at low  $\sqrt{\nu}$ , corresponding to low temperatures. This might be questionable in the case of 8.0 and 4.4‰ but is certainly confirmed for  $S = 5.9\text{‰}$ . The conclusion is that the precipitation of salts at low temperatures should affect the strength.

If  $\sigma$  is a unique function of  $\sqrt{\nu}$ , a superimposition of the curves in Figure 14a-c should result in one curve. This is actually the case for all practical purposes. Slight differences in the increasing branch at lower  $\sqrt{\nu}$  are to be expected according to the theory of salt reinforcement, suggested below. It is possible also that brine in contact with the ice surface around the brine inclusions causes a significant reduction in strength at higher temperatures (Assur, 1958, Fig. 16).

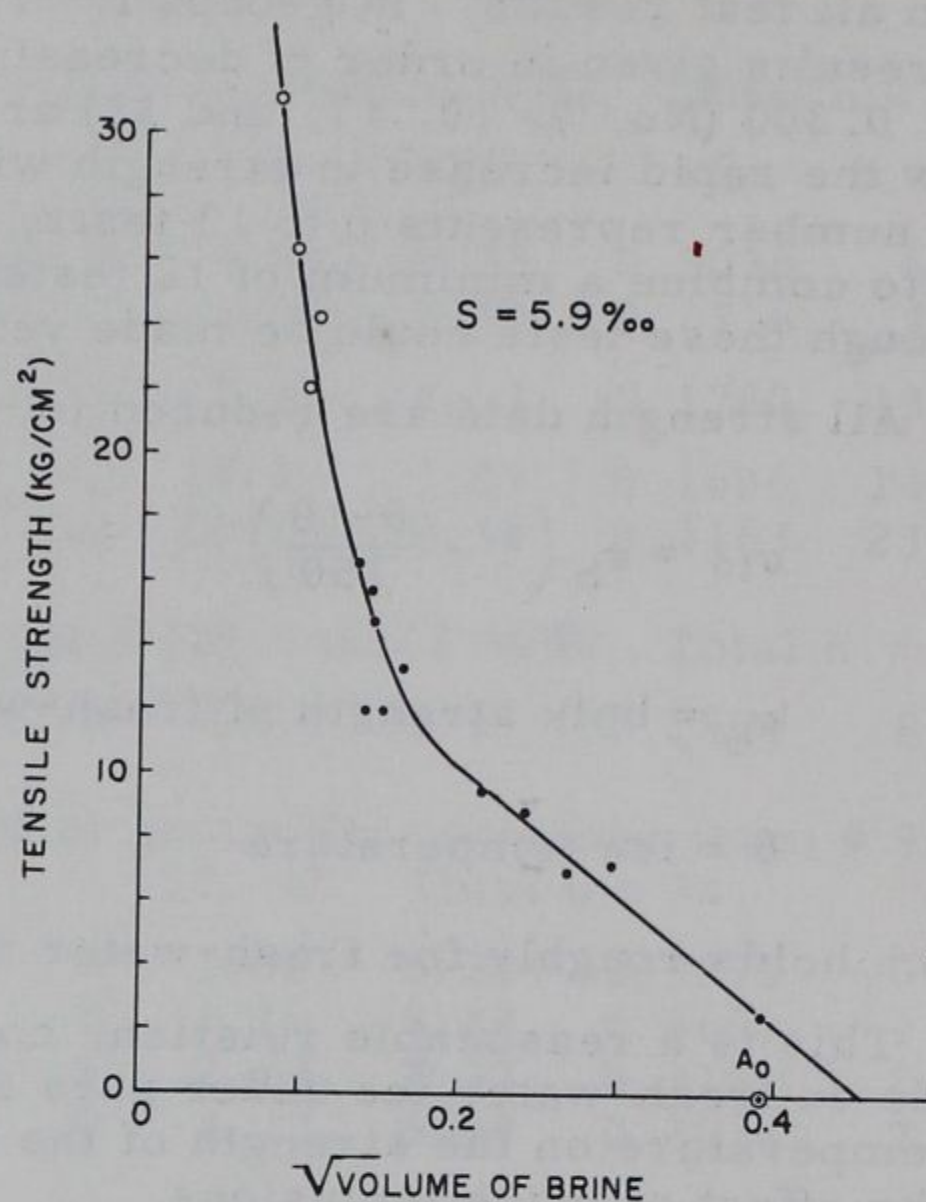
#### THEORETICAL ANALYSIS OF TEST RESULTS

After temperature correction (eq 63) the points fit the  $\sigma$ ,  $\sqrt{\nu}$  relation as shown in Figure 16. Ice samples with a temperature above  $-8.2^\circ\text{C}$  lie on line  $B_0 - B_f$  except for tests beyond  $B_2$  with  $\sqrt{\nu} = 0.300$ , when rapid deterioration begins. A few points with temperature  $-8.2 > \theta \geq -22.9^\circ\text{C}$  fall on this line, but about 70% of this group fall on line  $C - C_f$ , showing higher strength.

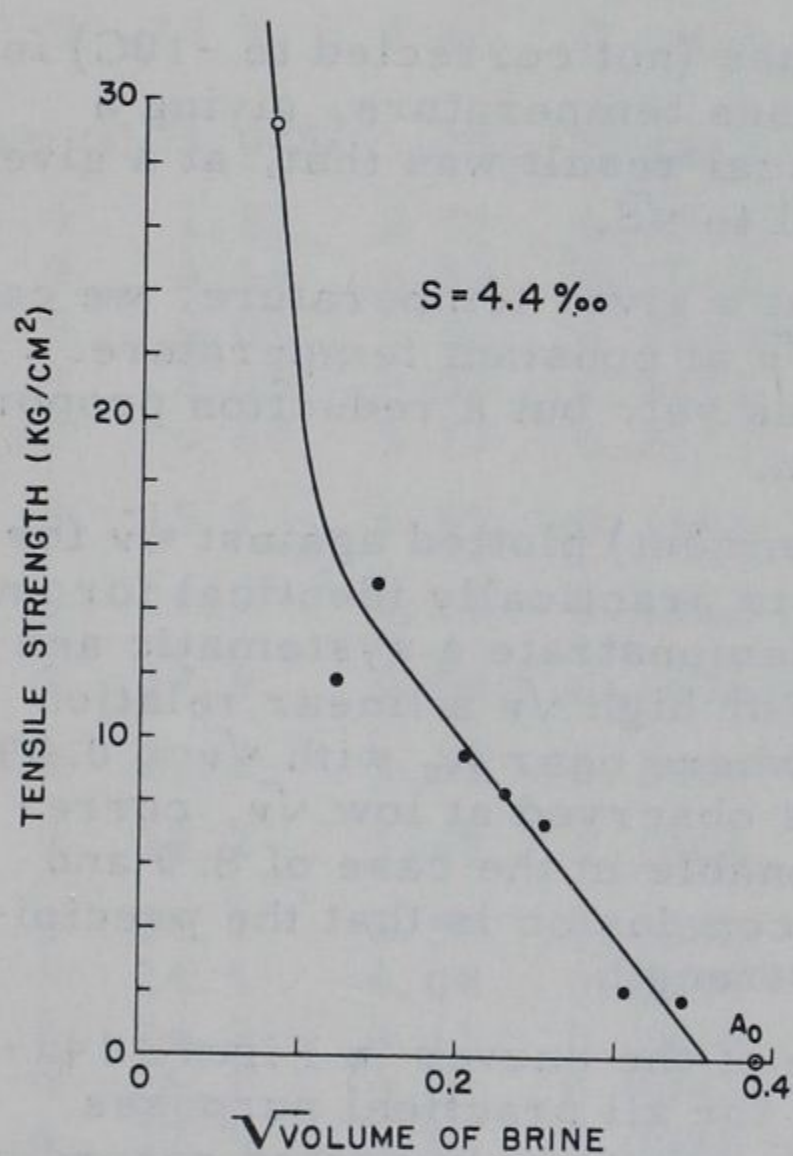




a.  $7.0 < S \leq 10.0$ , avg  $8.0\text{‰}$ , one test series with  $S = 11.6\text{‰}$



b.  $5.0 < S \leq 7.0$ , avg  $5.9\text{‰}$



c.  $3.0 < S \leq 5.0$ , avg  $4.4\text{‰}$

Figure 14a-c. Empirical relation of tensile strength of winter sea ice to  $\sqrt{v}$ , the square root of relative brine volume. Points with precipitated NaCl are given as circles, the remainder as dots. Each point represents an average of about 9 tests (not corrected for temperature; for a given  $S$ ,  $\sqrt{v}$  is determined only by the temperature).  $A_0$  indicates  $\sqrt{v} = 0.390$  where the strength is expected to be zero for theoretical reasons.

The slope of  $B_0 - B_f$  can be obtained from the data, in principle, giving the petrographic constant at the intercept of  $B_0$  with  $\sqrt{v}$ . The data, however, are not quite sufficient. We return, therefore, to eq 29 for an elliptical model.

A reasonable assumption is  $\gamma = 0.80$ ,  $\epsilon = 1.25$  and  $\gamma\epsilon = 1$ .  $\beta_1$  seems to be  $\frac{1}{2}$  (Table I). This combination gives the petrographic constant

$$p_2 = 2 \sqrt{\frac{\gamma\epsilon}{\pi\beta_0}} = 2 \sqrt{\frac{2}{\pi}} = 1.5958.$$

(64a)



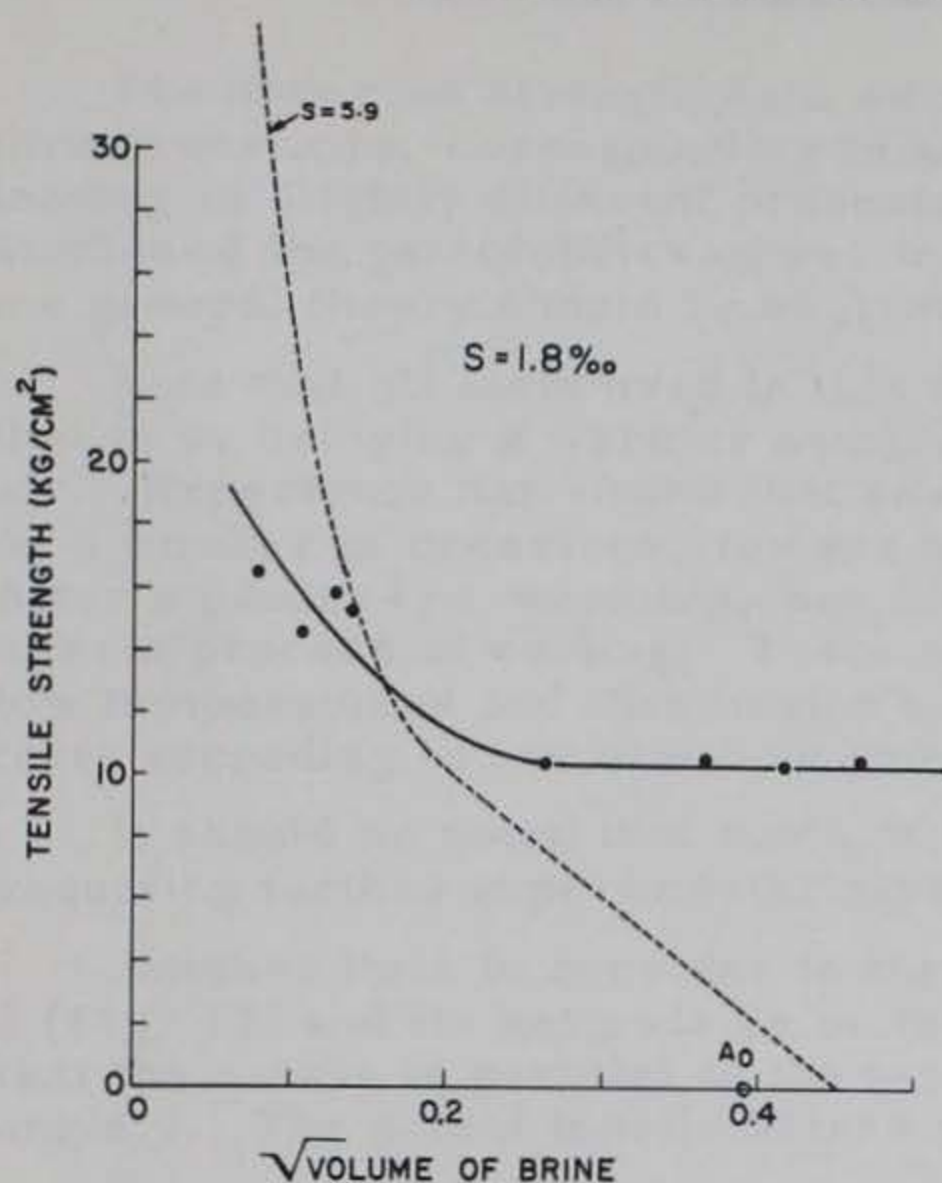


Figure 15. Empirical relation of tensile strength of perennial ice (Antarctica) to  $\sqrt{v}$ , the square root of relative brine volume. Data obtained during a short trip in the summer of 1957. (Curve for winter sea ice,  $S = 5.9\text{‰}$ , is shown for comparison.) The constant strength at high  $\sqrt{v}$  can be explained by hysteresis, due to the high  $\text{Na}_2\text{SO}_4 \cdot 10\text{H}_2\text{O}$  content. A very rapid breakdown and loss of strength occurs in perennial ice also after all  $\text{Na}_2\text{SO}_4$  goes into solution.

For the no strength condition we obtain

$$\sqrt{v}_{\sigma=0} = \frac{1}{p_2} = 0.6267. \quad (64b)$$

This is the location of point  $B_0$ . If  $\gamma\epsilon > 1$  (see note to eq 32) and  $\beta_0 < \frac{1}{2}$ , then  $p_2 > 1.5958$ . Further studies will determine its value.

Moderate changes in the petrographic constant  $p_2$  would not materially affect the relation, since no test data are available in the vicinity of point  $B_0$ . A condition whereby sea ice follows the path  $B_1 - B_0$  probably never exists, since a breakdown seems to occur soon after  $B_2$ .

Having assumed the location of point  $B_0$ , the slope of  $B_0 - B_f$  can be obtained by a method of least squares minimizing the relative errors of  $\sigma$  against  $\left(\frac{1}{p_2} - \sqrt{v}\right)$ . We then have

$$\sigma_0 p_2 = 22.66 \pm 0.50 \quad (\text{see eq 27b})$$

and

$$\sigma_0 = 14.20 \pm 0.31 \text{ for point } B_f.$$

Therefore (from eq 29)

$$\sigma = 14.20(1 - 1.596 \sqrt{v}). \quad (65)$$

The standard error of the constants is given.

Roughly the same strength ( $\sigma_0$ ) is observed for fresh-water ice in a wet condition. We define  $\sigma_0$  as the "basic strength" of sea ice for a particular type of test.

From Figure 16 we see that a linear relation  $\sigma$  versus  $\sqrt{v}$  might well hold for a certain part of the data (between  $D_0$  and  $B_2$ ). This indicates only that a relation of the general form of eq 16 and 21 is applicable, but not necessarily a circular nor even an elliptical model. The constants for eq 29 for an elliptical model were adopted for a preliminary computation of  $B_0$  only because no good petrographic data are available as yet.

For practical applications the elliptical model (eq 29) is preferred. This depends upon a knowledge of the petrographic constant

$$p_2 = 2\sqrt{\frac{\gamma\epsilon}{\pi\beta_0}}$$

in general and the constants  $\gamma$ , concerning the dimensions of the brine cylinders in the G-B plane,  $\epsilon$ , the elliptic ratio of the brine pockets and  $\beta_0$ , the relative spacing of brine pockets, in particular.

Note: Subsequent investigations, in particular those made in summer 1958 on the Arctic pack ice, revealed that the "basic strength" of sea ice is higher than computed here. In addition the "petrographic constant"  $p_2$ , as already suspected, appears to be higher than computed in eq 64a. More reasonable assumptions at present are  $\gamma = 0.9$   $\epsilon = 1.4$   $\beta = 0.4$ , which leads to  $1/p_2 = 0.49933$ .



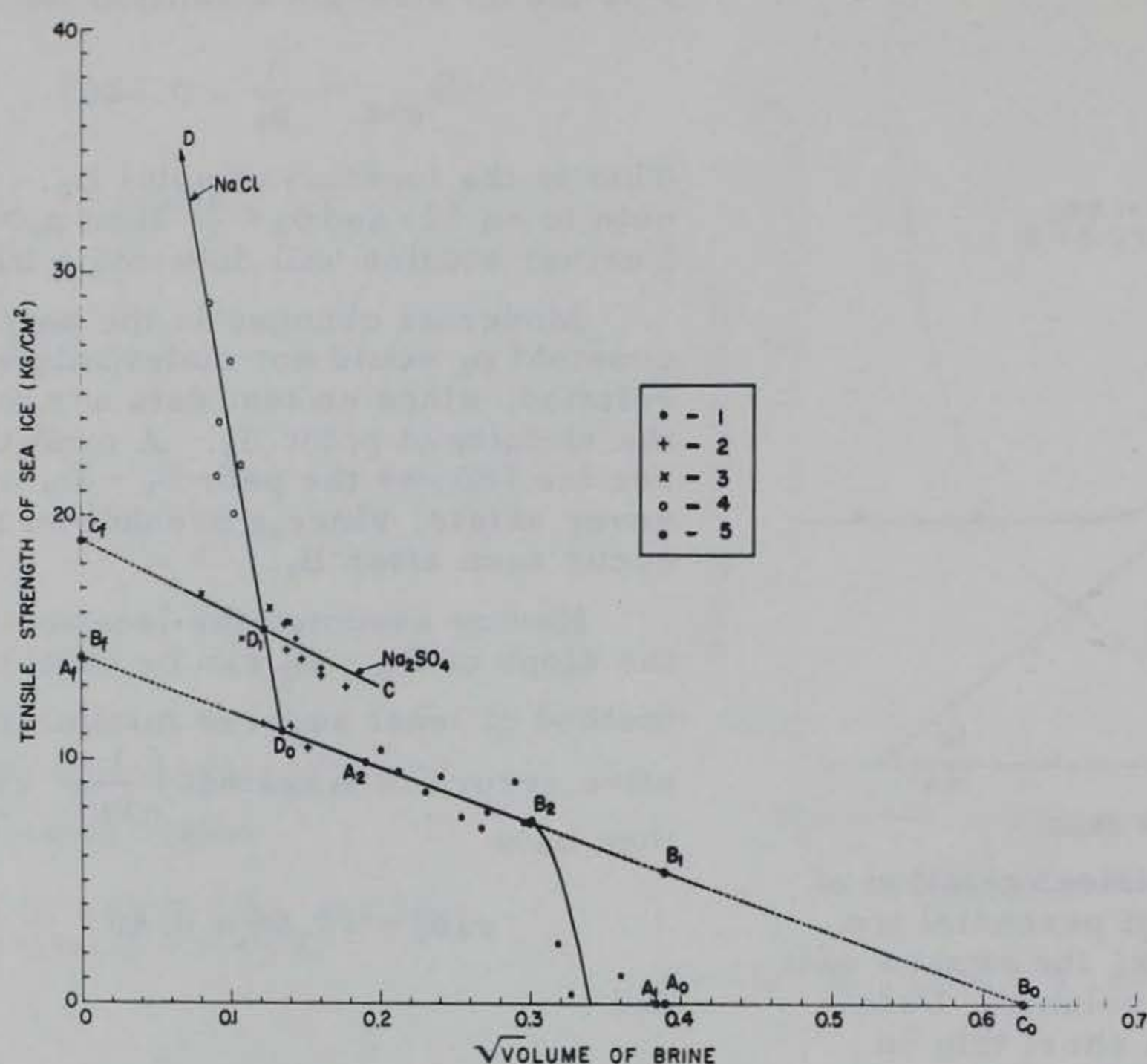


Figure 16. Measured tensile strength of sea ice versus  $\sqrt{v}$ , square root of the relative volume of brine. Each point represents an average of about 9 tests.

1. Winter ice,  $\theta > -8.2^\circ\text{C}$ . Ice-brine system. The "basic strength"  $\sigma_0 = 14.2 \text{ kg/cm}^2$ , is somewhat below the tensile strength of fresh-water ice.

2. Winter ice,  $-8.2 > \theta > -22.9^\circ\text{C}$ . Ice -  $\text{Na}_2\text{SO}_4 \cdot 10\text{H}_2\text{O}$  - brine system. The walls of the brine pockets are reinforced by salt particles. Initial rupture occurs in the reinforcement because of the high stress concentration. A relatively thin reinforcing layer increases the strength abruptly by one-third. Further thickening of the reinforcement layer does not lead to further increase in strength. Basic strength for  $\sqrt{v} = 0$  is  $\sigma_1 = 18.94 \text{ kg/cm}^2$ , with a few exceptions when reinforcement does not occur.

3. Perennial ice (Antarctica)  $-1.3 > \theta \geq -22.9^\circ\text{C}$ . Assumed ice -  $\text{Na}_2\text{SO}_4 \cdot 10\text{H}_2\text{O}$  - brine system. Probable enrichment in  $\text{SO}_4^{2-}$ . Walls reinforced by remaining salt particles.

4. Winter ice,  $\theta < -22.9^\circ\text{C}$ . Ice -  $\text{NaCl} \cdot 2\text{H}_2\text{O}$  - brine system. Walls effectively reinforced by salt particles. Initial rupture probably does not occur in reinforcement but in the ice bridging between elementary plates. The stresses in this ice bridging are reduced by the ratio of Young's moduli of the ice and the salt-ice reinforcement, as a first rough approximation.

5. Characteristic points:  $A_0$  - Transition from a non-strength "skeleton layer" to bridged plates with a sudden increase in strength. A layer with a sudden increase in strength can actually be observed in sea ice. It could be defined as the "bridging layer". The theoretical transition from a brine layer with parallel walls to elliptic brine pockets occurs from  $A_0$  to  $B_1$  - start of elliptic brine pockets after transition from parallel layer.  $\gamma_e = 1$  assumed here.  $A_1$  - initial bridging if brine pockets retain a constant width according to eq 38 with  $\gamma_0 = 0.390$ . The constant-width hypothesis results in a rather flat curve to point  $A_2$  - when the constant-width brine pockets may assume a circular shape with a further reduction according to the circular model, until the final point for  $v = 0$ ,  $A_f = B_f$  is reached, which gives the "basic strength"  $\sigma_0 = 14.20 \text{ kg/cm}^2$  for this case.  $B_0 = C_0$  - no-strength point, according to the elliptical model (eq 29) assuming  $\beta_0 = \frac{1}{2}$  and  $\gamma_e = 1$ .  $B_2$  - sudden drop in strength (according to experiments at  $\sqrt{v} = 0.30$ ; further drop empirically assumed as proportional to  $(v - 0.09)$ ). Transition from normal to deteriorating and bleeding sea ice. C -  $C_f$  - line for sea ice, reinforced by precipitation of  $\text{Na}_2\text{SO}_4 \cdot 10\text{H}_2\text{O}$ . Precipitation with (cont.)



The observed strength data were used (Figure 16) in order to derive essentially three constants, corresponding to assumed models. Other models may be assumed, leading to slightly different presentations. Final decision can be made after statistical studies of the petrofabrics of sea ice. In particular the nondimensional constants in the general theory should be evaluated.

Note that all tests used in this figure were performed using the same procedure, that is by bringing a warmer sample from the ice sheet to a colder environment, the air. Experience has shown that sea ice exhibits a considerable hysteresis, observed on a number of occasions, for example on our Antarctic samples (Fig. 15, 21). After a process of warming, sea ice shows different strength characteristics than after a process of cooling. Tests on samples which were stored for a longer time at low temperatures and then heated to a higher temperature should not be combined with tests according to our standard procedure, but should be discussed separately.

It should be noted that some of the assumptions are still working hypotheses, requiring further experimental verification.

Another item to consider is that the orientation of the elementary plates at point 2 (Fig. 13) and its antipode 2a on the other side of the hole is not necessarily such that the  $c$ -axis is parallel to the tensile stress. In general it will be inclined by an angle  $\delta$ . The actual tensile stress  $\sigma_t$  developed parallel to the  $c$ -axis is then

$$\sigma_t = \sigma \cos \delta. \quad (66)$$

Whether the sample breaks at point 2 or at its antipode will depend on the orientation of the elementary plates at these points. A complete theory of the failure of rings with the typical structure of sea ice will be worked out when the results of additional test series with  $\delta = \pi/2$  are available.

Before we adopt a (true) elliptical model, we will examine how the circular and constant-width models proposed by Anderson (1957) correspond to our data. Figure 17, essentially but not exclusively, illustrates Anderson's conclusions (1957) based upon a study of photomicrographs by Weeks (1958). The figure shows how these two models may be derived for the transformation of brine pockets with changing temperature.

Both the models have their deficiencies, if compared with the strength results and actual photographs of brine inclusions. The true shape of brine pockets is probably somewhere between these two assumptions. The (true) elliptical model, according to our eq 29, would also give a straight line in a  $\sigma, \sqrt{v}$  presentation but would correspond better to the actual shape of brine pockets and to their change with temperature.

Anderson (1957) observed that the minimum width of a brine layer is 0.07 mm. This gives directly a corresponding brine volume of

$$v_0 = \frac{0.07}{a_0} = \frac{0.07}{0.46} = 0.152$$

or  $\sqrt{v} = 0.390$  on Figure 16. He limited his discussion to the transition  $A_0 - B_1$ , from a parallel brine layer to a circular model. However, the constant  $v_0$  has broader implications. It appears in our derivation of eq 34 and in eq 38. The point  $A_1$  differs slightly from  $A_0$  due to the additional term in eq 38. Furthermore, the

---

Figure 16 (cont.)  
 reinforcement occurs in about 70% of all cases in winter ice and probably always in perennial ice.  $C_f$  - "basic strength" of sea ice, reinforced by  $\text{Na}_2\text{SO}_4 \cdot 10\text{H}_2\text{O}$ .  $\sigma = 18.94 \text{ kg/cm}^2$ .  $D_0 - D_1 - D$  line shows rapid increase in strength due to reinforcement by  $\text{NaCl} \cdot 2\text{H}_2\text{O}$ . Line adjusted to  $S = 6\%$ . Reinforcement is proportional to  $\sqrt{v_s} - \sqrt{v}$ , with  $\sqrt{v_s}$  equal to the relative brine volume at  $-22.9^\circ\text{C}$  (depends upon salinity).  $D_0$  - point, corresponding to  $-22.9^\circ\text{C}$ , when  $\text{NaCl} \cdot 2\text{H}_2\text{O}$  begins to precipitate; depends upon salinity.  $D_1$  - crossing of  $D_0 - D$  line with  $C - C_f$  line. Below  $D_1$  the actual strength is assumed to be the same as along  $C - C_f$ .



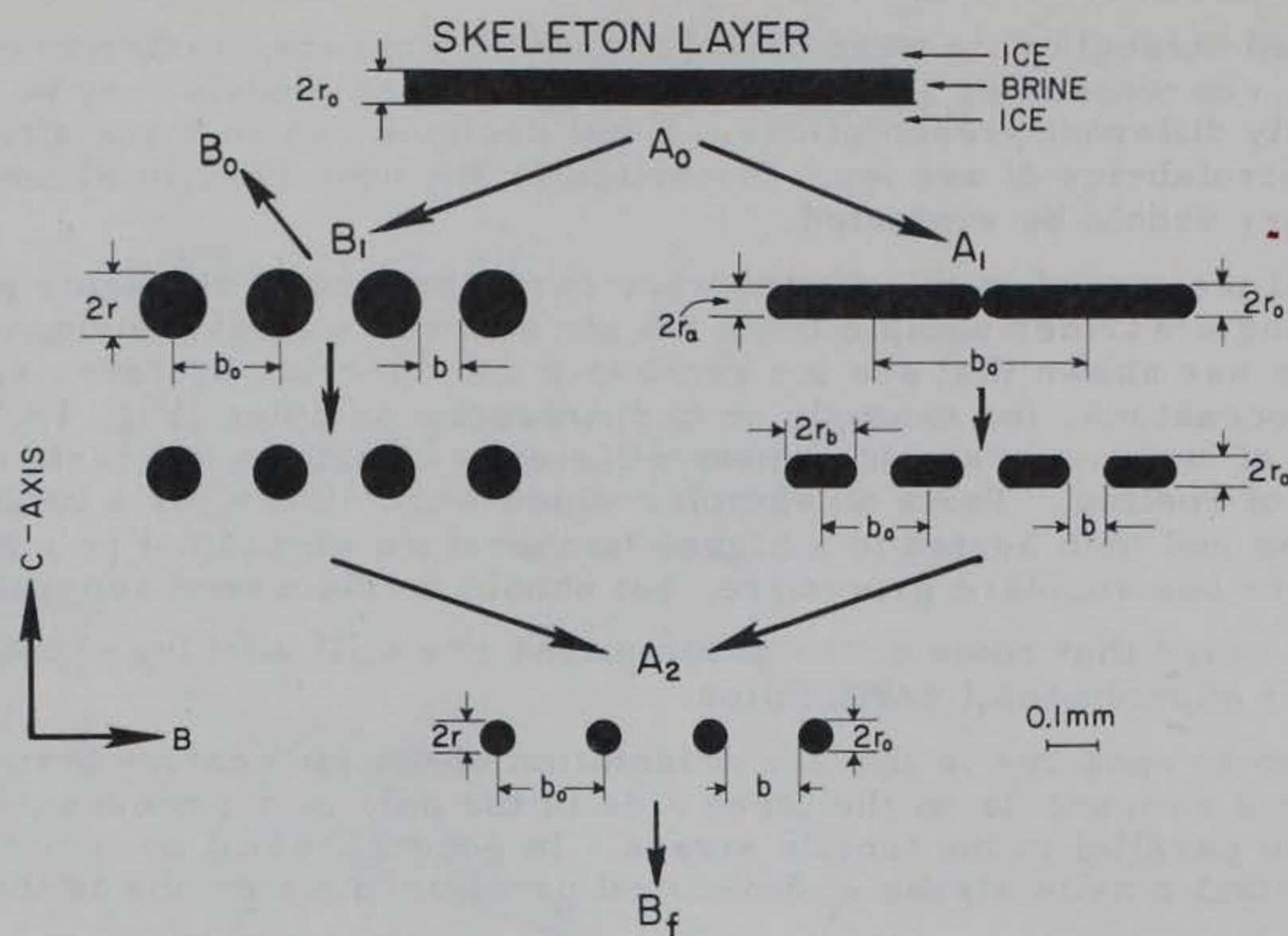


Figure 17. Two models for the transformation of brine pockets with changing temperatures (see Fig. 16 also). Shows an idealized cross section of brine pockets perpendicular to the direction of growth. At the lower surface of sea-ice sheets growth proceeds with vertically oriented pure ice plates, parallel within each individual ice crystal. These "elementary plates" later become the basic structural element of sea ice. The plates thicken gradually, leaving less and less brine in the interstitial layers. Finally surface tension causes splitting or necking of the brine layer, evidently with a sudden increase in strength. We designate the level where this transition from "elementary plates" occurs as the "bridging layer", the strengthless layer below that level as the "skeleton layer". Its normal thickness is 2.5 cm, independent of total thickness of the ice sheet. The minimum possible width of the brine layer before splitting is  $2r_0 \cong 0.07$  mm. Assuming that brine volume remains the same after splitting and following path  $A_0 - B$  for the circular model gives  $2r = 0.14$  for  $B_1$ . A relative spacing  $\beta_0 = b_0/a_0 = \frac{1}{2}$  with  $b_0 = 0.23$  mm is assumed. Further reduction in cross section can be computed from the brine volume, obtained from the phase diagram. The brine pockets are reduced to  $2r = 0.07$  mm at  $A_2$  and to  $2r = 0$  at  $B_f$  at extremely low temperatures. For the "constant width" model, path  $A_0 - A_1 - A_2 - B_f$  is followed. The brine pockets retain a constant width, with relative spacing  $\beta_0 = 1$  when initial necking occurs. In this case the increase in strength occurs only gradually. This gradual increase in strength is usually observed in very young sea ice. With further necking a relative spacing  $\beta_0 = \frac{1}{2}$  is achieved and finally circular pockets are left with  $2r = 0.07$  mm at  $A_2$  and further gradual transition to  $B_f$ . During warming cycles the process can take the  $B_f - A_2 - A_1$  path with brine pockets of constant width until the no-strength condition  $A_1$  is reached, or the path  $B_f - A_2 - B_1 - B_0$  with the circles enlarging until they touch with a breakdown of strength at  $B_0$ . The minimum condition under which a skeleton layer can exist is  $\sqrt{v} = 0.390$ . The first "circular" layer has the same  $\sqrt{v} = 0.390$ . The second circular and also the second "constant width" layer shown here corresponds to  $\sqrt{v} = 0.300$ . A rapid decrease of strength occurs if brine pockets enlarge beyond this value. The first constant-width layer has  $\sqrt{v} = 0.384$ . The  $A_2$  condition occurs at  $\sqrt{v} = 0.191$ . Acknowledgment: The concept of the two models and their changes explained in this diagram was first proposed by Anderson (1957). He defines the second model as "elliptical"; it is included in our general theory as a "constant width" model. Nakaya (1956) defined the criterion for the "splitting" of parallel layers into circular cylinders, as governed by surface tension. Applying this concept to sea ice, Anderson (1957) was the first to derive a criterion (cont.)



constant has to be used also in any elliptical model for the transition from a no-strength condition. It is unlikely, in my opinion, that a complete transition from the skeleton layer to a circular form occurs in the bridging layer. Most probably the transition process ends up with an incomplete circle, namely an ellipse, which gradually becomes smaller as the temperature drops. It would be very important to know the shape of the resulting initial ellipses, since the strength of the bridging layer obviously depends upon it. This strength again is important in the evaluation of the flexural strength of a sea-ice sheet.

The assumption of a sudden change in strength in the vicinity of  $A_0$  seems to be justified by the data available. No great significance should be attached to the fact that this strength transition occurs at a lower  $\sqrt{\nu}$  than  $A_0$ . There are a number of possible reasons for this, which will be discussed when more data are available from investigations on arctic pack ice in the summer of 1958. It must be pointed out, however, that the low strength data refer to conditions of spring time deterioration. Anderson assumes in his circular model that the circles gradually coalesce during warm-up, which would be a path along  $B_1 - B_0$  (Fig. 17) not a sharp drop after  $B_2$ , as actually observed (Fig. 16). The jump  $A_0 - B_1$  in his circular model is reserved for the freezing process.

The relation of the sharp drop after  $B_2$  to changes in brine inclusions is still to be investigated. Most probably  $\gamma$  becomes 1 at  $B_2$ , i. e. interrupted cylinders change to continuous cylinders and the brine inclusions enlarge in the interstitial planes in the B-direction, leading to a rapid breakdown of the interlaminar bridging.

The constant-width model would give a fairly flat curve from  $A_1$  to  $A_2$  both for cooling and warming conditions. The data do not necessarily suggest that eq 38 should hold.

For the time being, we assumed an empirical relation for the sharp drop in strength at  $B_2$ :

$$\sigma = \sigma_{(65)} [1 - 40 (\nu - 0.09)] \quad (67)$$

with  $\sigma_{(65)}$  computed from eq 65.

A part of future petrographic research should be to plot  $2r_b$ , the length of the brine pockets along the B line in the B - c plane (see Fig. 5), versus  $\sqrt{\nu}$ . This should result in a straight line going through 0, 0 if a circular, elliptical or any model according to eq 16 and 21 is correct. The sizes to be expected for circular and constant width models with spacing  $\beta_0 = \frac{1}{2}$  and  $\beta_0 = 1$  are given in Figure 18.

### THEORY OF REINFORCEMENT BY SALTS

None of the relations derived in the general theory for three groups of models should hold when salts start to precipitate. This occurs whenever the ice temperature drops below  $-8.2^\circ\text{C}$ . In perennial ice the effect of solid salts is evident almost up to the melting point (see Fig. 3).

Figure 19 represents a model of reinforced brine pockets. If the salt particles together with ice are deposited on the walls of the brine inclusions, there is effective reinforcement at the place of highest stress concentration (in the B-B plane at the walls). Tensile stresses in the direction of the c-axis are assumed, but shear in the B-B direction gives a similar effect in the case of the second model.

---

Figure 17 (cont.)  
for the sudden transition from the skeleton layer to sea ice proper. ( $A_0$  - called here the "Anderson point"). The strengthless "skeleton layer" itself with its distinct transition to stronger sea ice due to the internal "bridging" of the "elementary plates" was first found and defined by Assur in the winter of 1955. Its existence has been considered by SIPRE in routine computations since that time.



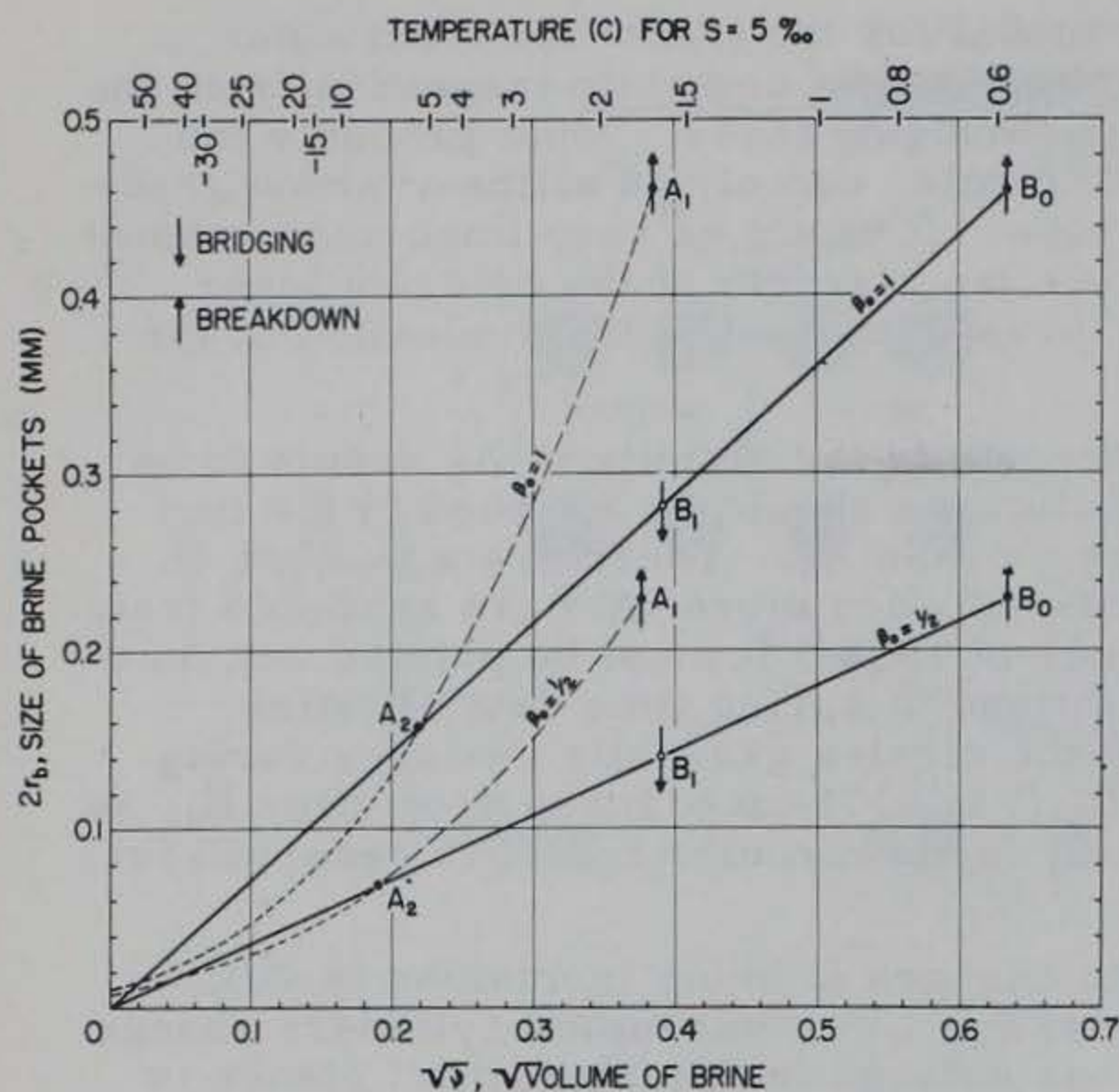


Figure 18. Expected length of brine pockets, depending upon model and spacing, as a function of the relative brine volume. Linear relations result for any model, satisfying eq 21. An elliptical model (eq 29) with  $\gamma\epsilon = 1$  is assumed for the solid lines and a constant width model (eq 38) for the dashed lines. This model will be valid from  $A_1$  to  $A_2$ , when a circular form is reached; the lines with short dashes below  $A_2$  are purely mathematical extensions. The upper scale shows the temperatures when the particular size of brine pockets should be observed for a salinity of 5‰ (average value for sea ice).

with the further thickening of the reinforcement, since the stress concentration is located only in the immediate vicinity of the wall. The rate of transition to this reinforcement and the minimum necessary width is not computed yet.

This model apparently holds for the relatively small concentration of salts when  $\text{Na}_2\text{SO}_4 \cdot 10\text{H}_2\text{O}$  precipitates, as evidenced by the increased strength of the corresponding group along the line  $C - C_f$  in Figure 16. Perennial ice still has this increased strength even if the temperature rises about  $-8.2^\circ\text{C}$ .

It is reasonable to assume that  $C_0 = B_0$  in Figure 16. Applying the same method of least squares gives

$$\sigma_1 = 18.94 \pm 0.27 \text{ kg/cm}^2. \quad (68)$$

The actual increase in strength due to the precipitation of  $\text{Na}_2\text{SO}_4 \cdot 10\text{H}_2\text{O}$  is

$$\frac{18.94}{14.20} = 1.334 \pm 0.035.$$

The standard error of the ratio is computed with the aid of the error propagation formula.

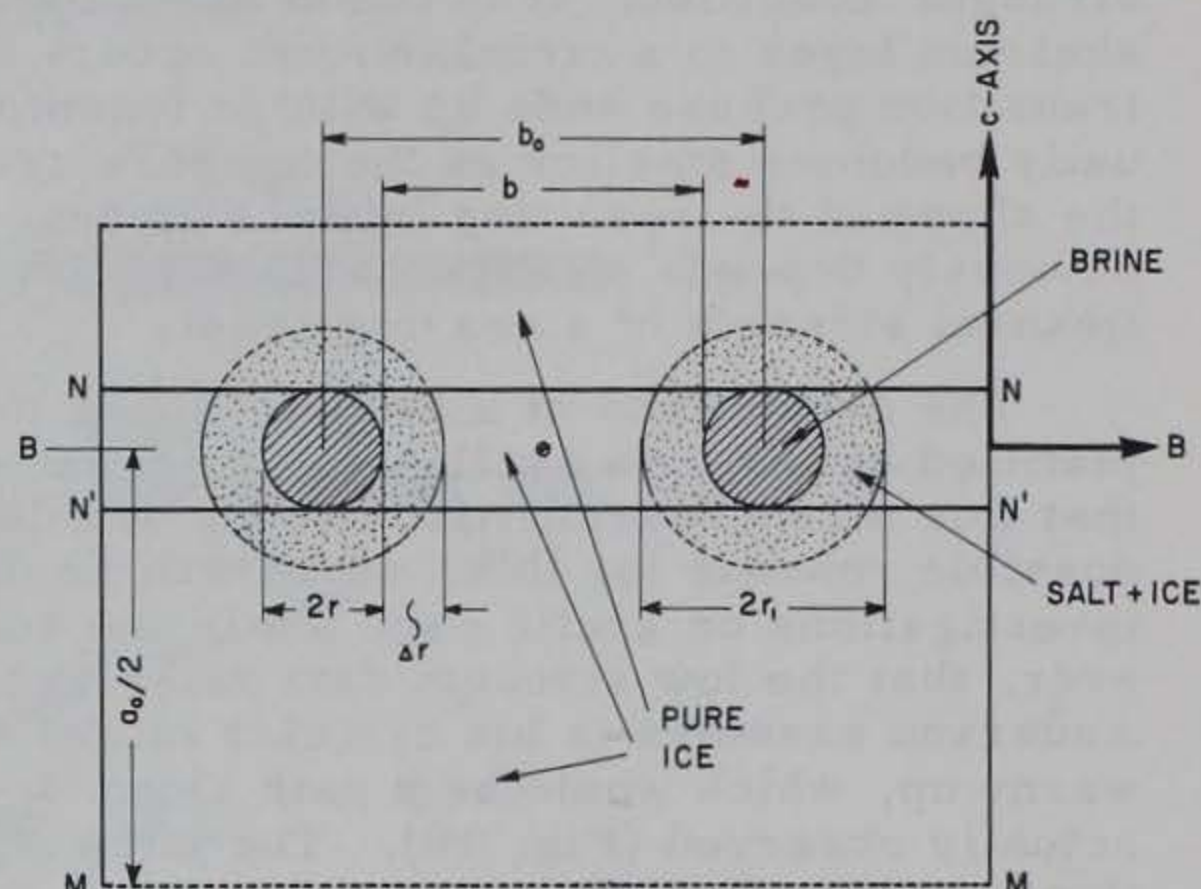


Figure 19. Reinforcement of brine pockets by salt-ice mixtures. For simplicity, circular pockets are drawn. The small bubble in the center is a symbol for stress concentrators or local defects in the B-B plane. Brine pockets are not drawn to scale.  $r_1$  = radius of brine pocket before precipitation of salt.  $r$  = radius of brine pocket after precipitation of salt.

Two models may be assumed. In the first, Young's modulus of the salt-ice reinforcement does not differ much from the modulus for ice. The rupture occurs within the reinforcement. A relatively thin layer of salt-ice rather abruptly increases the strength of sea ice but no further increase is observed



Stress concentration in a narrow layer around the brine pockets is essential for this concept. The low increase in strength by  $\frac{1}{3}$  can be explained by partial failure in shear. If, as suspected, the petrographic constant  $1/p_2 < 0.6267$ , as assumed above in eq 64b, then a lower computed increase in strength due to  $\text{Na}_2\text{SO}_4$  would result.

The second model assumes a substantial difference in Young's moduli. The strength of this salt-ice mixture might be so high that the initial failure occurs in the ice but not in the reinforcement. It is reasonable to assume that this initial failure occurs somewhere along the B-B line, because of remaining small stress concentrators or local defects, but not in the bulk of the ice between the layers with brine inclusions.

This might explain the strength behavior of sea ice when  $\text{NaCl}$  precipitates, which it does in much larger quantities than  $\text{Na}_2\text{SO}_4$  (Fig. 9). We see immediately that its presence in the form of  $\text{NaCl} \cdot 2\text{H}_2\text{O}$  increases the strength very appreciably and apparently in another manner than  $\text{Na}_2\text{SO}_4 \cdot 10\text{H}_2\text{O}$  (Fig. 16). The assumption of small remaining local defects is reasonable, considering Figure 11d in Nakaya (1956), as well as the use of the small quantity  $\epsilon$  by Nakaya in his eq 1-3, which all deal with similar phenomena in fresh-water ice (splitting of layers into columns). The nature of these defects still has to be studied.

The stress distribution can be treated as similar to a reinforced hole in a plate (collars around holes). However, we will apply a simplified approach, which can be used for tension as well as for shear with initial rupture in the B-G plane. Further rupture can occur around or through the reinforcement; the effect of increase in strength still remains.

Consider a 1 cm thick horizontal layer (perpendicular to the G-axis) between two assumed nondeformable plates (NN-N'N', Fig. 19). The force acting upon the length  $b_0$  in the direction of the c-axis at failure is  $\sigma b_0$ . Since  $2r$  is taken up by brine, only the length  $b$  is effective. The stresses in  $2\Delta r$  are higher in the proportion  $E_s/E_i$ , where

$E_i$  = Young's modulus for ice

$E_s$  = Young's modulus for salt-ice mixture.

Neglecting the curvature, which can be introduced later, the actual stress  $\sigma_0$  developed in the ice itself is

$$\sigma_0 = \frac{\sigma b_0}{b_0 - 2r - 2\Delta r + 2\Delta r (E_s/E_i) c} \quad (69)$$

The constant  $c$  accounts for the simplifications introduced, in particular the assumption that the layer NN - N'N' is included between two nondeformable plates. Actually only the line B - B and M - M do not deform for reasons of symmetry. Lines initially parallel to B - B do deform, which does not agree with eq 69.

The relative increase in strength is

$$\frac{\sigma}{\sigma_0} = 1 - \frac{2r}{b_0} + \frac{2\Delta r}{b_0} \left( \frac{E_s}{E_i} c - 1 \right). \quad (70)$$

This would hold for a circular model with  $\gamma = 1$ . For the more general case of any cylindrical model we obtain, similar to eq 13b

$$\frac{\sigma}{\sigma_0} = 1 - \frac{\gamma}{\beta_0} \frac{2r_b}{a_0} + \frac{r}{\beta_0} \frac{2\Delta r_b}{a_0} \left( \frac{E_s}{E_i} c - 1 \right). \quad (71)$$



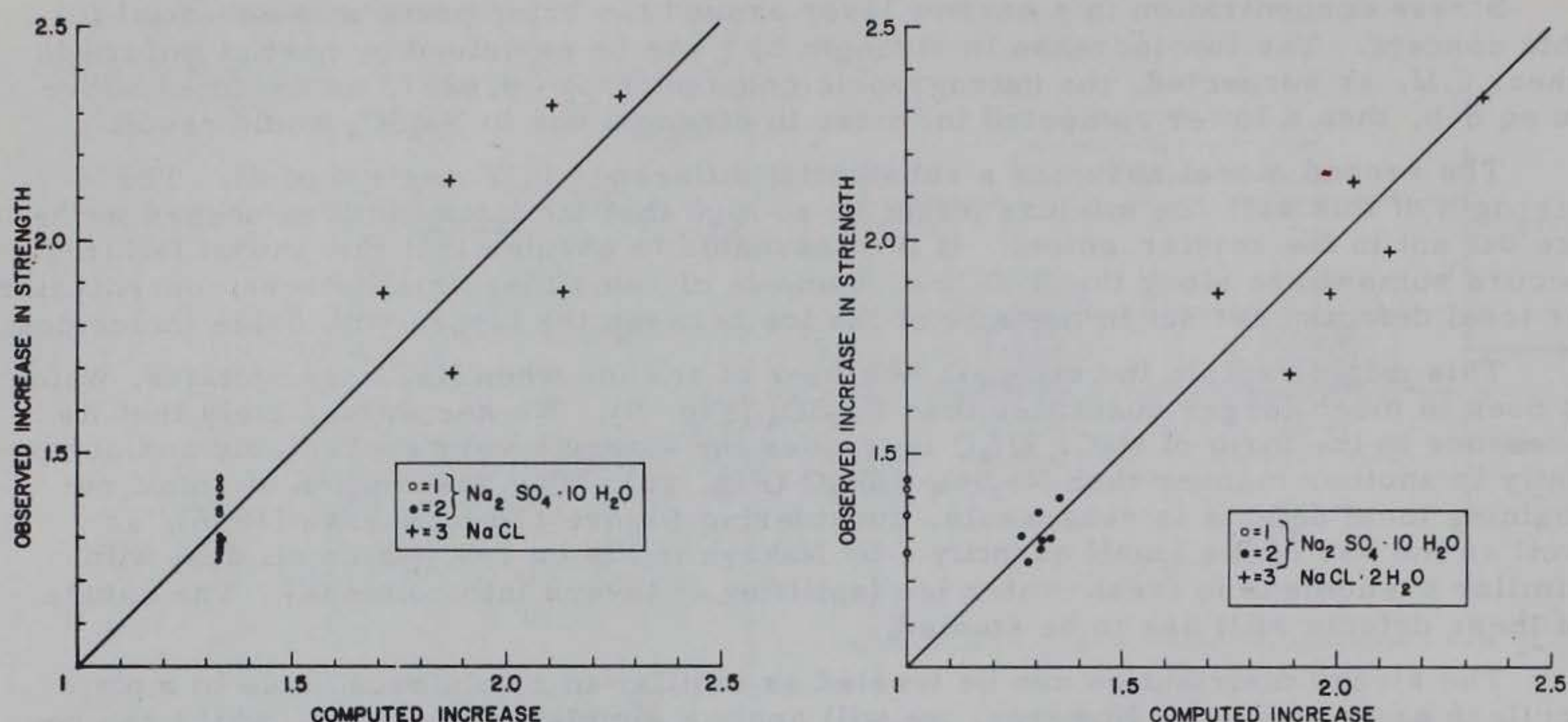


Figure 20. Increase of strength due to the precipitation of salts. Each point represents an average of about 9 tests. 1 - Perennial ice (Antarctica)  $-1.3 \geq \theta > -9^\circ\text{C}$ . Reinforcement by remaining  $\text{Na}_2\text{SO}_4 \cdot 10\text{H}_2\text{O}$  suspected. (High  $\text{SO}_4^{=}/\text{Cl}$  ratio.) 2 - Winter ice  $-8.2 > \theta \geq -22.9^\circ\text{C}$ . Reinforcement by  $\text{Na}_2\text{SO}_4 \cdot 10\text{H}_2\text{O}$ . 3 - Winter ice  $-22.9 > \theta$  C. Reinforcement by  $\text{NaCl} \cdot 2\text{H}_2\text{O}$ .

Similar to the reasoning in eq 18 - 21 and 27 - 29, we find for the elliptical model

$$\frac{\sigma}{\sigma_0} = 1 - 2\sqrt{\frac{\gamma\epsilon\nu}{\pi\beta_0}} + 2\sqrt{\frac{\gamma\epsilon}{\pi\beta_0}} \left( \frac{E_s}{E_i} c - 1 \right) \Delta\sqrt{\nu} \quad (72)$$

where

$$\Delta\sqrt{\nu} = \sqrt{\nu_s} - \sqrt{\nu}$$

and

$$\nu_s = \text{brine volume at } -22.9^\circ\text{C}.$$

Thus, the strength of sea ice after NaCl starts to precipitate can be computed according to eq 29, accounting for the reduction in cross section by the remaining brine and adding a term which accounts for the reinforcement.

Following an earlier concept

$$\sigma_1 = \sigma_{(65)} (1 + c_1 \Delta\sqrt{\nu}) \quad (73)$$

with  $\sigma_{(65)}$  computed according to eq 65; the constant  $c_1$  was determined as

$$c_1 = 26.25 \quad (73a)$$

by the method of least squares, minimizing the relative error in the observed ratio  $\sigma_1/\sigma_{(65)}$  versus  $\Delta\sqrt{\nu}$ . The numerical difference between eq 73 and 72 is small.

The position of the line  $D_0 - D$  in Figure 16 depends upon the location of  $\sqrt{\nu_s}$ , which in turn is a function of salinity. All these data, shown by circles, were adjusted to  $S = 6\text{‰}$ .

Figure 20a shows how the observed increase in strength compares with the computed increase. The agreement is not startling but the effect of solid salts is quite



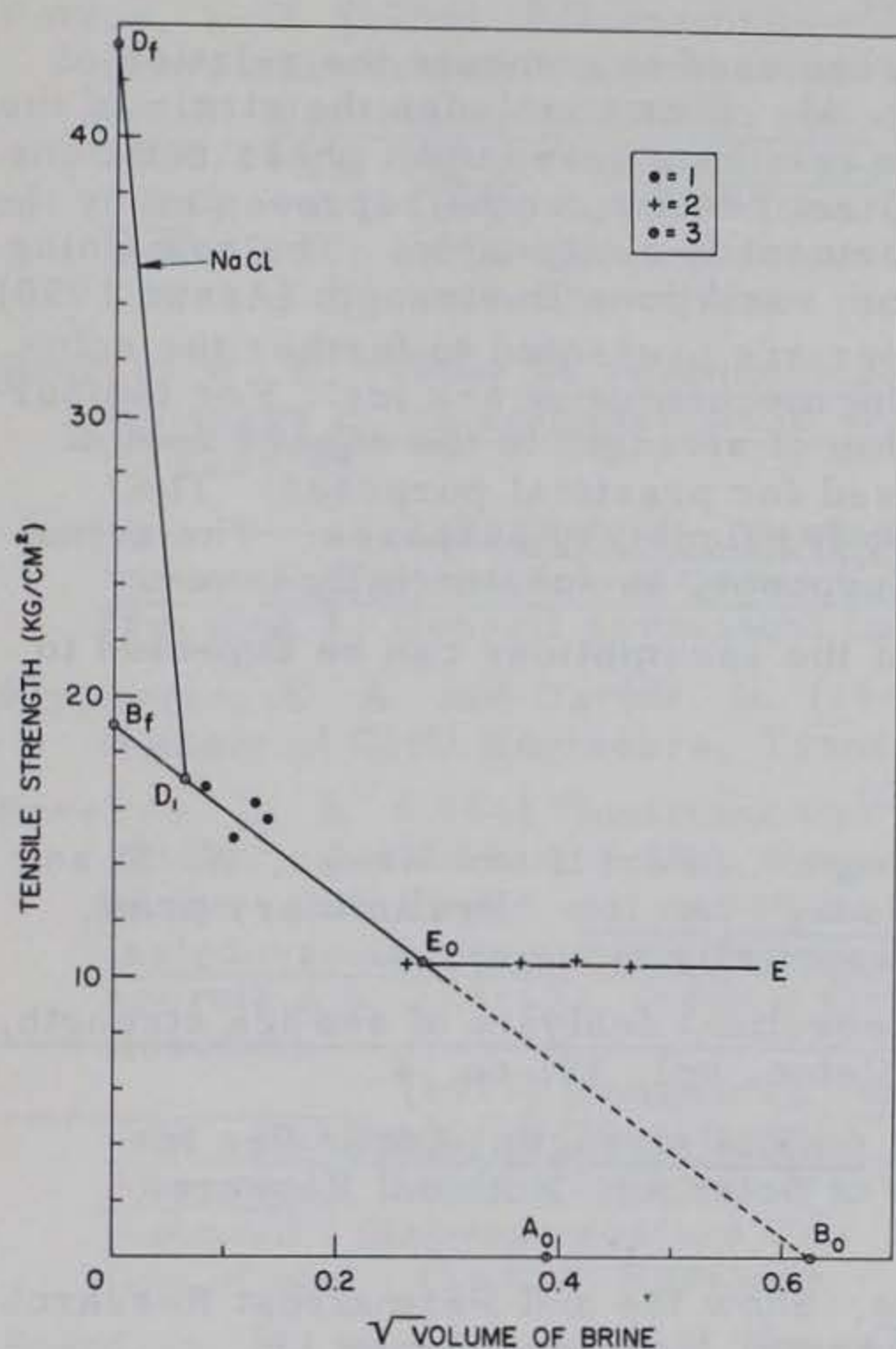


Figure 21. Hypothetical strength relations for perennial ice, compared with actual tests. Each point represents an average of about 9 tests, all made in Antarctica. 1 - Perennial ice  $-1.3 \geq \theta > -9^\circ\text{C}$ . 2 - Perennial ice  $-8.2 > \theta \geq -22.9^\circ\text{C}$ . 3 - Characteristic points  $A_0$ ,  $B_0$ ,  $B_f$ ,  $D_1$  and  $D_f$  correspond to the points used in Fig. 16, 18. Point  $E_0$  corresponds to the upper temperature of formation of  $\text{Na}_2\text{SO}_4 \cdot 10\text{H}_2\text{O}$ , which is  $-1.25^\circ\text{C}$  according to Nelson (1953). The assumption is that the strength decreased with increasing temperatures (higher  $\sqrt{v}$ ) until  $-1.25^\circ\text{C}$  is reached. Then, as the test data show, the strength remains constant, apparently until all  $\text{Na}_2\text{SO}_4$  went into solution (path  $E_0 - E$ , hysteresis effect). The following collapse in strength with transition to mush occurs suddenly, as evidenced by the extremely rapid deterioration of the McMurdo ice runway.  $B_0$  corresponds to  $\sqrt{v} = 0.627$ ; for  $B_f$   $\sigma_1 = 18.94 \text{ kg/cm}^2$ .  $D_1 - D_f$  line corresponds to  $S = 2\text{‰}$ .

evident. Figure 20 shows that a somewhat better agreement with data can be obtained by computing the increase in strength, as compared to eq 65, as proportional to  $\Delta\sqrt{v}/\sqrt{S}$  for reinforcement by  $\text{Na}_2\text{SO}_4 \cdot 10\text{H}_2\text{O}$  and by  $\text{NaCl} \cdot 2\text{H}_2\text{O}$ , using different constants. (The increased strength of perennial ice cannot be readily represented in this case). Such an assumption, however, does not appear reasonable at present although further studies in this direction would be justified. Since  $\sqrt{v} = \sqrt{S}v(1)$ , with  $v(1)$  the brine volume for  $S = 1\text{‰}$ , we obtain

$$\Delta\sqrt{v}/\sqrt{S} = v_1(1) - v(1).$$

$v_1(1) = 0.00305$  is a constant, equal to the brine volume at  $-22.9^\circ\text{C}$  for  $S = 1\text{‰}$ . The minimum value of  $v(1)$  is zero, so that the maximum increase in strength would be a constant, independent of salinity. The approach to the maximum would be proportional to the decrease of brine volume after the precipitation of  $\text{NaCl}$  has begun.

Figure 21 summarizes data and hypothetical relations for perennial ice. The coverage is inadequate. In particular no data are available for line  $D_1 - D_f$  which is a very substantial region according to Figure 3.

We have shown here three models for the effect of solid inclusions upon strength, with another simplification introduced in eq 73. A fifth possibility would be to base a theory upon the assumption that crack propagation is reduced by the presence of salt inclusions. Further experiments should decide between the different models. In particular, further limited tests by Assur and Frankenstein on the Arctic pack ice in the fall of 1958 have not yet substantiated the increase in strength with higher salinity at a given temperature below  $-22.9^\circ\text{C}$ , as required by the second model and as shown in Figure 3. The possibility exists that either the first or the third model is more suitable.



## CONCLUSION

The relationships developed for Figure 16 were used to compute the relation of tensile strength to salinity and temperature (Fig. 3). This concludes the circle of the investigation leading to a formulation of strength relations based upon phase relations and models. Figure 1 shows to what degree the test results can be represented by the theoretical relations discussed above. The agreement is reasonable. The remaining scatter even up to 30% can be explained by random variations in strength (Assur 1958).

Most of the interpretations given in this paper are presented to further the solution of basic problems in our understanding of the mechanics of sea ice. For temperatures up to  $-22.9^{\circ}\text{C}$ , one straight line relationship of strength to the square root of brine volume, as shown in Figure 14, may be used for practical purposes. The strength relations should not be used directly for trafficability purposes. The actual flexural strength of ice sheets, used for these purposes, is substantially lower.

Much work still has to be done and not all of the assumptions can be expected to stand up under further study.

## REFERENCES

- Anderson, D. L. (1957) "Theory of sea ice strength". Part II of: Weeks, W. F. and Anderson, D. L., A study of strength of "young" sea ice. Preliminary print, Air Force Cambridge Research Center. Essentially same as:
- \_\_\_\_\_ and Weeks, W. F. (1958) A theoretical analysis of sea ice strength, Transactions of the American Geophysical Union, vol. 39, no. 4.
- Assur, A. (1958) Composition of sea ice and its tensile strength, Arctic Sea Ice Conference proceedings, National Academy of Sciences, National Research Council Publication 598.
- Butkovich, T. R. (1954) Ultimate strength of ice, Snow Ice and Permafrost Research Establishment, Corps of Engineers, U. S. Army, Research Paper 11.
- \_\_\_\_\_ (1956a) Strength studies of high-density snow, SIPRE Research Report 18.
- \_\_\_\_\_ (1956b) Strength studies of sea ice, SIPRE Research Report 20.
- \_\_\_\_\_ (1958) Some physical properties of ice from the TUTO tunnel and ramp, Thule, Greenland, SIPRE Research Report 47.
- Gitterman, K. E. (1937) Akad. Nauk, SSSR Leningrad, Institut Galurgii, Solianaia laboratoria, Trudy 15.
- Jellinek, H. H. G. (1957a) Adhesive properties of ice, Snow Ice and Permafrost Research Establishment, Corps of Engineers, U. S. Army, Research Report 38.
- \_\_\_\_\_ (1957b) Tensile strength properties of ice adhering to stainless steel, SIPRE Research Report 23.
- Lyman, J. and Fleming, R. H. (1940) Composition of sea water, Journal of Marine Research, vol. 3, p. 134-146.
- Makarov, S. (1901) Ermak vo l'dakh (Ermak in ice), St. Petersburg.
- Malmgren, F. (1927), On the properties of sea ice, Scientific Results, Maud Expedition 1918-1925, vol. 1, no. 5, Bergen: John Greig.
- Moskatov, K. A. (1938) O posadke samoletov na led (Landing of airplanes on ice), Arkticheskii institut, (Leningrad) Trudy 110, p. 43-55 (text in Russian).
- Nakaya, N. (1956) Properties of single crystals of ice, revealed by internal melting, Snow Ice and Permafrost Research Establishment, Corps of Engineers, U. S. Army, Research Paper 13.
- Nelson, K. H. (1953) A study of the freezing of sea water, Thesis, Univ. Washington.
- \_\_\_\_\_ and Th. G. Thompson (1954) Deposition of salt from sea water by frigid concentration, Univ. Washington, Dept. of Oceanography, Technical Report 29.



- Petrov, I. G. (1955) "Fiziko-mekhanicheskie svoistva i tolshchina ledianogo pokrova. (Physical-mechanical properties and thickness of the ice cover)," in Somov, M. M. (ed.), Materialy nabliudenii nauchno-issledovatel'skoi dreifuishchei stantsii 1950/51 gg. (Observational data of the scientific-research drifting station of 1950-1951), vol II (6) p. 103-165 (text in Russian), Leningrad: Izd. "Morskoi Transport". Translation by D. Kraus (Meteorol. Soc.) available from US Dept. of Commerce, Office of Technical Services.
- Ringer, W. E. (1906) De veranderingen in samenstelling van zeewater bij het bevriesen (Changes in the composition of sea water upon freezing), Chem. Weekblad, 3 p. 223-249.
- (1928) Über die Veränderungen in der Zusammensetzung des Meereswassersalzes beim Ausfrieres (Changes in the composition of sea-water salt during freezing.) Conseil permanent intern. exploration mer, Rapp. 47, p. 226-231.
- Ripperger, E. A. and Davids, N. (1947) Critical stresses in a circular ring, American Society of Civil Engineers, Transactions, vol. 12, p. 619-635.
- Savel'ev, B. A. (1954) "Instruktivnye ukazaniia po opredeleniiu soderzhaniia tverdoi, zhidkoi i gasoobraznoi fazy v zasolennykh l'dakh (Instructions for the determination of the solid, liquid and gas phase in salt-water ice)," in Materialy po laboratornym issledovaniiam merzlykh gruntov (Laboratory investigations of frozen ground), sbornik 2 p. 176-192, Institut merzlotovedeniia, Akademiia Nauk SSSR, (text in Russian).
- (1957) (compiler): Izuchenie mekhanicheskikh i fizicheskikh svoist l'da. Rukovodstvo (Investigation of the mechanical and physical properties of ice - A manual), Année géophysique Internationale, Moscow. (See Ch. II: Izmerenie plotnosti i fazovogo sostava l'da (Determination of the density and phase composition of ice). (Text in Russian).
- Sverdrup, H. W. et al. (1942) The oceans. New York: Prentice Hall.
- Tabata, T. and Ono, N. (1957) Kaihyō no kōzō ni Tsuite (On the structure of sea ice) (Low Temperature Science), Ser. A. vol. 16 (Text in Japanese).
- Thompson, T. G. (1932) The physical properties of sea water, US National Research Council, Bull. 85: p. 84.
- Tsurikov, V. L. (1939) Problema prochnosti morskogo l'da (The problem of sea ice strength), Severnyi Morskoi Put; vol. 16, p. 45-74. (Text in Russian).
- Weeks, W. F. (1958) The structure of sea ice: A progress report, Arctic Sea Ice Conference Proceedings, National Academy of Sciences - National Research Council Publication 598.
- Wright, C. S. and Priestley, R. N. (1922) Glaciology. British Antarctic Expedition 1910-1913.
- Zubov, N. N. (1945) L'dy Arktiki. (The Arctic ice), Moscow: Izd. Glasevmorputi. (Text in Russian).



APPENDIX A: Relative volume of brine  $v$  (‰) in standard sea ice of 1‰ salinity, depending upon temperature (C), 1957.

The relative volume of brine for sea ice is obtained by multiplying the values in the table by the observed salinity of the ice in ‰. The excess salts in sea ice (for example an enrichment in  $\text{Na}_2\text{SO}_4$ ) should be subtracted from the salinity, but not enough experimental data are available yet to estimate them. This table was computed from the phase relations in standard sea ice (Table III) in combination with information derived from Figure 6 (freezing point of brine). The procedure is explained in the text. Eq 40 was used up to  $-2^\circ\text{C}$  with some adjustment to the results computed from Table II. Graphical interpolation was used to obtain the values for each  $0.1^\circ\text{C}$ . The table is dated since refinements and improvements are to be expected in the future.

Volume of brine

$\theta(^{\circ}\text{C})$	0	0.1	0.2	0.3	0.4	0.5	0.6	0.7	0.8	0.9
-0	-	500.9	250.5	167.1	125.4	100.3	83.66	71.74	62.08	55.85
-1	50.28	45.77	41.87	38.60	35.77	33.29	31.17	29.06	27.23	25.56
-2	24.0	22.8	21.8	20.9	20.1	19.3	18.5	17.9	17.3	16.7
-3	16.2	15.7	15.2	14.8	14.4	14.0	13.6	13.3	13.0	12.7
-4	12.4	12.1	11.8	11.6	11.4	11.2	11.0	10.8	10.6	10.4
-5	10.2	10.0	9.81	9.64	9.48	9.32	9.16	9.01	8.87	8.73
-6	8.60	8.48	8.36	8.25	8.14	8.03	7.92	7.82	7.72	7.62
-7	7.52	7.43	7.34	7.25	7.16	7.07	6.99	6.91	6.83	6.75
-8	6.67	6.60	6.53	6.46	6.39	6.32	6.26	6.20	6.14	6.08
-9	6.02	5.97	5.92	5.87	5.82	5.77	5.72	5.67	5.62	5.57
-10	5.53	5.49	5.45	5.41	5.37	5.33	5.29	5.26	5.22	5.18
-11	5.15	5.12	5.08	5.05	5.01	4.98	4.95	4.92	4.88	4.85
-12	4.82	4.79	4.76	4.74	4.71	4.68	4.66	4.63	4.61	4.58
-13	4.56	4.54	4.51	4.49	4.46	4.44	4.42	4.40	4.37	4.35
-14	4.33	4.31	4.29	4.27	4.25	4.23	4.21	4.19	4.17	4.15
-15	4.13	4.11	4.09	4.08	4.06	4.04	4.02	4.00	3.99	3.97
-16	3.95	3.93	3.92	3.90	3.89	3.87	3.85	3.84	3.82	3.81
-17	3.79	3.78	3.76	3.75	3.73	3.72	3.71	3.69	3.68	3.66
-18	3.65	3.64	3.62	3.61	3.59	3.58	3.57	3.55	3.54	3.52
-19	3.51	3.50	3.48	3.47	3.45	3.44	3.43	3.42	3.40	3.39
-20	3.38	3.37	3.36	3.34	3.33	3.32	3.31	3.30	3.28	3.27
-21	3.26	3.25	3.24	3.22	3.21	3.20	3.19	3.18	3.16	3.15
-22	3.14	3.13	3.12	3.11	3.10	3.09	3.08	3.07	3.06	3.05
-23	2.97	2.89	2.81	2.72	2.64	2.56	2.50	2.43	2.37	2.30
-24	2.24	2.19	2.14	2.08	2.03	1.98	1.94	1.89	1.85	1.80
-25	1.76	1.72	1.69	1.65	1.62	1.58	1.55	1.52	1.49	1.46
-26	1.44	1.41	1.38	1.36	1.33	1.31	1.29	1.27	1.25	1.23
-27	1.21	1.19	1.18	1.16	1.15	1.13	1.12	1.11	1.09	1.08
-28	1.07	1.06	1.05	1.04	1.03	1.02	1.01	1.00	0.990	0.980
-29	0.970	0.960	0.950	0.940	0.930	0.920	0.912	0.904	0.897	0.889
-30	0.881	0.875	0.869	0.864	0.858	0.852	0.846	0.840	0.835	0.829
-31	0.823	0.818	0.813	0.808	0.803	0.798	0.793	0.788	0.783	0.778
-32	0.773	0.769	0.764	0.760	0.756	0.752	0.747	0.743	0.739	0.734
-33	0.730	0.726	0.723	0.720	0.716	0.712	0.709	0.706	0.702	0.698



## Volume of brine

$\theta(^{\circ}\text{C})$	0	0.1	0.2	0.3	0.4	0.5	0.6	0.7	0.8	0.9
-34	0.695	0.692	0.689	0.686	0.683	0.680	0.678	0.675	0.672	0.669
-35	0.666	0.664	0.661	0.658	0.656	0.654	0.651	0.648	0.646	0.644
-36	0.641	0.639	0.636	0.634	0.632	0.630	0.627	0.625	0.623	0.620
-37	0.618	0.616	0.614	0.611	0.609	0.607	0.605	0.603	0.600	0.598
-38	0.596	0.594	0.592	0.590	0.588	0.585	0.583	0.581	0.579	0.577
-39	0.575	0.573	0.571	0.569	0.567	0.565	0.563	0.561	0.559	0.557
Temp: -40	-42	-44	-46	-48	-50	-52	-54			
Brine: 0.555	0.522	0.395	0.242	0.162	0.118	0.0914	0.0750			



APPENDIX B: Gravimetric constants for the main constituents in the brine-salt system of sea ice. Based on International Atomic Weights 1956. Ratios primarily used for the derivation of Table III are given.  
(Compiled for the convenience of investigators studying the chemistry of sea ice).

Ratio		Value	Reciprocal
$\text{CaCO}_3$		100.091	0.0099909
$\text{CaCO}_3 \cdot 6\text{H}_2\text{O}$		208.187	0.0048034
$6\text{H}_2\text{O}$	to $\text{CaCO}_3 \cdot 6\text{H}_2\text{O}$	0.51923	2.0800
Ca	to $\text{CaCO}_3 \cdot 6\text{H}_2\text{O}$	0.19252	5.1943
O	to $\text{CaCO}_3 \cdot 6\text{H}_2\text{O}$	0.076854	13.012
Ca	to $\text{CaCO}_3$	0.40044	2.4973
$\text{CO}_2$	to $\text{CaCO}_3$	0.43971	2.2742
$\text{CO}_3$	to $\text{CaCO}_3$	0.59956	1.6679
$\text{CaO}$		56.08	0.017832
Ca	to $\text{CaO}$	0.7174	1.399
$\text{CO}_3$		60.011	0.016664
Ca	to $\text{CO}_3$	0.66788	1.4973
$\text{HCO}_3$		61.019	0.016388
$\text{CaCO}_3 \cdot 6\text{H}_2\text{O}$	to $\text{HCO}_3$	3.4118	0.29310
$\text{NaSO}_4$		142.048	0.0070399
$\text{NaSO}_4 \cdot 10\text{H}_2\text{O}$		322.208	0.0031036
$10\text{H}_2\text{O}$	to $\text{Na}_2\text{SO}_4 \cdot 10\text{H}_2\text{O}$	0.55914	1.7885
$\text{Na}_2$	to $\text{Na}_2\text{SO}_4 \cdot 10\text{H}_2\text{O}$	0.14271	7.0073
$\text{SO}_4$	to $\text{Na}_2\text{SO}_4 \cdot 10\text{H}_2\text{O}$	0.29815	3.3540
$\text{Na}_2\text{SO}_4$	to $\text{Na}_2\text{SO}_4 \cdot 10\text{H}_2\text{O}$	0.44086	2.2683
$\text{Na}_2\text{S}$		78.048	0.012813
$\text{Na}_2$	to $\text{Na}_2\text{S}$	0.58915	1.6974
$\text{SO}_4$		96.066	0.010410
$\text{SO}_3$	to $\text{SO}_4$	0.83345	1.1998
$\text{Na}_2$	to $\text{SO}_4$	0.47865	2.0892
$\text{NaCl}$		58.448	0.017109
$\text{NaCl} \cdot 2\text{H}_2\text{O}$		94.480	0.010584
$2\text{H}_2\text{O}$	to $\text{NaCl} \cdot 2\text{H}_2\text{O}$	0.38137	2.6221
$\text{NaCl}$	to $\text{NaCl} \cdot 2\text{H}_2\text{O}$	0.61863	1.6165
Na	to $\text{NaCl} \cdot 2\text{H}_2\text{O}$	0.24334	4.1094
Cl	to $\text{NaCl} \cdot 2\text{H}_2\text{O}$	0.37529	2.6646
Na	to $\text{NaCl}$	0.39336	2.5422
Cl	to $\text{NaCl}$	0.60664	1.6484
Na	to Cl	0.64842	1.5422
$\text{Na}_2\text{O}$		61.892	0.026134
Na	to $\text{Na}_2\text{O}$	0.37093	2.6959
$\text{MgCl}_2$		95.234	0.010500
$\text{MgCl}_2 \cdot 8\text{H}_2\text{O}$		239.362	0.0041778
$8\text{H}_2\text{O}$	to $\text{MgCl}_2 \cdot 8\text{H}_2\text{O}$	0.60213	1.6608
Mg	to $\text{MgCl}_2 \cdot 8\text{H}_2\text{O}$	0.10160	9.8422
$\text{Cl}_2$	to $\text{MgCl}_2 \cdot 8\text{H}_2\text{O}$	0.29626	3.3754
$\text{MgCl}_2 \cdot 12\text{H}_2\text{O}$		311.426	0.0032110
$12\text{H}_2\text{O}$	to $\text{MgCl}_2 \cdot 12\text{H}_2\text{O}$	0.69420	1.4405
Mg	to $\text{MgCl}_2 \cdot 12\text{H}_2\text{O}$	0.078092	12.805
$\text{Cl}_2$	to $\text{MgCl}_2 \cdot 12\text{H}_2\text{O}$	0.22771	4.3916
Mg	to $\text{MgCl}_2$	0.25537	3.9159
$\text{Cl}_2$	to $\text{MgCl}_2$	0.74463	1.3430
Mg	to $\text{Cl}_2$	0.34295	2.9159



## APPENDIX B:

	<u>Ratio</u>	<u>Value</u>	<u>Reciprocal</u>
Mg	to Cl	0.68590	1.4579
KCl		74.557	0.013413
K	to KCl	0.52443	1.9068
Cl	to KCl	0.47557	2.1027
Cl	to K	0.90683	1.1027
CaCl <sub>2</sub>		110.994	0.0090095
CaCl <sub>2</sub> ·6H <sub>2</sub> O		219.090	0.0045643
6H <sub>2</sub> O	to CaCl <sub>2</sub> ·6H <sub>2</sub> O	0.49339	2.0268
Ca	to CaCl <sub>2</sub> ·6H <sub>2</sub> O	0.18294	5.4663
Cl <sub>2</sub>	to CaCl <sub>2</sub> ·6H <sub>2</sub> O	0.32368	3.0895
Cl <sub>2</sub>	to CaCl <sub>2</sub>	0.63890	1.5652
Ca	to Cl <sub>2</sub>	0.56519	1.7693
NaBr		102.907	0.00971751
Na	to NaBr	0.22342	4.4759
NaBr·2H <sub>2</sub> O		138.939	0.00719740
KBr		119.016	0.00840223
K	to KBr	0.32852	3.0439